Estimating the Critical Height of Unsupported Trenches in Unsaturated Soil

by

Adin Richard

B.Sc.E. (Civil Engineering), University of New Brunswick, 2016

A Thesis Submitted in Partial Fulfillment
of the requirements for the Degree of

Master of Science in Engineering

In the Graduate Academic Unit of Civil Engineering

Supervisor: Won Taek Oh, Ph.D., P.Eng., Department of Civil Engineering

Examining Board: Kaveh Arjomandi, Ph.D., P.Eng., Department of Civil Engineering
Othman Nasir, Ph.D., P.Eng., Department of Civil Engineering
Mohsen Mohammadi, Ph.D., Department of Mechanical Engineering

This Thesis is accepted by the Dean of Graduate Studies

THE UNIVERSITY OF NEW BRUNSWICK

August 2018

ABSTRACT

Trenching (or excavating) is integral to construction activities in the practice of geotechnical, mining, tunnelling, and geo-environmental engineering. Many projects are initiated by excavating trenches for infrastructure to be installed. Workers are often required to enter trenches during the construction process, which may present serious risks. Trench failures can result in death and/or damage to adjacent properties, therefore trenches should be excavated with extreme precaution. The critical height (i.e. maximum depth that can be excavated without failure) is the most important design consideration for ensuring the stability of unsupported trenches. Excavation work is often done in unsaturated soils, in which case the critical height of unsupported trenches can be more reliably estimated by considering the influence of matric suction.

The purpose of this study is to investigate the influence of soil type, the matric suction distribution, and surcharge pressure in assessing the critical height of unsupported trenches. Extended Rankine earth pressure theory, the limit equilibrium method, and finite element analyses were used to estimate the critical height of unsupported trenches in two unsaturated soils.

ACKNOWLEDGEMENTS

Thank you to all friends, family, and faculty for the emotional and the financial support. There are countless individuals that made this degree possible. First of all, my parents, Sean and Holly, you have positioned me to succeed and for that I will be forever grateful. I am especially thankful for the number of times you have been my shuttle for kayaking. Dad, I am sorry for the number of times us dirtbags have piled in the truck and messed it up. Mom, thank you for continually making him take us. I genuinely could not have asked for better parents. Stuart, my brother, I am most thankful for the number of times you cooked me supper over the last two years. Seriously, you should open a stir-fry restaurant (name it Stu-Fry ©). I was fortunate enough to share an office with two great colleagues, Vitus Ileme, and Greg Brennan. I am happy to call both of you my friends. Our creative discussions always kept me thinking. Vitus, your positive attitude and composure always helped me on my down days. Greg, your knack for problem solving is something to admire. Thank you both for all that you contributed to this thesis. Dr. Haralampides and Dr. MacQuarrie, I thoroughly enjoyed each class I had with you going all the way back to undergrad. Thank you both for helping round out my knowledge in hydraulics and hydrology. Lastly, thank you, my supervisor, Dr. Oh. I am honoured to have been accepted as your first ever graduate student. I think we both took a leap of faith. I did not actually understand soil mechanics until that first semester when you taught us the 'Mechanics of Unsaturated Soils'. You have brought me a long way. And of course, thank you to my friends that were always there to help me unwind. I could not have done without every one of you!

TABLE OF CONTENTS

ABSTRACT ii
ACKNOWLEDGEMENTS iii
TABLE OF CONTENTS iv
LIST OF TABLES vi
LIST OF FIGURES vii
LIST OF SYMBOLS & ABBREVIATIONS xii
CHAPTER 1 - Introduction 1
1.1 Problem Statement 1
1.2 Objectives of the Thesis 2
1.3 Scope of the Thesis 3
1.4 Organization of the Thesis 3
CHAPTER 2 – Trenching Hazards and Regulations in Canada 5
2.1 Trench Collapse Statistics 6
2.2 Trench Failure Mechanisms 8
2.3 Trench Failure Modes 10
2.4 Work Protection Methods 12
2.5 Trench Economics 16
CHAPTER 3 – Theoretical Background 18
3.1 Properties of Unsaturated Soil 18
3.2 Shear Strength of Unsaturated Soil 23
3.3 Critical Height of Unsupported Vertical Trenches 29
3.3.1 Rankine's Earth Pressure Theory (1857) 29
3.3.2 Pufahl et al. (1983) 33
3.3.3 Vanapalli & Oh (2012) 36
CHAPTER 4 – Estimating the Critical Height of Unsupported Vertical Trenches in Sand 39
4.1 Soil Properties 40
4.2 Estimating the Critical Height with EREPT 44

4.3 Estimating the Critical Height with BSM 51
4.4 Comparison of Critical Heights from EREPT and BSM 58
4.5 Summary and Conclusions 61
CHAPTER 5 – Estimating the Critical Height of Unsupported Trenches with Different Wall Slopes in Sand 62
5.1 Estimating the Critical Height with the Finite Element Approach 63
5.1.1 Hydraulic Conductivity Function 63
5.1.2 Analysis in SIGMA/W 65
5.1.3 Analysis in SLOPE/W 67
5.2 Estimating the Critical Height with the Limit Equilibrium Method 70
5.3 Comparison of Limit Equilibrium and Finite Element Approaches 74
5.4 Summary and Conclusions 86
CHAPTER 6 – Estimating the Critical Height of Unsupported Vertical Trenches Subjected to Surcharge Pressure 88
6.1 Soil Properties 88
6.2 Estimating the Critical Height without Foundation Stress 90
6.2.1 Estimating the Critical Height with EREPT 90
6.2.2 Estimating the Critical Height with BSM 95
6.2.3 Comparison of Critical Heights from EREPT and BSM 97
6.3 Estimating the Critical Height with Foundation Stress 99
6.4 Summary and Conclusions 107
CHAPTER 7 – General Conclusions 108
7.1 Recommendations for Future Research 111
REFERENCES 112
CURRICULUM VITAE

LIST OF TABLES

Table 2.1. Summary of the maximum allowable height of an unsupported vertical trench 6
Table 2.2. Total cost breakdown for pipe-laying crew (Gulf Operators 2018)..... 17
Table 4.1. Basic soil properties of Unimin 7030 sand (Mohamed & Vanapalli 2006).... 41
Table 4.2. Summary of fitting parameters used to plot the SWCC of Unimin 7030 sand 42
Table 4.3. Variation of the critical height in Unimin 7030 sand..... 58
Table 6.1. Basic soil properties of IHT (Vanapalli et al. 1997, Oh & Vanapalli 2010)... 89
Table 6.2. Variation of the critical height in IHT..... 97

LIST OF FIGURES

Figure 2.1. Factors affecting trench stability (Ontario 2017) 9
Figure 2.2. Excavation adjacent to existing foundations (Ontario 2017) 9
Figure 2.3. Trench parallel with backfill material (Ontario 2017)..... 10
Figure 2.4. Sequential trench failure (Alberta 2009) 11
Figure 2.5. Trench failure modes (Manitoba 2011) 12
Figure 2.6. Sloping standards (Ontario 2017)..... 14
Figure 2.7. Placement of spoil pile (Ontario 2017)..... 14
Figure 2.8. Shored trench with partially sloped walls (Ontario 2017)..... 15
Figure 2.9. Typical shored trench (Ontario 2017) 16
Figure 3.1. Surface tension phenomenon at air-water interface; (a) intermolecular forces acting on contractile skin and (b) surface tension forces associated with curved 2D surface (Fredlund et al. 2012) 19
Figure 3.2. Typical SWCC showing different zones of desaturation (Nishimura et al. 2008) 20
Figure 3.3. Pore-water profiles in the vadose zone (Fredlund & Rahardjo 1993a) 21
Figure 3.4. Typical SWCC for silt soil (Fredlund et al. 2012) 22
Figure 3.5. Extended Mohr-Coulomb failure envelope for unsaturated soil (Fredlund & Rahardjo 1993b)..... 25
Figure 3.6. Variation of shear strength with respect to suction for four sands (modified after Donald 1957) 26
Figure 3.7. Relationship between κ and I_p (Garven & Vanapalli 2006) 28
Figure 3.8. Soil structure system for the Rankine solution for $\alpha = 90°$ (modified after Bowles 2001) 30
Figure 3.9. General conditions of Mohr's circle to derive the Rankine earth pressure equations (modified after Bowles 2001)..... 31
Figure 3.10. AEP and critical height in saturated soil (modified after Pufahl et al. 1983) 32

Figure 3.11. Lateral earth pressure states for saturated and unsaturated conditions (Pufahl et al. 1983) 33
Figure 3.12. Components of AEP distribution and critical height in unsaturated soil 35
Figure 3.13. Unsupported vertical trench (unsaturated, intact, modified after Pufahl et al. 1983) 36
Figure 3.14. Field tests on the stability of an unsupported excavation in an unsaturated soil (modified after Whenham et al. 2007) 37
Figure 4.1. Measured matric suction profile and assumed hydrostatic matric suction profile with the water table at a depth of 600-mm from the soil surface (modified after Mohamed & Vanapalli 2006) 40
Figure 4.2. Grain size distribution curve of Unimin 7030 sand..... 41
Figure 4.3. SWCC of Unimin 7030 sand (modified after Mohamed & Vanapalli 2006) 42
Figure 4.4. Direct shear test results on Unimin 7030 sand (modified after Mohamed & Vanapalli 2006)..... 43
Figure 4.5. Example of regression curve for the net AEP distribution with D = 0.6-m .. 45
Figure 4.6. Positive, negative, and net AEP distribution (D = 0.3-m)..... 47
Figure 4.7. Positive, negative, and net AEP distribution (D = 0.6-m)..... 48
Figure 4.8. Positive, negative, and net AEP distribution (D = 1.0-m)..... 49
Figure 4.9. Positive, negative, and net AEP distribution (D = 1.5-m)..... 50
Figure 4.10. Forces acting on the i^{th} slice in Bishop's simplified method of slices (Craig 2004) 51
Figure 4.11. Establishing PWP profile with In-situ analysis in SIGMA/W 53
Figure 4.12. Analysis tree for Bishop's simplified method with In-situ as the parent analysis..... 53
Figure 4.13. Calculation of PWP based on the location of GWT in SIGMA/W 54
Figure 4.14. Schematic of the 'Entry and Exit' slip surface method in SLOPE/W..... 55
Figure 4.15. Slope stability analysis in SLOPE/W using Bishop's simplified method (D = 0.3-m) 56
Figure 4.16. Slope stability analysis in SLOPE/W using Bishop's simplified method (D = 0.6-m) 56

Figure 4.17. Slope stability analysis in SLOPE/W using Bishop's simplified method (D = 1.0-m) 57
Figure 4.18. Slope stability analysis in SLOPE/W using Bishop's simplified method (D = 1.5-m) 57
Figure 4.19. Variation of the critical height with respect to the depth of the GWT using extended Rankine earth pressure theory and Bishop's simplified method (Unimin 7030 sand) 60
Figure 5.1. Different types of trenches considered in this chapter 63
Figure 5.2. Hydraulic conductivity function of Unimin 7030 sand 65
Figure 5.3. Boundary conditions required for coupled analyses in SIGMA/W 67
Figure 5.4. Example of slope stability analysis tree used in the coupled analyses (10-s time steps between excavations) 68
Figure 5.5. Example of slope stability analysis using SIGMA-Stress method in SLOPE/W (1.5V:1H) 69
Figure 5.6. Example of half-sine function used in M-P analyses (λ = 0.25) 71
Figure 5.7. Forces acting on a slice within an arbitrary slip surface (GEO-SLOPE 2015) 72
Figure 5.8. Variation of deformation, PWP, and FOS with time for (a) 10-s, (b) 250-s, (c) 500-s, and (d) 750-s after 1.3-m excavation stage with initial D = 0.7-m 76
Figure 5.9. FOS vs. Time for 1.3-m excavation stage (1.5V:1H) with initial D = 0.7-m 76
Figure 5.10. Variation of the critical height for different sloping angles in Unimin 7030 sand (10-s time steps, coupled analysis) 78
Figure 5.11. Variation of the critical height for different sloping angles in Unimin 7030 sand (1,000-s time steps, coupled analysis) 79
Figure 5.12. Variation of the critical height for different sloping angles in Unimin 7030 sand (M-P method) 79
Figure 5.13. Variation of the critical height for 90° slope in Unimin 7030 sand 80
Figure 5.14. Variation of the critical height for 3V:1H slope in Unimin 7030 sand 80
Figure 5.15. Variation of the critical height for 2V:1H slope in Unimin 7030 sand 81
Figure 5.16. Variation of the critical height for 1.5V:1H slope in Unimin 7030 sand 81

Figure 5.17. Distribution of total normal stress during 0.3-m excavation stage for 1.5V:1H slope with initial D = 1.2-m (10-s time steps) 84
Figure 5.18. Distribution of shear stress during 0.3-m excavation stage for 1.5V:1H slope with initial D = 1.2-m (10-s time steps) 84
Figure 5.19. Vertical trench with D = 0.9-m (M-P method) 85
Figure 5.20. Partially sloped (1:1) vertical trench with D = 0.9-m (M-P method) 85
Figure 5.21. Variation of the critical height for 90*** slope in Unimin 7030 sand 86
Figure 6.1. Grain size distribution curve of IHT (Oh &Vanapalli 2010) 89
Figure 6.2. SWCC of IHT (Oh & Vanapalli 2018) 90
Figure 6.3. Positive, negative, and net AEP distribution (D = 0-m) 91
Figure 6.4. Positive, negative, and net AEP distribution (D = 1-m) 92
Figure 6.5. Positive, negative, and net AEP distribution (D = 3-m) 93
Figure 6.6. Positive, negative, and net AEP distribution (D = 5-m) 94
Figure 6.7. Slope stability analysis in SLOPE/W using Bishop's simplified method (D = 0-m) 95
Figure 6.8. Slope stability analysis in SLOPE/W using Bishop's simplified method (D = 1-m) 95
Figure 6.9. Slope stability analysis in SLOPE/W using Bishop's simplified method (D = 3-m) 96
Figure 6.10. Slope stability analysis in SLOPE/W using Bishop's simplified method (D = 5-m) 96
Figure 6.11. Variation of the critical height with respect to the depth of the GWT using extended Rankine earth pressure theory and Bishop's simplified method (IHT) 98
Figure 6.12. SLOPE/W model used to consider foundation stress 100
Figure 6.13. Stability analysis considering 50-kPa surcharge at a distance of 3-m (D = 5-m) 101
Figure 6.14. Critical height vs. distance of foundation stress from excavation (D = 0-m) 101
Figure 6.15. Critical height vs. distance of foundation stress from excavation (D = 1-m) 102

Figure 6.16. Critical height vs. distance of foundation stress from excavation (D = 2-m) 102
Figure 6.17. Critical height vs. distance of foundation stress from excavation (D = 3-m) 103
Figure 6.18. Critical height vs. distance of foundation stress from excavation (D = 5-m) 103
Figure 6.19. Critical height vs. depth of the GWT with distance of foundation stress from excavation = 0-m 105
Figure 6.20. Critical height vs. depth of the GWT with distance of foundation stress from excavation = 1-m 105
Figure 6.21. Critical height vs. depth of the GWT with distance of foundation stress from excavation = 2-m 106
Figure 6.22. Critical height vs. depth of the GWT with distance of foundation stress from excavation = 3-m 106

LIST OF SYMBOLS & ABBREVIATIONS

Abbreviations

AEP = active earth pressure

AEV = air-entry value

BSM = Bishop's simplified method

CW = constant water content triaxial test

EREPT = extended Rankine earth pressure theory

FOS = factor of safety

GWT = groundwater table

IHT = Indian Head till

LEM = limit equilibrium method

M-P = Morgenstern-Price

MESA = modified effective stress approach

MTSA = modified total stress approach

PAP = pore-air pressure

PWP = pore-water pressure

SWCC = soil-water characteristic curve

Symbols

α = inclination of slice base (°)

wall inclination (°)

β = length of slice base (m)

backfill inclination (°)

γ = unit weight of soil (kN/m^3)

Θ =	normalized water content
θ =	volumetric water content
	failure angle
θ' =	the first derivative of the SWCC with respect to suction
κ =	fitting parameter for shear strength
λ =	scaling factor for specified force function used in the Morgenstern-Price method
ν =	Poisson's ratio
σ =	total stress (kPa)
σ' =	effective stress (kPa)
$\sigma - u_a$ =	net normal stress (kPa)
τ =	shear strength (kPa)
ϕ' =	internal friction angle (˚)
ϕ^b =	angle describing rate of change between suction and shear strength (˚)
χ =	soil specific parameter for effective stress in unsaturated soil
ψ =	soil suction (kPa)
a, m, n =	fitting parameters for Fredlund & Xing's equation (1994)
C =	total cohesion (kPa)
C_{cw} =	total cohesion from constant water content triaxial test (kPa)
c' =	effective cohesion (kPa)
D =	depth of the groundwater table from the soil surface (m)
E =	elastic modulus (kPa)
	interslice normal force (kN/m)

e = Napier's constant (2.71828…)

void ratio

$f(x)$ = specified force function in the Morgenstern-Price method

G_s = specific gravity of soil particles

H = height (m)

I_p = plasticity index

i = the interval between the range of j to N

j = the least negative pore-water pressure to be described by the final hydraulic conductivity function (kPa)

K_a = Rankine's active earth pressure coefficient

K_0 = Rankine's earth pressure coefficient for at-rest conditions

k = hydraulic conductivity (m/s)

m_{cr} = ratio of the depth of the groundwater table to the critical height

N = slice base normal force (kN/m)

the maximum negative pore-water pressure to be described by the final hydraulic conductivity function (kPa)

p_a = net active earth pressure (kPa)

R, f, x = geometric parameters as described in Figure 5.7

R_s = radius of curvature of meniscus (m)

S = degree of saturation

S_r = shear resistance (kN/m)

S_m = mobilized shear force (kN/m)

T_s = tensile force per unit length (kN/m)

u_a = pore-air pressure (kPa)

u_w = pore-water pressure (kPa)

Δu = pressure difference (kPa)

$u_a - u_w$ = matric suction (kPa)

$(u_a - u_w)_b$ = matric suction at the air-entry value (kPa)

$(u_a - u_w)_r$ = matric suction at the residual suction value (kPa)

W = weight of a slice within a sliding mass (kN/m)

X = interslice shear force (kN/m)

y = a dummy variable of integration representing the logarithm of negative pore-water pressure

Z_t = depth of tension zone (m)

z = depth below soil surface (m)

Subscripts

FOS

f = factor of safety for force equilibrium

m = factor of safety for moment equilibrium

γ

sat = unit weight of saturated soil

unsat = unit weight of unsaturated soil

w = unit weight of water

θ

s = saturated water content

r = residual water content

σ

1 = major principal stress (kPa)

3 = minor principal stress (kPa)

h = lateral pressure (kPa)

v, z = overburden pressure (kPa)

τ

sat = shear strength of saturated soil

unsat = shear strength of unsaturated soil

H

cr = critical height of a trench

max = maximum negative pressure head

sat = height of saturated soil layer

unsat = height of unsaturated soil layer

k

sat = the measured hydraulic conductivity for saturated conditions (m/s)

unsat = the calculated hydraulic conductivity for unsaturated conditions (m/s)

CHAPTER 1

INTRODUCTION

1.1 Problem Statement

Most engineering projects involving foundations, landfills, pipelines, storm drains, etc., are initiated with an excavation for infrastructure to be installed. Workers are often required to enter the excavation or trench during the construction process, which may present serious risks. Trenching is inherently dangerous due to the risk of cave-in, which may result in severe injury, death, and/or consequential damage to adjacent property. Thousands of work-related deaths and injuries in the construction industry have been attributed to trench collapses. An average of 50 fatalities were reported each year from 1992 to 2007 in the U.S. alone (NIOSH 2013). In Canada, each province enforces strict regulations with respect to safe excavation practices in an attempt to prevent fatalities and serious injuries resulting from trench collapses. The regulations specify the maximum allowable height of an unsupported vertical trench (i.e. safe height), maximum sloping and benching angles, and the minimum distance from the trench for stockpiling excavated or backfill materials. Regardless of in-situ field conditions, Canadian provinces enforce safe heights in the range of 1.2-m (New Brunswick 1991) to 1.5-m (Alberta 2009).

Trench boxes are often a practical solution in protecting workers since they allow them to safely access the work space. However, typical trench boxes are eight metres in length and weigh multiple tons (Trench Shoring Company 2016). Hence, the process of lifting a box, setting it in place, and repositioning it when necessary can be very time consuming. They

also create an obstacle for the workers and the equipment that are used for setting infrastructure. Lost production time results in lost profit, making it desirable to excavate and work in unsupported vertical trenches whenever possible. However, unsupported trenches risk collapsing and therefore must be designed and excavated with extreme precaution, especially when workers are required to enter the excavation.

The critical height (i.e. maximum depth of a trench that can be excavated without failure, H_{cr}) is the most important design consideration for ensuring the stability of unsupported trenches. Many construction projects involve trenching and setting infrastructure in the vadose zone; thus, the critical height of unsupported trenches should be determined by extending the mechanics of unsaturated soils. Trench stability is mainly governed by the matric suction distribution between the soil surface and the groundwater table (Pufahl et al. 1983, Whenham et al. 2007, De Vita et al. 2008, Vanapalli & Oh 2012). In other words, adhering to a universal safe height suggested by provincial regulations may not be a reasonable approach in geotechnical engineering practice, because in-situ field conditions are not considered.

1.2 Objectives of the Thesis

The main objective of this study is to investigate the variation of the critical height of unsupported trenches in unsaturated soil considering various field conditions and matric suction distributions. More details are as follows:

- Review current trenching regulations and procedures in Canada.
- Review methodologies for estimating the critical height of unsupported vertical trenches in unsaturated soil.

- Estimate the critical height of unsupported trenches in unsaturated cohesionless (Unimin 7030 sand) and cohesive (Indian Head till) soils using analytical and numerical approaches.

1.3 Scope of the Thesis

Multiple excavation scenarios were simulated considering five major factors; i) level of the groundwater table (hereafter referred to as GWT) ii) slope of the trench wall, iii) excavation rate, iv) magnitude of surcharge pressure, and v) distance between a trench and a surcharge pressure. The critical heights were estimated using three distinct approaches; i) analytical approach with extended Rankine earth pressure theory, ii) limit equilibrium methods (Bishop's simplified method and Morgenstern-Price method), and iii) slope stability analyses based on finite element analyses. Geotechnical modelling software, SLOPE/W and SIGMA/W (GEO-SLOPE International Ltd.), were used for the limit equilibrium methods and finite element analyses. The critical heights obtained from the three different approaches are discussed. The results were also compared to the guidelines set by Canadian provinces. Lastly, recommendations were provided for the direction of future studies in estimating the critical height of unsupported trenches.

1.4 Organization of the Thesis

This thesis consists of seven chapters including 'Introduction' (Chapter 1) and 'General Conclusions' (Chapter 7).

Chapter 2 discusses trenching regulations and general trenching guidelines in Canada. The modes and mechanisms of trench failure are described, and field procedures for mitigating worker risks are discussed. Trenching economics are briefly noted.

Chapter 3 is an extensive literature review pertaining to the mechanical properties of unsaturated soil and analytical approaches for estimating the critical height of unsupported vertical trenches in unsaturated soil.

Chapter 4 details the procedures to estimate the critical height of unsupported vertical trenches in an unsaturated sand using two independent methods; i) extended Rankine earth pressure theory and ii) Bishop's simplified method, which is a form of the Limit Equilibrium Method (hereafter referred to as LEM). The critical heights obtained from both approaches are compared. In addition, details of the geotechnical modelling software, SLOPE/W and SIGMA/W, are provided.

Chapter 5 investigates the influence of excavation rate on the critical height of various sloped trenches in an unsaturated sand through coupled stress-PWP analyses, which is a finite element approach. The estimated critical heights for different time steps (i.e. fast and slow excavation rates) are compared with those from the Morgenstern-Price method, which is also a form of the LEM. Additional details of SIGMA/W are provided.

Chapter 6 examines the critical height of unsupported vertical trenches in an unsaturated cohesive soil using the LEM (Morgenstern-Price method). The trenches being modelled are subjected to surcharges pressures at various distances from the edge of excavation.

CHAPTER 2

TRENCHING HAZARDS AND REGULATIONS IN CANADA

'Trench' is defined as an excavation in which the measurement of depth exceeds the width. Working in trenches is inherently dangerous because workers are subjected to the risk of cave-ins. According to NIOSH (2013), trenches as shallow as 1.2-m deep have reportedly collapsed and resulted in deaths. To avoid these types of tragedies, each Canadian province enforces strict regulations with respect to safe excavation practices. Table 2.1 summarizes the maximum allowable height of an unsupported vertical trench as regulated by each Canadian province before safety measures such as benching, sloping, bracing, or trench boxes must be implemented to access the workspace (i.e. safe height). The problem with enforcing a universal safe height throughout each province is that the standards are solely based on empirical data without any theoretical background, rather than considering the soil type and field conditions. More importantly, the factor of safety used in determining the safe height in each province is unknown. This may lead to over, or under conservative protective measures being used during construction. De Vita et al. (2008) reported that stable vertical cuts can be approximately 15-m deep in a Pozzolan deposit, while Richard et al. (2017) concluded that the critical height in an unsaturated sand can be even less than 1-m. These studies indicate that the safe height of an unsupported trench should be estimated based on the job site conditions.

Table 2.1. Summary of the maximum allowable height of an unsupported vertical trench

Provinces in Canada	Safe height
BC, NB, NS, ON, QC, SK (NL, PE)	1.2-m (4-ft)
AB, MB	1.5-m

2.1 Trench Collapse Statistics

According to NIOSH (2013), an average of 50 fatalities were reported annually in the U.S. from 1992-2007 due to trench collapses. Eivemark & Hall (2000) stated that approximately 1% of work-related deaths in the U.S. were caused by trenching accidents. Other studies showed that approximately 1,000 injuries, and between 60 and 100 deaths per year were associated with trench failures in the U.S. (Thompson & Tanenbaum 1977, Suruda et al. 1988, White 2008). Most deaths occurred in sewer line construction when the trenches were not shored. 80% of reported fatalities occurred in trenches less than 4.5-m deep, and 40% occurred in trenches less than 3-m deep (Eivemark & Hall 2000). Shoring or trench boxes normally provide sufficient worker protection. However, workers should exit the trench before shoring or a trench box is moved (Hinze 2005).

The number of deaths and injuries related to trenching have significantly declined as regulations have been improved. In New Brunswick, the last death that was caused by trenching was reported on May 28, 2001 (WorkSafeNB 2017). The employer was charged with non-compliance of regulations 181(1) and 182(1)(a) of the Occupational Health & Safety Act (1991), which are listed below:

181(1): An employer shall ensure that the walls of an excavation or trench are supported by shoring, bracing, or caging, except when the excavation or trench

(a) is less than 1.2-m deep,

(b) subject to subsection (2), is cut in solid rock,

(c) is sloped or benched to within 1.2-m of the bottom of the excavation or trench with the slope or bench not exceeding 1-m of vertical rise to each 1-m of horizontal run, or

(d) is one that an employee is not required to enter.

181(2): Where the walls or crests of an excavation or trench are cut in solid rock and are not stable, an employer shall ensure that the walls and crests are adequately supported by rock bolts, wire mesh, shoring, or a method that provides equivalent support.

182(1): An employer shall ensure that an employee does not, and no employee shall, enter an excavation or trench 1.2-m or more in depth unless

(a) the walls of the excavation or trench are supported by shoring, bracing, or caging, the excavation or trench is cut in solid rock, or the excavation or trench is sloped or benched to within 1.2-m of the bottom of the excavation or trench with the slope not exceeding 1-m of vertical rise to each 1-m of horizontal run.

Only infraction codes were provided in the investigation report without site-specific details. The employer was fined $4,800 for their negligence.

2.2 Trench Failure Mechanisms

Changes in pore-water pressure (hereafter referred to as PWP), surface loading, and vibration are the most predominant causes of trench instability (Ontario 2017). Figure 2.1 illustrates the causes of trench failure.

The base and walls of a trench experience elastic rebound immediately after excavating due to the relief of confining pressures. This causes an increase in the soil's void space and a decrease in PWP, thus increasing the soil's shear strength. Hence, a trench may appear stable immediately after excavating. However, the trench destabilizes over time as PWP rises back to equilibrium within the soil nearby the trench base and walls. Rainfall infiltration, development of cracks, and a rising GWT can further increase PWP and accelerate a trench failure. Thus, the risk of trench collapse increases as exposure time to the atmosphere increases. Trenches should be backfilled as soon as the job is complete.

Many forms of static and dynamic loading can cause a trench to collapse. Surcharge loads from excavated material and construction equipment, and vibration induced by vehicular traffic, compaction, pile driving, blasting, other adjacent excavations, etc. may trigger a collapse. Trenches excavated near existing foundations may collapse if the bearing pressure enters the active zone of the trench (Figure 2.2).

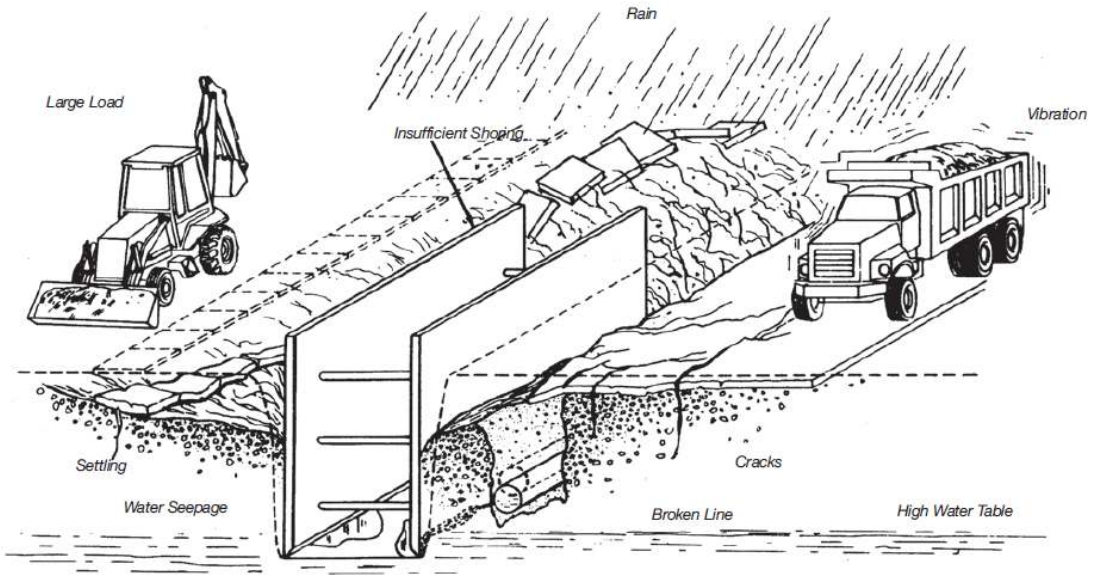

Figure 2.1. Factors affecting trench stability (Ontario 2017)

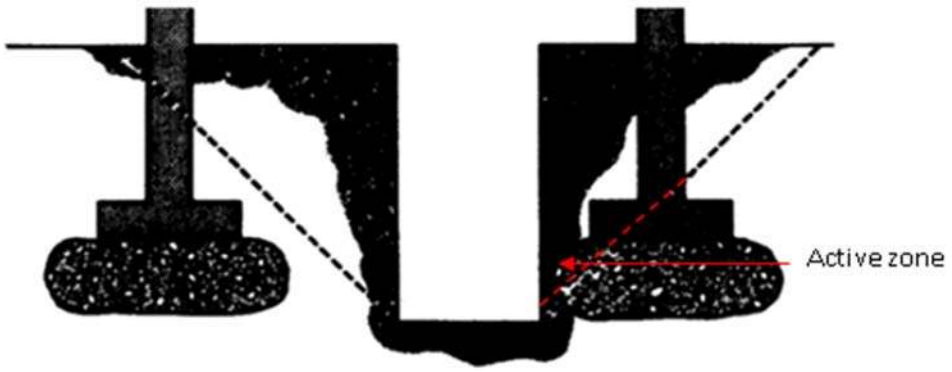

Figure 2.2. Excavation adjacent to existing foundations (Ontario 2017)

The presence of buried utilities adjacent to an open excavation can result in an unexpected failure because the backfill materials encasing the utility are typically weaker than undisturbed native soil (Figure 2.3). This type of failure mechanism not only endangers workers, but may also result in excessive strain causing structural damage to the utilities

(Symons et al. 1982). Shoring is typically required when excavating near buried utilities or foundation structures to ensure ground movement is minimized.

Figure 2.3. Trench parallel with backfill material (Ontario 2017)

Heterogeneity should also be monitored when excavating, especially over long distances. Some soils such as gravel deposits may have a high variance with respect to local mechanical properties (Krahn & Fredlund 1983, Dai et al. 2016). Thus, the critical height may vary significantly between locations in the same soil deposit. In such cases, it may be necessary to perform a probabilistic analysis to determine minimum values for the soil properties of interest to quantify a critical height.

2.3 Trench Failure Modes

The Occupational Health & Safety Division of Alberta (2009) described how rescue attempts may be more difficult and dangerous when the wall failure occurs sequentially as shown in Figure 2.4. In this case, failure is initiated at the base of the trench wall. Cracking near the ground surface and local failures in Zone 1 should raise alarms. This localized failure or movement leads to failure in Zone 2. Finally, the failure in Zone 3 occurs due to the self-weight of the soil. This failure sequence is a plausible explanation for why rescuers

are sometimes trapped along with the first victim(s). Someone attempting to intervene and help uncover a victim when failure in Zone 3 has not yet occurred can put themselves at risk.

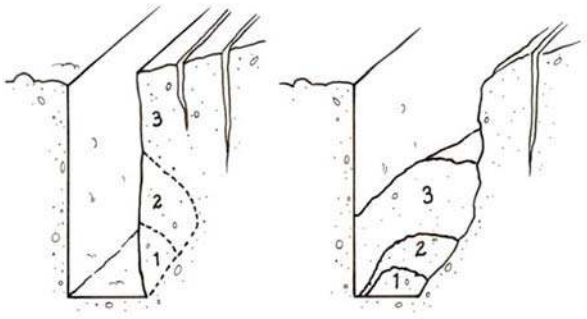

Figure 2.4. Sequential trench failure (Alberta 2009)

The Workplace Safety & Health Division of Manitoba (2011) categorizes the modes of trench collapse into four types (Figure 2.5).

(a) Spoil pile slide - occurs when the excavated material is not placed far enough away from the edge of the excavation. A minimum distance of 0.6-m is recommended for every one-metre of excavation depth.

(b) Side wall shear - common to fissured or desiccated clay-type or alluvial soils that are exposed to drying.

(c) Slough-in (cave-in) - common to previously excavated material, fill, and granular soils where the water table is above the base of the excavation, or where soils are organic or peat.

(d) Rotation - common in clay-type soils when excavation walls are too steep, or when moisture content increases rapidly.

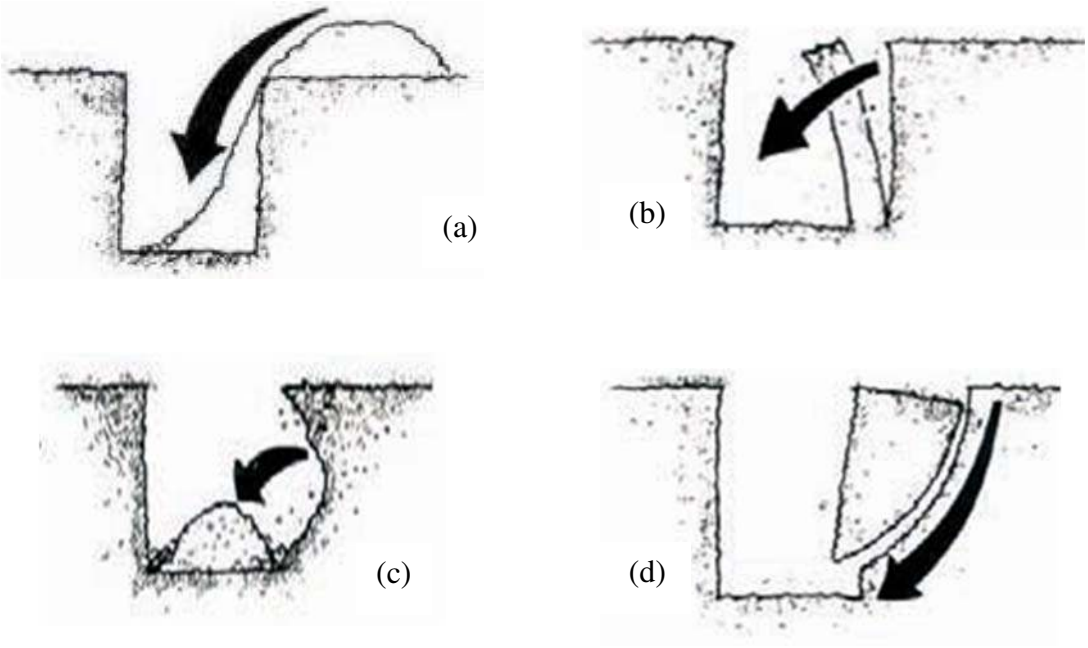

Figure 2.5. Trench failure modes (Manitoba 2011)

2.4 Work Protection Methods

At least one of benching, sloping, shoring, or worker-protective trench boxes must be implemented in the trenching process when it is necessary to excavate deeper than the regulated safe height. The preferred safety measure depends on the application and the soil properties. Protection methods have been devised based on four soil types (Figure 2.6; Ontario 2017):

(a) ***Type 1*** - includes hardpan, consolidated clay, and some glacial tills. It is hard to drive a pick into Type 1 soil. The sides remain vertical with no water released from the trench wall during excavation. Rain may cause soil to break down along the edges of the excavation.

(b) ***Type 2*** - Includes silty clay and less dense tills. It is relatively easy to drive a pick into Type 2 soil and can be easily excavated with a backhoe. The sides will remain vertical for short periods of time before tension cracks appear as the soil starts to dry.

(c) ***Type 3*** - Includes sand, granular materials, silty or wet clays, and all backfill or previously disturbed material. Type 3 soil can be excavated without difficulty using a backhoe and will not stand vertically when dry. Soil will stand vertically for short periods of time when wet, however it dries quickly and is prone to deterioration by vibration from heavy equipment.

(d) ***Type 4*** - Includes quicksand, Leta clays, silty clays, muskeg, or other organic deposits with high moisture content. Type 4 soil is flowable material that can be excavated with no difficulty and must be supported or contained to excavate to any significant depth.

Regardless of the material, the spoil pile should be placed further away from the edge of excavation as depth increases (Figure 2.7; Ontario 2017). It is necessary to slope the trench walls 1:1 once the excavation extends deeper than the safe height in Type 1 and 2 soils. Type 3 and 4 soils warrant 1:1 and 1V:3H slopes from the base of the excavation, respectively (Figure 2.6). The main restriction with sloping is the space allotted to achieve an adequate slope, and therefore other reinforcement may be required in certain practical scenarios. Figure 2.8 illustrates the case of using shoring in conjunction with sloping.

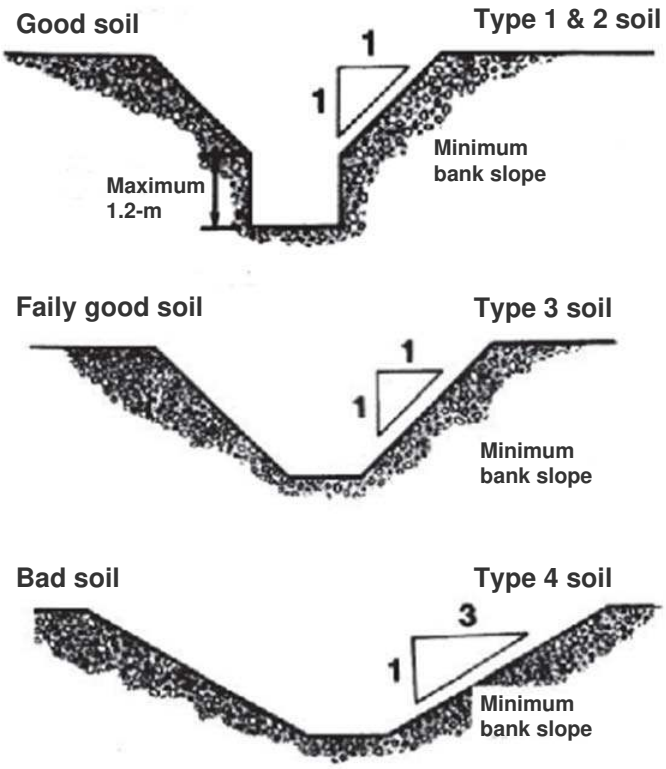

Figure 2.6. Sloping standards (Ontario 2017)

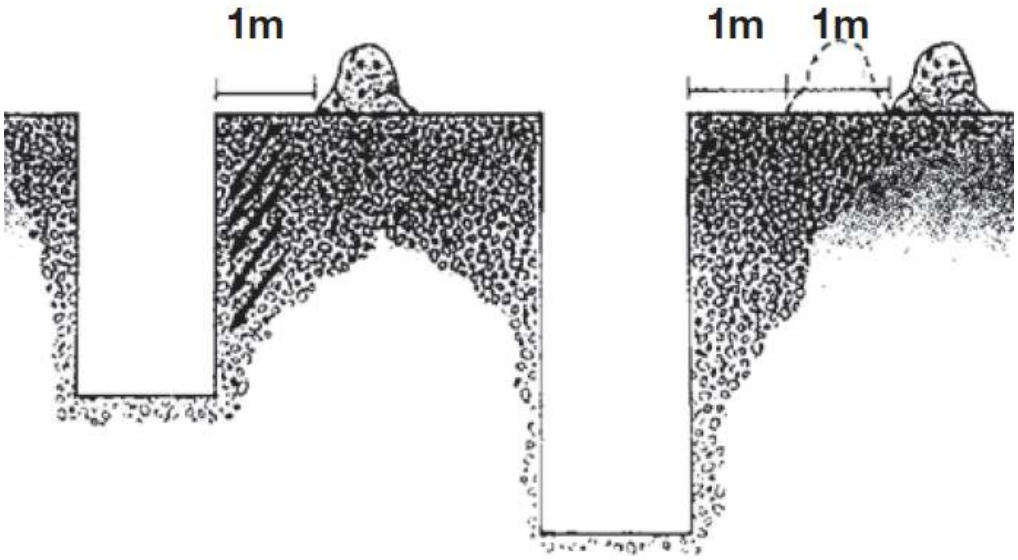

Figure 2.7. Placement of spoil pile (Ontario 2017)

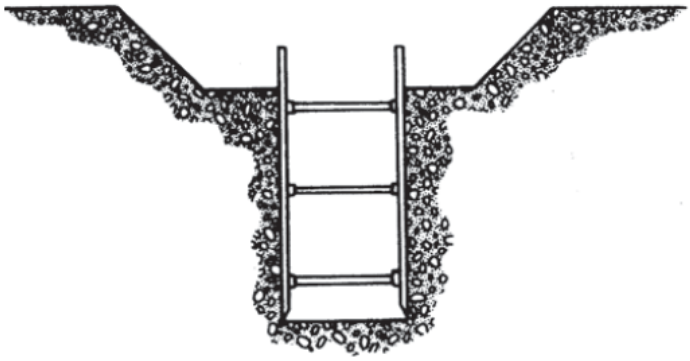

Figure 2.8. Shored trench with partially sloped walls (Ontario 2017)

Shoring involves supporting trench walls with a braced structure as shown in Figure 2.9. Shoring systems are used to transfer and resist the loads acting on opposing sides of the trench. Hydraulic shoring is more frequently used in practice than timber shoring (Hinze 2005). Hydraulic shores are prefabricated sections in which the width can be adjusted with a pneumatic device, making them much more practical than timber shores that must be cut to the exact width of the excavation. Trench boxes are different from shores as they do not provide structural support to trenches unless the void space between the box and the walls are backfilled; their sole purpose is to prevent soil from collapsing onto the workers. For this reason, trench boxes should always be accessed by a ladder which rests inside the box. The space between the box and the wall should be minimized to provide easier access to the ladder from the edge of the excavation, and to limit soil movement in the event of a collapse. It is often necessary to use shoring rather than trench boxes while working in the proximity of infrastructure such as buried utilities, roads with nearby traffic, or buildings.

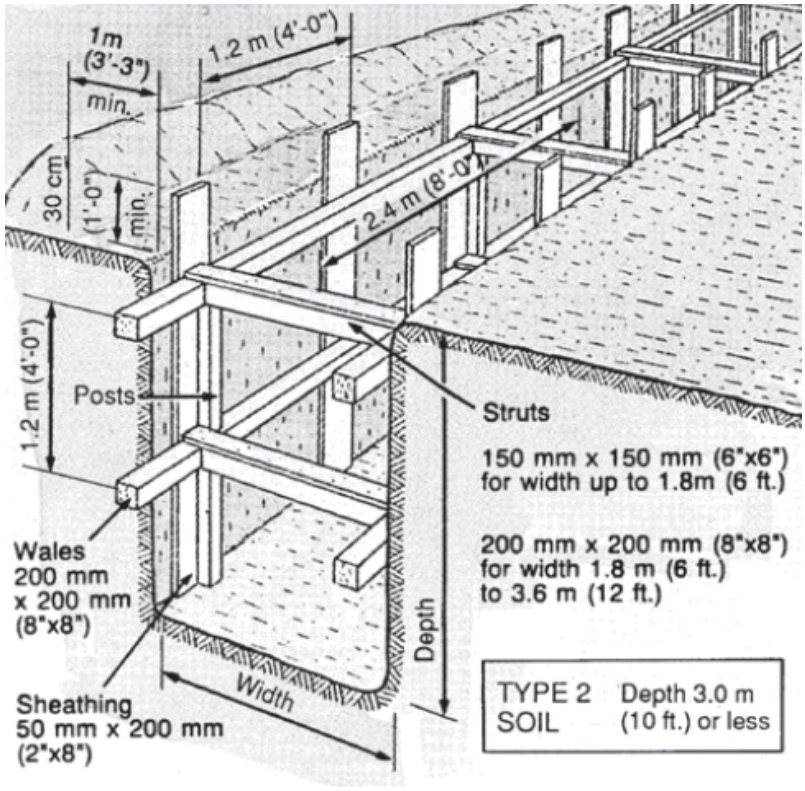

Figure 2.9. Typical shored trench (Ontario 2017)

2.5 Trench Economics

Unsupported trenches require the least amount of excavation work and are therefore the most desirable form of trenches from an economical perspective. Benching and sloping require more time for excavating since more soil is removed per linear distance, yet the installation process may be unimpeded if the infrastructure cannot be installed as fast as the trench is being excavated. However, production is inevitably slowed when using shoring or trench boxes. An anonymous construction company was capable of setting 6 to 8 (0.6-m diameter, 6-m long) pipes per day when working in and around a trench box, compared to 12 to 15 per day when working without one. Inconsistencies in day-to-day operations were mostly attributed to human resources, and trench dewatering associated

with groundwater seepage or rainfall. The opportunity cost of employing an entire pipe-laying crew with heavy equipment for a 12-hour day is approximately $10,000. A total cost breakdown is shown below in Table 2.2. Other costs that are not listed in Table 2.2 include the cost of quality control inspectors, surveyors, and rental equipment. Over an entire construction season on a large-scale project, hundreds of thousands of dollars could be saved if working without a trench box or shoring could be justified.

Table 2.2. Total cost breakdown for pipe-laying crew (Gulf Operators 2018)

Equipment	**Cost per hour ($CAD/hr)**	**Quantity**	**Cost per 12-hour day ($CAD/day)**
Cat 345 Excavator	215.00	1	2,580.00
Cat 336 Excavator	190.00	1	2,280.00
Cat D-4 Dozer	95.00	1	1,140.00
Compactor	85.00	1	1,020.00
Labour	37.00	4	1,776.00
Lead Hand	41.00	1	492.00
Supervisor	68.00	1	816.00
	Total cost per day		10,104.00

CHAPTER 3

THEORETICAL BACKGROUND

3.1 Properties of Unsaturated Soil

Unsaturated soil consists of soil particles, water, and air (i.e. solid, liquid, and gas phases). The three phases interact to create the contractile skin (or air-water interface), which is referred to as the fourth phase. As shown in Figure 3.1(a), a molecule of water within a body experiences equal forces in all directions, while a molecule along the air-water interface experiences an unbalanced force towards the interior of the water body. Thus, a tensile force is generated tangentially to the air-water interface to satisfy static equilibrium. Surface tension causes the contractile skin to behave like an elastic membrane; somewhat like an inflated balloon that has a greater air pressure inside than in the atmosphere. The membrane forms a concave curvature towards the larger pressure (Figure 3.1(b)). The radius of curvature is directly related to the pressure difference as shown in Eq. (3.1). The tensile force is temperature dependant. In an unsaturated soil, the air pressure (u_a = 0-gauge pressure) becomes greater than the water pressure (u_w = negative gauge pressure) which creates a contractile skin. The pressure difference between u_a and u_w is referred to as matric suction (Eq. (3.2)).

$$\Delta u = \frac{2T_s}{R_s} \tag{3.1}$$

$$\left(u_a - u_w\right) = \frac{2T_s}{R_s} \tag{3.2}$$

where Δu = pressure difference, T_s = tensile force per unit length, R_s = radius of curvature, and (u_a – u_w) = matric suction

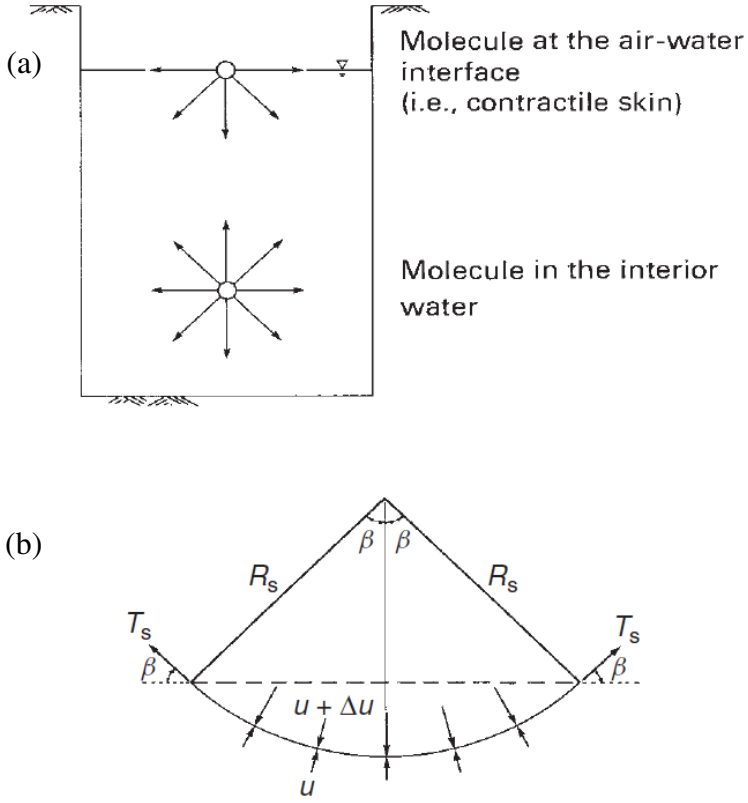

Figure 3.1. Surface tension phenomenon at air-water interface; (a) intermolecular forces acting on contractile skin and (b) surface tension forces associated with curved 2D surface (Fredlund et al. 2012)

Eq. (3.1) shows that matric suction approaches infinity as the radius of curvature approaches zero, indicating that smaller radii can exert greater matric suction than larger radii. In terms of the radii within the void space of an unsaturated soil, fine-grained soils with small pore-sizes have a higher affinity for matric suction than coarse-grained soils

with relatively large pores. In other words, the ability for a soil to retain water is strongly related to the pore-size (or particle-size) distribution.

The soil-water characteristic curve (hereafter referred to as SWCC) is a soil specific relationship between matric suction and the degree of saturation (or volumetric water content). A typical SWCC can be divided into three main zones; boundary effect zone, transition zone, and residual zone (Figure 3.2).

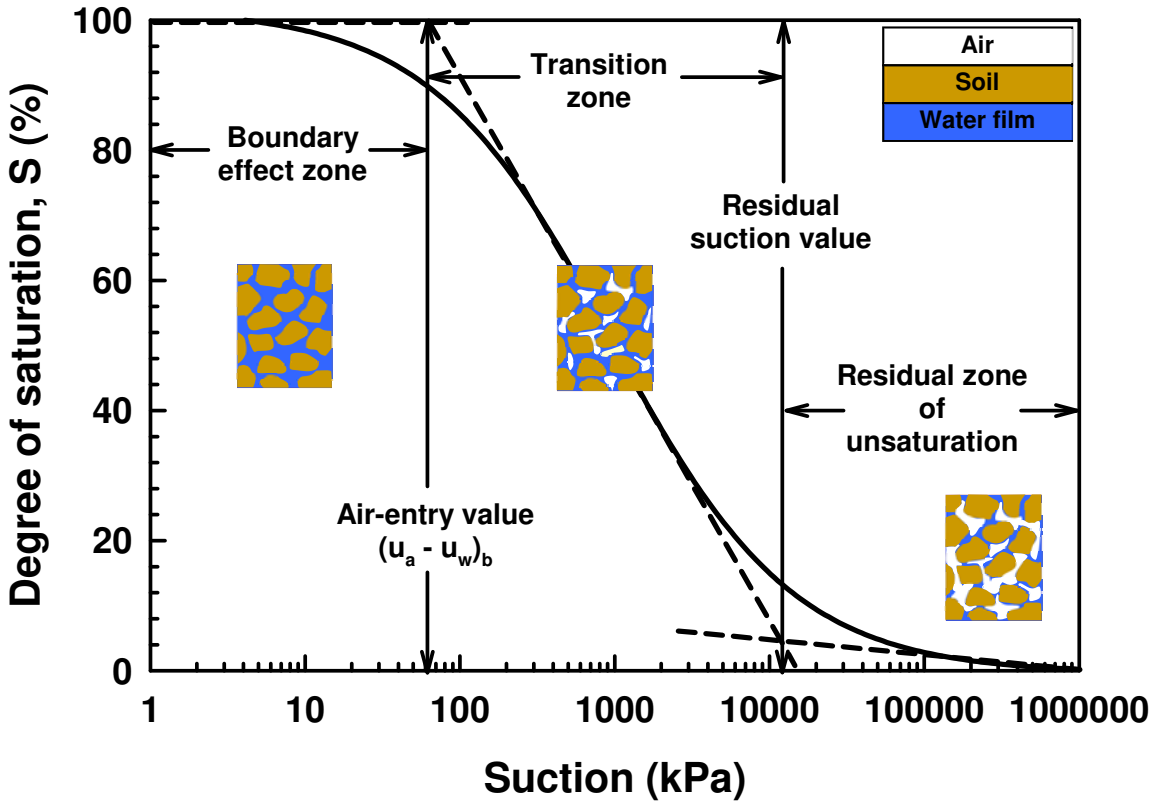

Figure 3.2. Typical SWCC showing different zones of desaturation (Nishimura et al. 2008)

The boundary effect zone ranges from zero matric suction (i.e. saturation) up to the air-entry value (hereafter referred to as AEV). The AEV is the suction required to force air into the largest voids in a soil and is the first point of importance on a SWCC for a drying

cycle. Soil begins desaturating once matric suction is increased past the AEV. Most desaturation occurs in the transition zone. The degree of saturation (or water content) is reduced significantly with relatively small increases in matric suction. In the residual zone, large increases in suction result in small changes in the degree of saturation.

Figure 3.3 demonstrates possible PWP profiles with respect to depth above and below the GWT. In the saturated zone, the pore-water is in compression (i.e. zero matric suction) and the magnitude of pressure increases linearly with depth. In the unsaturated zone (or vadose zone), the pore-water is in tension and the soil is subjected to a matric suction distribution that can vary linearly or nonlinearly above the GWT (Fredlund & Rahardjo 1993a). Ideal hydrostatic conditions (i.e. linear matric suction distribution; ① in Figure 3.3) often do not represent true field conditions due to environmental factors such as evaporation (② in Figure 3.3) and rainfall infiltration (③ in Figure 3.3).

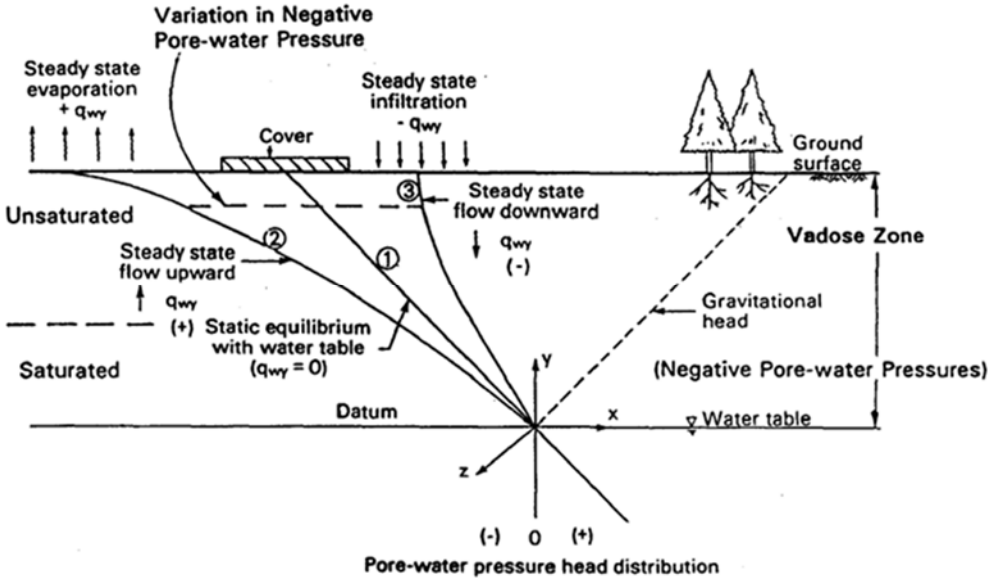

Figure 3.3. Pore-water profiles in the vadose zone (Fredlund & Rahardjo 1993a)

Soils in nature experience cycles of wetting and drying (i.e. rainfall infiltration and evaporation), which alter the SWCC of the soil accordingly. Increasing or decreasing a soil's moisture content by the same volume of water does not cause the same change in suction. This phenomenon is known as hysteresis. The first drying (desorption curve) and wetting (adsorption curve) cycle form the two boundaries for the possible SWCCs that a soil can experience (Figure 3.4). Larger pores drain first due to better interconnectivity, while smaller pores are more reluctant to release water when drying since there is more surface contact between the available water and the soil grains. Conversely, larger pores are filled last during wetting because smaller pores absorb water more easily due to a higher affinity for matric suction. Thus, the drying SWCC always corresponds to higher suction than the wetting SWCC for a given moisture content (Yang et al. 2004, Goh et al. 2014). It is therefore more conservative to analyze the mechanical behaviours of unsaturated soils using a wetting-cycle SWCC.

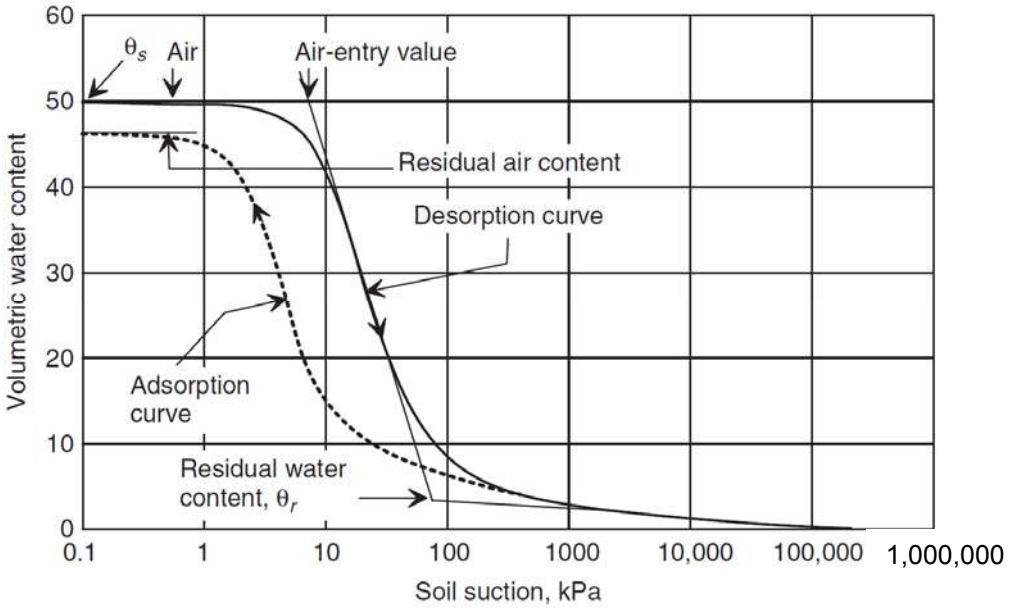

Figure 3.4. Typical SWCC for silt soil (Fredlund et al. 2012)

3.2 Shear Strength of Unsaturated Soil

The effective stress equation proposed by Terzaghi (1936) laid a foundation towards establishing geotechnical engineering as one of the independent fields of civil engineering (Vanapalli 2009). Effective stress is the difference between total stress and PWP (Eq. (3.3)). In conjunction with Mohr-Coulomb theory, effective stress can be used to interpret the shear strength of saturated soils (Eq. (3.4)).

$$\sigma' = \sigma - u_w \tag{3.3}$$

$$\tau_{sat} = c' + \sigma' \tan \phi' \tag{3.4}$$

where σ' = effective stress, σ = total stress, u_w = pore-water pressure, τ_{sat} = shear strength of saturated soil, c' = effective cohesion, and ϕ' = effective internal friction angle

Most soils, especially in arid or semi-arid regions, exist in unsaturated conditions. In this case, the influence of matric suction should be considered to reliably estimate the shear strength of unsaturated soil. Bishop (1959) was one of the first researchers to recognize that suction contributes to the strength of unsaturated soil and proposed Eq. (3.5) by extending Terzaghi's equation for effective stress (i.e. Eq. (3.3)).

$$\sigma' = \sigma - u_a + \chi\left(u_a - u_w\right) \tag{3.5}$$

where u_a = pore-air pressure, $(\sigma - u_a)$ = net normal stress, and χ = a soil parameter related to degree of saturation (or matric suction) ranging from 0 to 1

The effective stress parameter, χ, is equal to zero for dry soil. When the soil is saturated, χ is equal to one and Eq. (3.5) becomes equal to Eq. (3.3). Jennings & Burland (1962) and Bishop & Blight (1963) pointed out that there are limitations to Eq. (3.5) since different χ values are required to explain shear strength and volume change behaviour of unsaturated soils. In other words, Eq. (3.5) cannot universally describe the mechanical behaviours of unsaturated soil. The parameter, χ, can be evaluated using Eq. (3.6) to determine the shear strength of unsaturated soils depending on the range of matric suction values (Khalili & Khabbaz 1998).

$$\begin{cases} \chi = \dfrac{(u_a - u_w)}{(u_a - u_w)_b} & \text{if } (u_a - u_w) > (u_a - u_w)_b \\ \chi = 1 & \text{if } (u_a - u_w) \le (u_a - u_w)_b \end{cases} \tag{3.6}$$

where $(u_a - u_w)_b$ = air-entry value of a soil

Fredlund & Morgenstern (1977) concluded that net normal stress and matric suction are the two independent stress-state variables that are to be used for evaluating the mechanical behaviour of unsaturated soil. Fredlund et al. (1978) proposed Eq. (3.7) to estimate the shear strength of unsaturated soil based on the extended Mohr-Coulomb failure envelope (Figure 3.5).

$$\tau_{unsat} = c' + (\sigma - u_a)\tan\phi' + (u_a - u_w)\tan\phi^b \tag{3.7}$$

where τ_{unsat} = shear strength of unsaturated soil ϕ^b = angle indicating the rate of increase in shear strength with respect to a change in matric suction

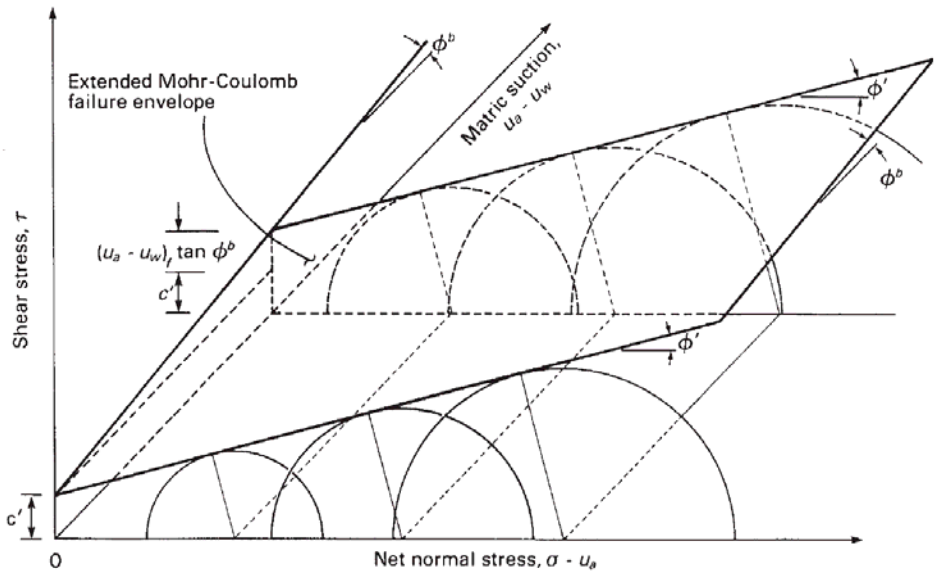

Figure 3.5. Extended Mohr-Coulomb failure envelope for unsaturated soil (Fredlund & Rahardjo 1993b)

However, determining ϕ^b is time-consuming and requires elaborate testing equipment. Previous research also showed that ϕ^b is not a constant, but varies nonlinearly with respect to matric suction (Escario & Saez 1987, Gan et al. 1988). For matric suction values less than the AEV, $\phi^b = \phi'$, and ϕ^b becomes less than ϕ' once matric suction exceeds the AEV (i.e. $\phi^b < \phi'$). It is interesting to note that shear strength approaches that of saturated condition for suction values greater than residual suction in coarse-grained soils (Figure 3.6). This is attributed to a decrease in the net contribution of matric suction towards shear strength as the residual condition is approached. The contractile skin becomes discontinuous in the residual stage and becomes incapable of maintaining peak strength.

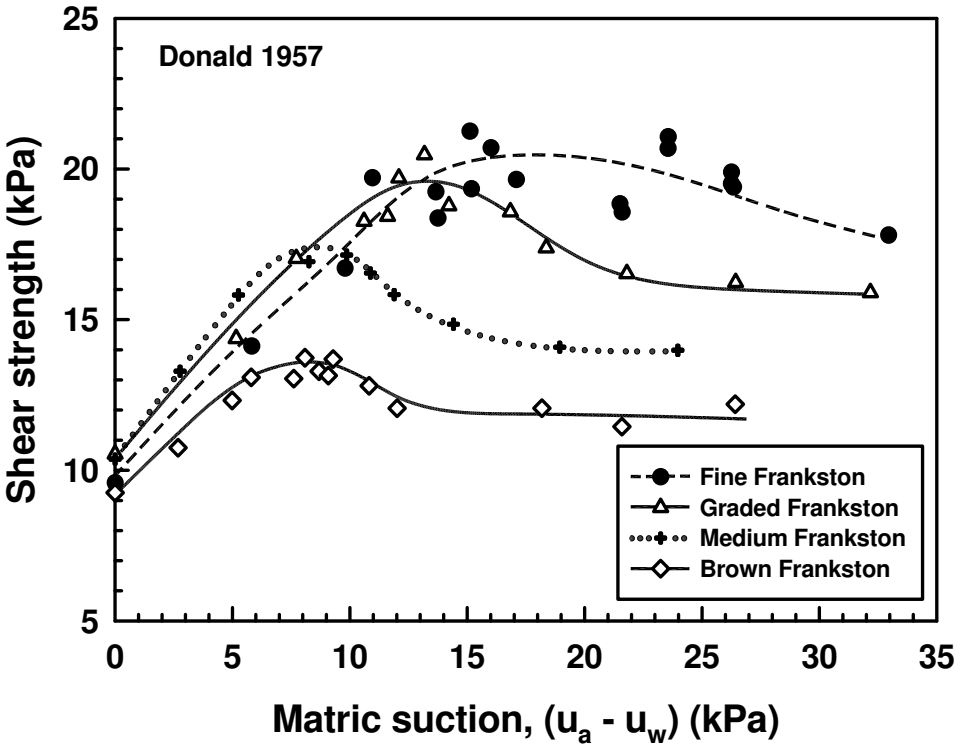

Figure 3.6. Variation of shear strength with respect to suction for four sands (modified after Donald 1957)

Vanapalli et al. (1996) proposed equations to estimate the variation of ϕ^b with respect to suction in terms of volumetric water content/degree of saturation as shown in Eq. (3.8) and (3.9), respectively.

$$\tan\phi^b = \left(\frac{\theta - \theta_r}{\theta_s - \theta_r}\right)\tan\phi' \tag{3.8}$$

$$\tan\phi^b = \left(\frac{S - S_r}{100 - S_r}\right)\tan\phi' \tag{3.9}$$

where S = degree of saturation, θ = volumetric water content, subscript s = saturated condition, and subscript r = residual condition

The SWCC for the entire range of suction is required to accurately identify the volumetric water content or degree of saturation for a soil's residual condition. Vanapalli et al. (1996) proposed another equation that requires the degree of saturation (or volumetric water content) along with a fitting parameter.

$$\tan \phi^b = \left(\Theta^\kappa\right) \tan \phi' = \left(S^\kappa\right) \tan \phi' \tag{3.10}$$

where Θ = normalized volumetric water content (= θ/θ_s) and κ = fitting parameter for the shear strength of an unsaturated soil

Vanapalli & Fredlund (2000) provided a relationship between the fitting parameter, κ, and the plasticity index, I_p, as shown in Eq. (3.11) using five data sets of shear strength of unsaturated soils. Garven & Vanapalli (2006) further improved Eq. (3.11) by using ten data sets of shear strength for compacted soils (Eq. (3.12) and Figure 3.7). Eq. (3.11) and (3.12) show that κ = 1 for estimating the variation of shear strength of unsaturated non-plastic soils with respect to matric suction.

$$\kappa = -0.0008(I_p^2) + 0.0801(I_p) + 1 \tag{3.11}$$

$$\kappa = -0.0016(I_p^2) + 0.0975(I_p) + 1 \tag{3.12}$$

where I_p = plasticity index

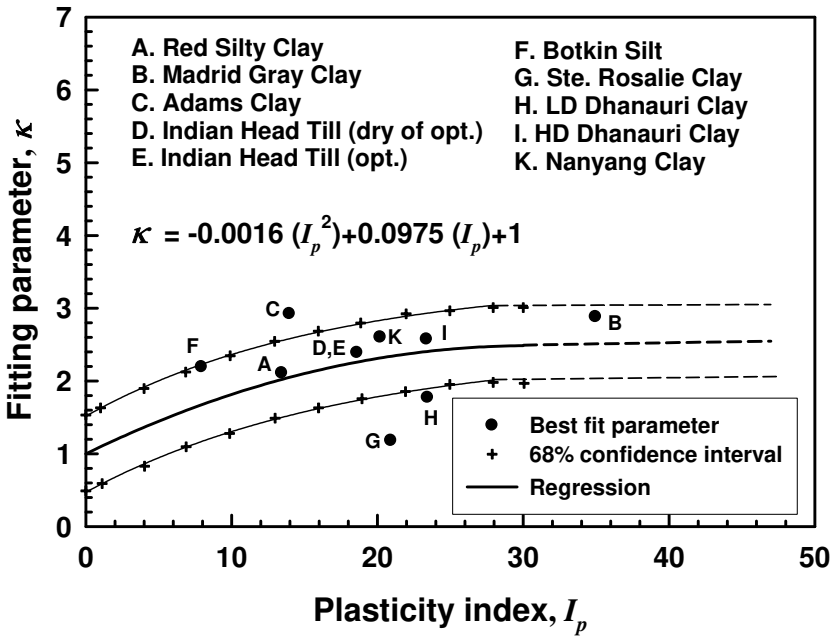

Figure 3.7. Relationship between κ and I_p (Garven & Vanapalli 2006)

Total cohesion is the sum of effective and apparent cohesion as shown in Eq. (3.13).

$$C = c' + \left(u_a - u_w\right)\tan\phi^b \tag{3.13}$$

where C = total cohesion c' = effective cohesion, and $(u_a - u_w)\tan\phi^b$ = apparent cohesion

Substituting Eq. (3.10) into Eq. (3.13), and then into Eq. (3.7) yields Eq. (3.14).

$$\begin{aligned}
\tau_{unsat} &= c' + \left(\sigma - u_a\right)\tan\phi' + \left(u_a - u_w\right)\tan\phi^b \\
&= c' + \left(\sigma - u_a\right)\tan\phi' + \left(u_a - u_w\right)\left(S^\kappa\right)\tan\phi' \\
&= \left[c' + \left(u_a - u_w\right)\left(S^\kappa\right)\tan\phi'\right] + \left(\sigma - u_a\right)\tan\phi' \\
&= \left[c' + \left(u_a - u_w\right)\left(\Theta^\kappa\right)\tan\phi'\right] + \left(\sigma - u_a\right)\tan\phi' \\
&= C + \left(\sigma - u_a\right)\tan\phi'
\end{aligned} \tag{3.14}$$

3.3 Critical Height of Unsupported Vertical Trenches

3.3.1 Rankine's Earth Pressure Theory (1857)

Rankine (1857) investigated the stress conditions of a soil in a state of plastic equilibrium. Bowles (2001) summarized the major assumptions made in Rankine's theory as listed below:

(a) Soil is isotropic and homogeneous and has internal friction but no cohesion.

(b) The rupture surface (AC in Figure 3.8) is a plane surface and the backfill surface (BC in Figure 3.8) is planar (it may slope but is not irregularly shaped).

(c) The frictional resistance is distributed uniformly along the rupture surface and the soil-to-soil friction coefficient, $f = \tan\phi$.

(d) The failure wedge (ABC in Figure 3.8) is a rigid body undergoing translation.

(e) There is no wall friction.

(f) Failure is a plane strain problem - that is, consider a unit interior slice from an infinitely long wall.

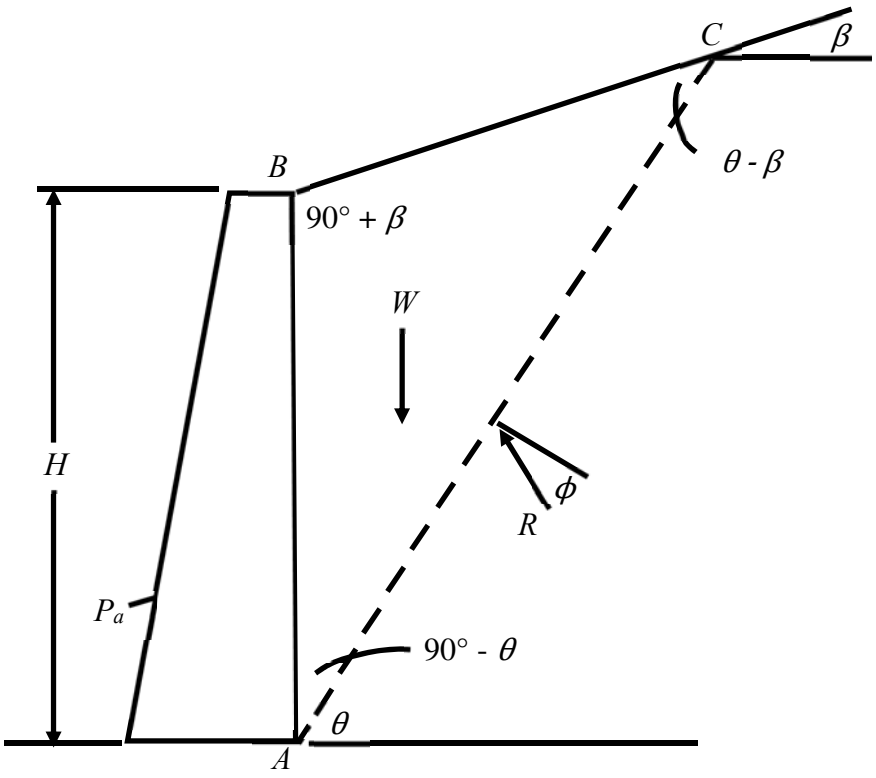

Figure 3.8. Soil structure system for the Rankine solution for $\alpha = 90°$ (modified after Bowles 2001)

Plastic equilibrium is achieved if a wall moves sufficiently far away from a soil mass, in which the effective lateral earth pressure acting on the vertical plane is denoted as Rankine's active earth pressure (hereafter referred to as AEP). For the case shown in Figure 3.9, AEP can be calculated using Eq. (3.15) assuming the soil's unit weight is constant.

$$p_a = \gamma z \cos\beta K_a' = \gamma z K_a$$
$$K_a = \cos\beta \frac{\cos\beta - \sqrt{\cos^2\beta - \cos^2\phi}}{\cos\beta + \sqrt{\cos^2\beta - \cos^2\phi}} \tag{3.15}$$

where p_a = active earth pressure, γ = unit weight of soil, z = depth, β = angle of backfill, and K_a = active earth pressure coefficient

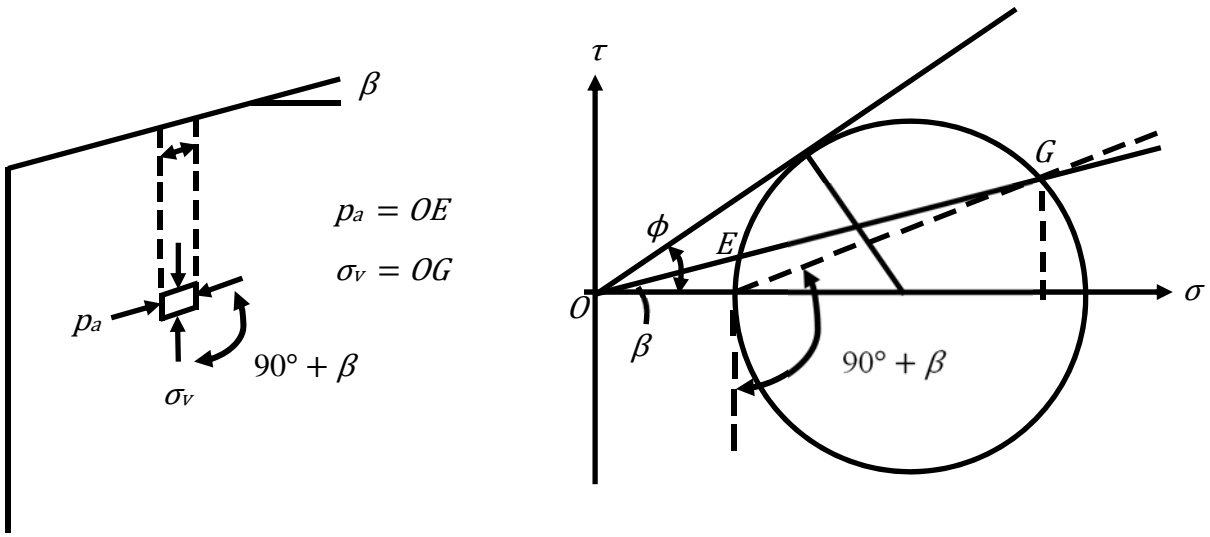

(a) General case: only for +β as shown (b) Mohr's circle

Figure 3.9. General conditions of Mohr's circle to derive the Rankine earth pressure equations (modified after Bowles 2001)

When the backfill surface is horizontal, the AEP coefficient can be calculated with Eq. (3.16).

$$K_a = \frac{1-\sin\phi}{1+\sin\phi} \tag{3.16}$$

Rankine did not incorporate soil cohesion in estimating AEP. This issue is resolved by combining Eq. (3.17) with Rankine's theory as shown in Eq. (3.18).

$$\sigma_3' = \sigma_1' \tan^2\left(45° - \frac{\phi'}{2}\right) - 2c' \tan\left(45° - \frac{\phi'}{2}\right) \tag{3.17}$$

$$p_a = \gamma z K_a - 2c'\sqrt{K_a} \tag{3.18}$$

where σ_3' = minor principal stress, σ_1' = major principal stress

The lateral earth pressure (positive, negative, and net) distribution in a saturated cohesive soil is shown in Figure 3.10. From the ground surface to a depth of zero net AEP is referred to as the tension zone. The depth of the tension zone can be calculated using Eq. (3.19). Theoretically, by setting the sum of horizontal forces equal to zero, a vertical trench can be excavated up to twice the depth of the tension zone without failure if effective cohesion and the unit weight are constant. In which case, the critical height of an unsupported vertical trench is calculated using Eq. (3.20).

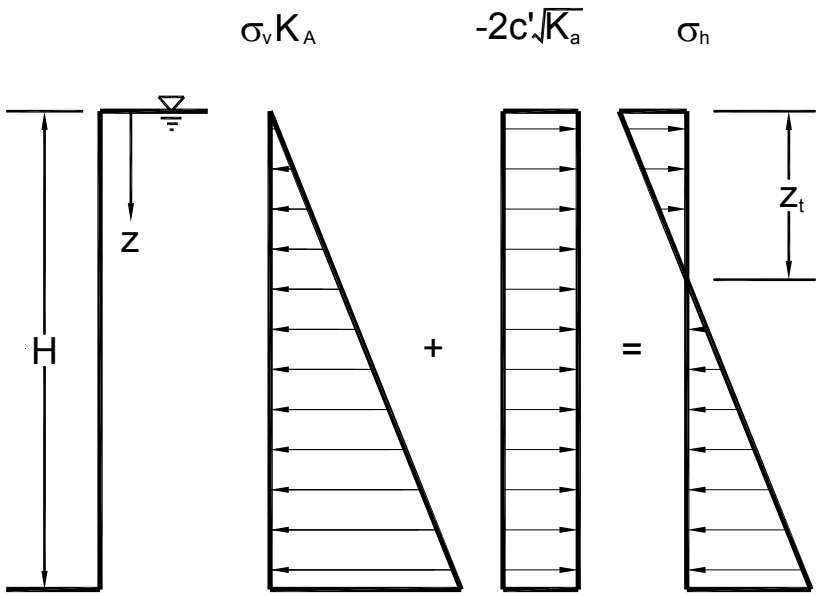

Figure 3.10. AEP and critical height in saturated soil (modified after Pufahl et al. 1983)

$$Z_t = \frac{2c'}{\gamma\sqrt{K_a}} \tag{3.19}$$

$$H_{cr} = 2Z_t = \frac{4c'}{\gamma\sqrt{K_a}} \tag{3.20}$$

Where H_{cr} = critical height, Z_t = depth of tension zone

By assuming a planar rupture surface and a horizontal backfill surface, the AEP in an unsupported trench in unsaturated soil can be interpreted by extending Rankine's earth pressure theory.

3.3.2 Pufahl et al. (1983)

Pufahl et al. (1983) investigated lateral earth pressure (i.e. active and passive pressures) for a vertical trench extending the mechanics of unsaturated soil. Conventional Rankine earth pressure theory for saturated soil was modified to incorporate the influence of matric suction using the Mohr-Coulomb failure criteria (i.e. extended Rankine earth pressure theory). The lateral earth pressures (i.e. active and passive) for both saturated and unsaturated conditions are illustrated in Figure 3.11.

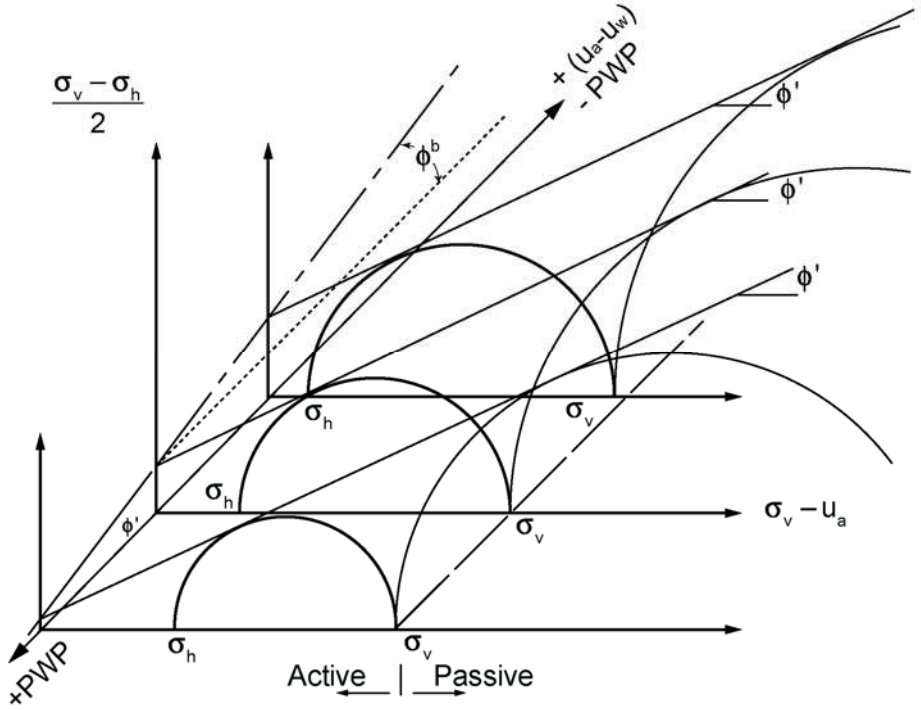

Figure 3.11. Lateral earth pressure states for saturated and unsaturated conditions (Pufahl et al. 1983)

The AEP decreases as a soil desaturates due to increasing contribution from matric suction. From the geometrics of the Mohr circle in Figure 3.11, the net AEP can be written as Eq. (3.21) by replacing effective cohesion in Eq. (3.18) with total cohesion (Eq. (3.13)) to incorporate the influence of matric suction.

$$\left(\sigma_h - u_a\right) = \left(\sigma_v - u_a\right) K_a - 2\left[c' + \left(u_a - u_w\right)\tan\phi^b\right]\sqrt{K_a} \tag{3.21}$$

where ($\sigma_h - u_a$) = net lateral pressure, and ($\sigma_v - u_a$) = net overburden pressure

If the pore-air pressure (hereafter referred to as PAP) is assumed to be atmospheric pressure (i.e. $u_a = 0$), the AEP in an unsaturated soil can be calculated using Eq. (3.22).

$$p_a = \sigma_v K_a - 2\left[c' + \left(u_a - u_w\right)\tan\phi^b\right]\sqrt{K_a} \tag{3.22}$$

Substituting Eq. (3.10) into Eq. (3.22) yields Eq. (3.23).

$$\begin{aligned} p_a &= \sigma_v K_a - 2\left[c' + \left(u_a - u_w\right)\tan\phi^b\right]\sqrt{K_a} \\ &= \sigma_v K_a - 2\left[c' + \left(u_a - u_w\right)\left(S^\kappa\right)\tan\phi'\right]\sqrt{K_a} \\ &= \sigma_v K_a - 2C\sqrt{K_a} \end{aligned} \tag{3.23}$$

Typically, matric suction varies nonlinearly with depth. In other words, the critical height in unsaturated soils may not be simply two times the depth of the tension zone. In this case, the critical height can be estimated by locating the depth that equates ‘Area I’ and ‘Area II’ as shown in Figure 3.12.

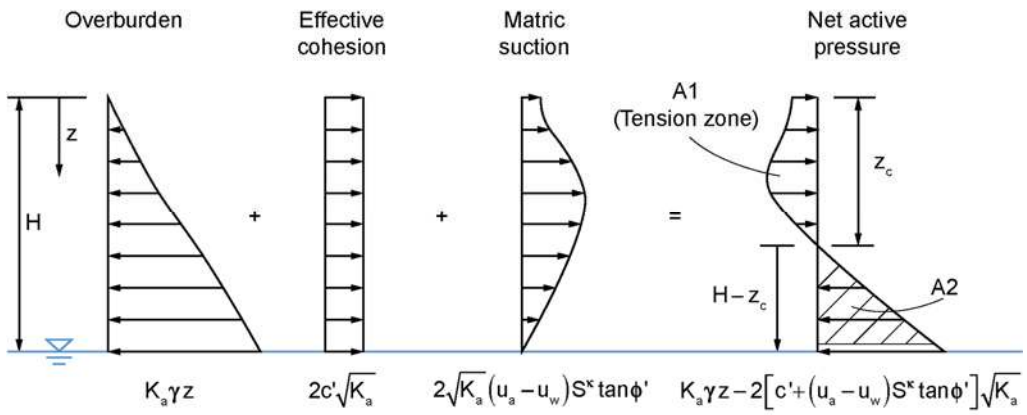

Figure 3.12. Components of AEP distribution and critical height in unsaturated soil

By assuming a planar failure surface, the critical height in unsaturated soil can also be determined by considering a balance of forces on the sliding wedge shown in Figure 3.13. Trial and error must be used to solve for H_{cr} since it appears on both sides of Eq. (3.24).

$$H_{cr} = \frac{\dfrac{4}{\sqrt{K_a}}\left(c' + \dfrac{m_{cr}}{2}(u_a - u_w)\tan\phi^b\right)}{\left(1-{m_{cr}}^2\right)\left(\gamma_{sat} + \dfrac{2\gamma_w \tan\phi'}{\sqrt{K_a}}\right) + m_{cr}\left(2-m_{cr}\right)\gamma_{unsat}} \tag{3.24}$$

where $m_{cr} = D/H_{cr}$, D = depth of the GWT from the soil surface, γ_w = unit weight of water, and γ_{sat}, γ_{unsat} = unit weight of soil for saturated and unsaturated condition, respectively

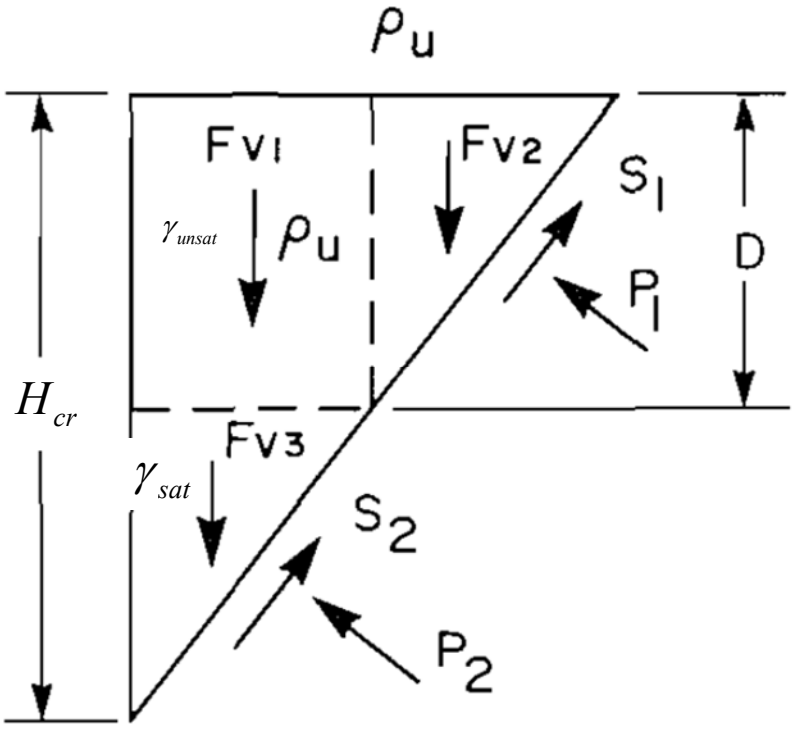

Figure 3.13. Unsupported vertical trench (unsaturated, intact, modified after Pufahl et al. 1983)

3.3.3 Vanapalli & Oh (2012)

Vanapalli & Oh (2012) extended the work by Pufahl et al. (1983) to analyze the stability of an unsupported vertical trench in an unsaturated soil. The excavation dimensions were 3-m deep, 6-m wide, and 20-m long. The variation of matric suction with depth was measured using tensiometers installed at depths of 1, 1.5, 2.5, and 3.5-m from the ground surface (Whenham et al. 2007). The trench was first excavated in June 2004. The first localized and generalized failures were observed in January 2005 and February 2005, respectively, due to a decrease in matric suction associated with precipitation activity (Figure 3.14).

Figure 3.14. Field tests on the stability of an unsupported excavation in an unsaturated soil (modified after Whenham et al. 2007)

Two different approaches were used to calculate AEP; the Modified Effective Stress Approach (hereafter referred to as MESA; Eq. (3.22)) and the Modified Total Stress Approach (hereafter referred to as MTSA; Eq. (3.25)). The MTSA implies that excess PAP is assumed to drain and the excess PWP is an undrained condition. Therefore, AEP is estimated by replacing total cohesion, C, in Eq. (3.22) with total cohesion from the constant-water content triaxial test (C_{cw}; Rahardjo et al. 2004, Thu et al. 2006).

$$p_a = \sigma_v K_a - 2C_{cw}\sqrt{K_a} \tag{3.25}$$

The factor of safety (hereafter referred to as FOS) estimated using the MESA and the MTSA were 0.31 and 1.14, respectively, at the time when first localized failures occurred.

This implies that the stability analysis using the MESA is more conservative, but the analysis done with constant-water content test results provides more realistic estimates compared to the field observations. At the time general failures occurred, matric suction remained relatively constant at depth and the wetting front remained stable even after a small rainfall event. This indicates that general failure of the excavation can be attributed to an increase in the AEP associated with an increase in the soil's unit weight.

In this study, Eq. (3.23) was used to calculate the net AEP distribution for an unsupported vertical trench in unsaturated soil.

CHAPTER 4

ESTIMATING THE CRITICAL HEIGHT OF UNSUPPORTED VERTICAL TRENCHES IN SAND

In this chapter, an attempt is made to estimate the critical height of an unsupported vertical trench in an unsaturated sand. Two independent approaches were used; i) extended Rankine's earth pressure theory (hereafter referred to as EREPT) and ii) Bishop's simplified method (hereafter referred to as BSM) with geotechnical modelling software, SLOPE/W. It was assumed that the trenches were excavated into Unimin 7030 sand with various levels of the GWT (i.e. different matric suction distributions).

Mohamed & Vanapalli (2006) conducted model-footing tests in a sand (Unimin 7030) for both saturated and unsaturated conditions in a specially designed soil tank. Unsaturated conditions were achieved by setting a water level at some depth, and the matric suction distribution was established by measuring matric suction at various depths using conventional tensiometers. Figure 4.1 shows the measured and the assumed matric suction distributions with the water table at a depth of 600-mm in the soil tank, in which there is a negligible difference. Hence, a hydrostatic matric suction distribution was assumed for both approaches used in this chapter.

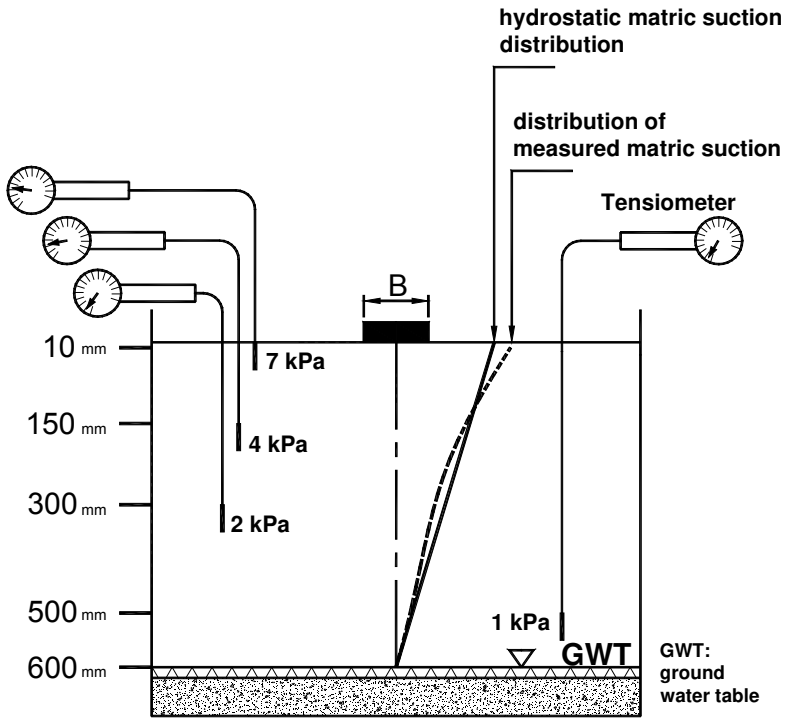

Figure 4.1. Measured matric suction profile and assumed hydrostatic matric suction profile with the water table at a depth of 600-mm from the soil surface (modified after Mohamed & Vanapalli 2006)

4.1 Soil Properties

Basic soil properties of Unimin 7030 sand are summarized in Table 4.1. The grain size distribution curve of the sand is shown in Figure 4.2. The SWCC was measured using a Tempe Cell apparatus extending the axis-translation technique (Figure 4.3; Hilf 1956). The AEV [$(u_a - u_w)_b$] and residual suction value [$(u_a - u_w)_r$] were estimated to be 4 kPa and 7.8 kPa, respectively. This was done using the procedure detailed in Vanapalli et al. (1999), (i.e. the matric suction values corresponding to the intersection of the two linear slope segments of the SWCC; Figure 4.3). A best-fit analysis for the SWCC was conducted using Fredlund & Xing's (1994) model (Eq. (4.1)), and the fitting parameters are summarized in Table 4.2.

Table 4.1. Basic soil properties of Unimin 7030 sand (Mohamed & Vanapalli 2006)

Properties	Value
Plasticity Index, I_p	NP
Saturated unit weight, γ_{sat} (kN/m^3)	20.4
Saturated water content, θ_s (%)	38.7
Void ratio, e	0.63
Specific gravity, G_s	2.65
Effective cohesion, c' (kPa)	0
Effective internal friction angle, ϕ' (˚)	36.2
Saturated hydraulic conductivity, k_{sat} (m/s)	5×10^{-5}
Elastic modulus, E (kPa)**	10,000
Poisson's ratio, v **	0.33

** = assumed value

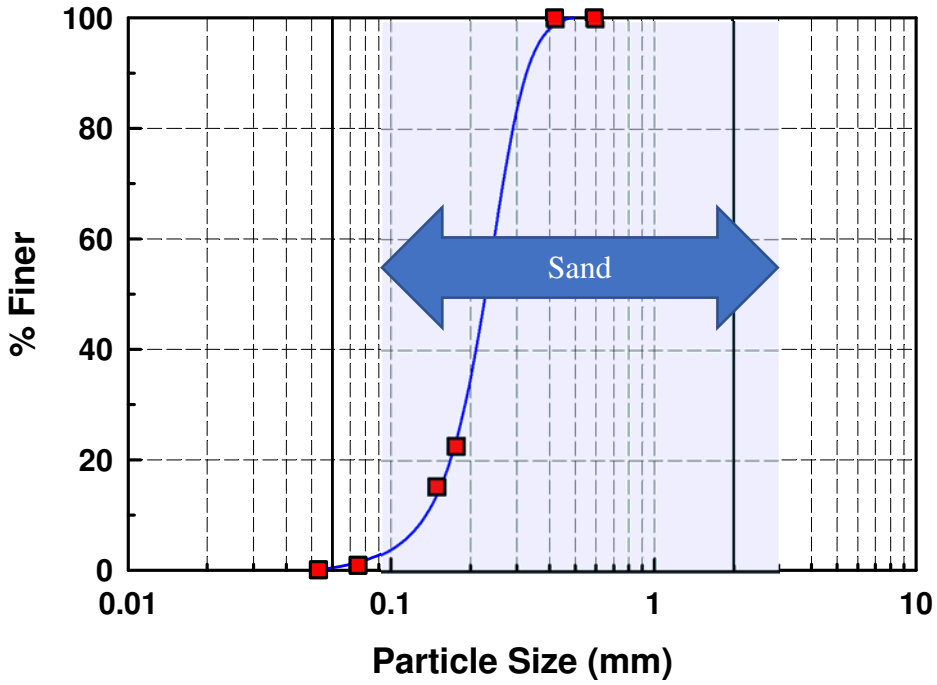

Figure 4.2. Grain size distribution curve of Unimin 7030 sand

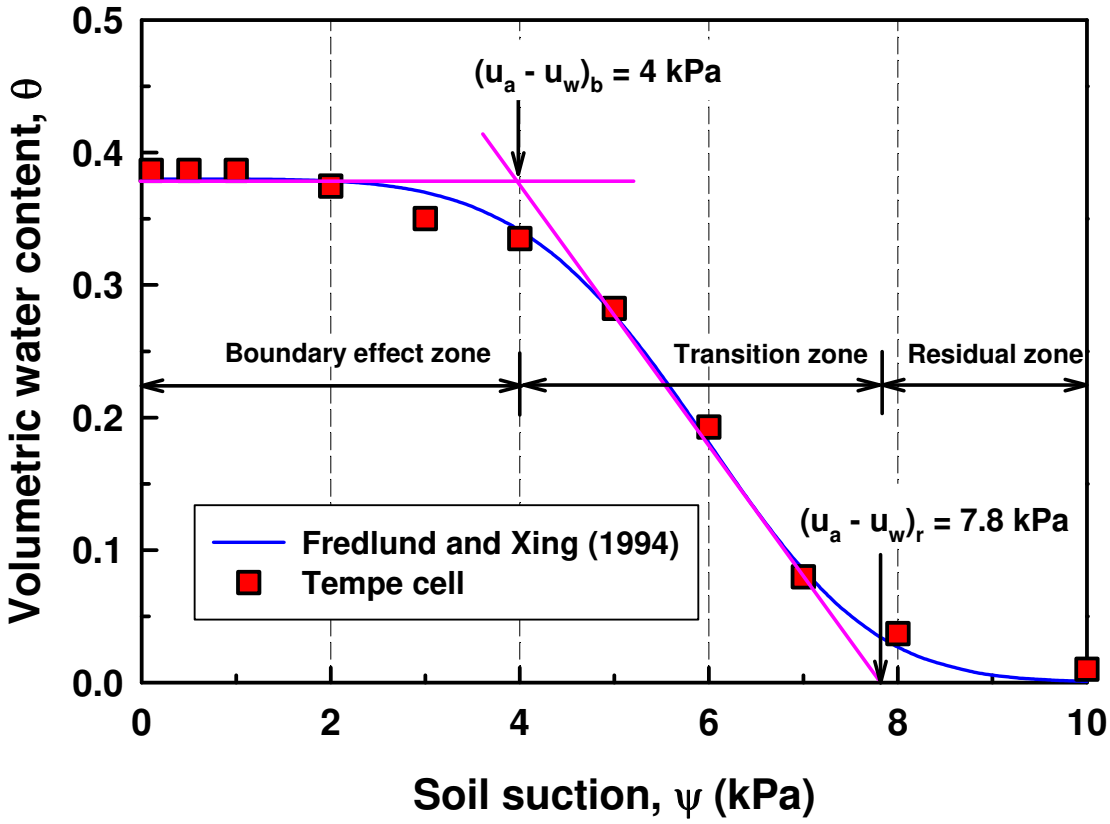

Figure 4.3. SWCC of Unimin 7030 sand (modified after Mohamed & Vanapalli 2006)

$$\frac{\theta}{\theta_s} = S = \left[\frac{1}{\ln\left[e + \left(\psi / a \right)^n \right]} \right]^m \tag{4.1}$$

where e = Napier's constant (2.71828…), ψ = soil suction, and a, n, m = fitting parameters

Table 4.2. Summary of fitting parameters used to plot the SWCC of Unimin 7030 sand

Parameter	*a*	*m*	*n*
Value	11.415	54.202	5.1322

Volume changes can be neglected in cohesionless soils during drying/wetting cycles (i.e. void ratio, e = constant); therefore, the unit weight of the sand is a function of volumetric water content as shown in Eq. (4.2). The variation of the unit weight with respect to volumetric water content (or matric suction) was accounted for in both approaches discussed in this chapter.

$$\gamma = \frac{G_s + \theta(1+e)}{(1+e)}\gamma_w \tag{4.2}$$

where G_s = specific gravity, and e = void ratio

Effective cohesion and the internal friction angle of the sand were determined from the direct shear test (Figure 4.4).

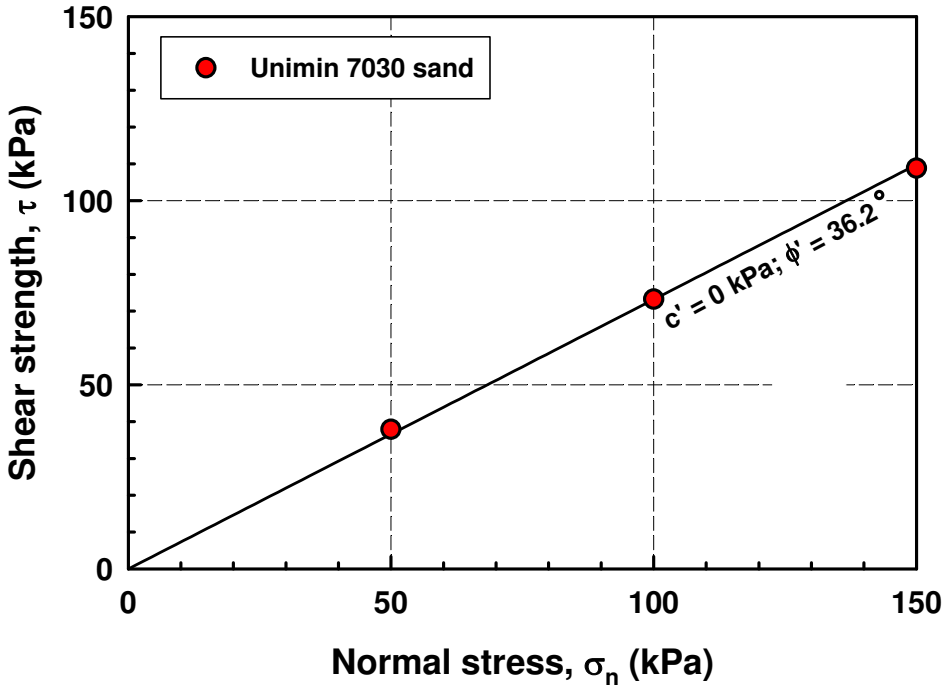

Figure 4.4. Direct shear test results on Unimin 7030 sand (modified after Mohamed & Vanapalli 2006)

4.2 Estimating the Critical Height with EREPT

The procedure for estimating the critical height of an unsupported vertical trench using extended Rankine earth pressure theory is as follows:

(a) Set a desired elevation of the GWT.

(b) Set the increment size (i.e. ΔH) for calculating pressures. ΔH = 1-mm was used in this study for calculating the AEP distribution.

(c) Establish the matric suction distribution with depth by multiplying the unit weight of water by the distance from the GWT [$(u_a - u_w) = 0$ in the saturated zone].

(d) Calculate the distribution of volumetric water content with the computed values of matric suction by using Eq. (4.1) and the values in Table 4.2.

(e) Calculate the distribution of the unit weight with depth using Eq. (4.2) and the values in Table 4.1. Use effective unit weight in the saturated zone.

(f) Establish the overburden pressure distribution with depth by multiplying the unit weight at a specific depth by the depth increment and adding the stress from the previous increment. This causes the overburden pressure to compound with depth while accounting for the variation of the unit weight.

(g) Plot the variation of positive earth pressure (i.e. $\sigma_v K_a$) with depth. Use effective stress in the saturated zone.

(h) Convert volumetric water content to the degree of saturation and plot the variation of negative earth pressure (i.e. $2C\sqrt{K_a}$) with depth.

(i) Plot the net AEP distribution as the difference between (g) and (h).

(j) Attain the regression curve for the AEP distribution.

(k) Using a tool such as Wolfram Alpha, integrate the regression curve (Figure 4.5) from the ground surface to the depth where net AEP equals zero to determine A1 (i.e. resultant force in tension zone). Integrate from the depth where AEP = 0 to the depth which provides A1 = A2 to find the critical height. This may involve integrating beyond the depth of the GWT. In this case, the first part of A2 is determined by integrating up to the depth of the GWT. The remaining area is found by integrating the function for the saturated zone. The critical height is taken as the depth from the ground surface to where A1 = A2.

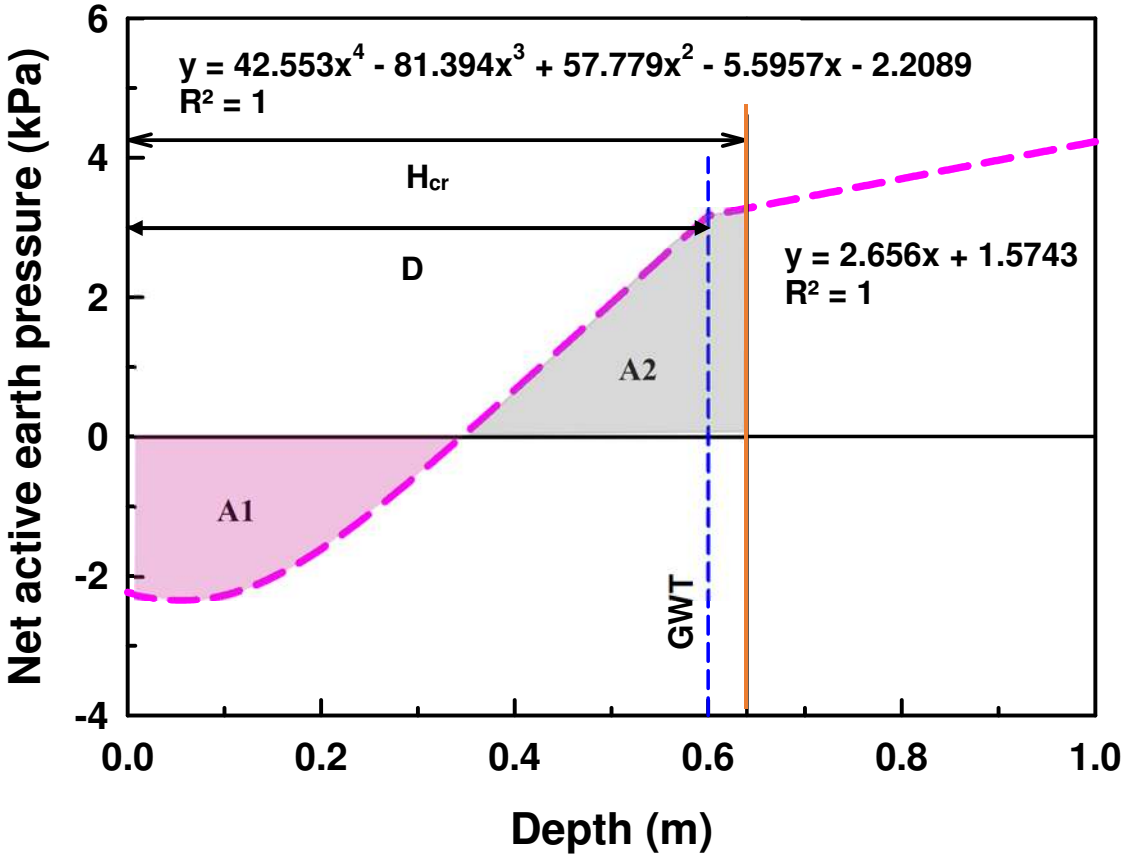

Figure 4.5. Example of regression curve for the net AEP distribution with D = 0.6-m

Figure 4.6 to Figure 4.9 show the distributions of the positive, negative, and net AEP with depth for D = 0.3, 0.6, 1.0, and 1.5-m, respectively. The absolute value of negative earth pressure is plotted such that the magnitude of the positive and negative earth pressures can be compared more easily. The negative sign in the net AEP distribution indicates the tension zone, and the positive sign indicates the compression zone. When the lateral earth pressure is zero, the stress-state is transitioning from tension to compression or vice versa. When D = 1.0-m, the magnitude of negative earth pressure is not sufficient to match the positive pressure. Also, in the case with D = 1.5-m, the net AEP is positive throughout the entire soil profile. This indicates that an unsupported vertical trench fails immediately upon initiating the excavation (i.e. H_{cr} = 0-m).

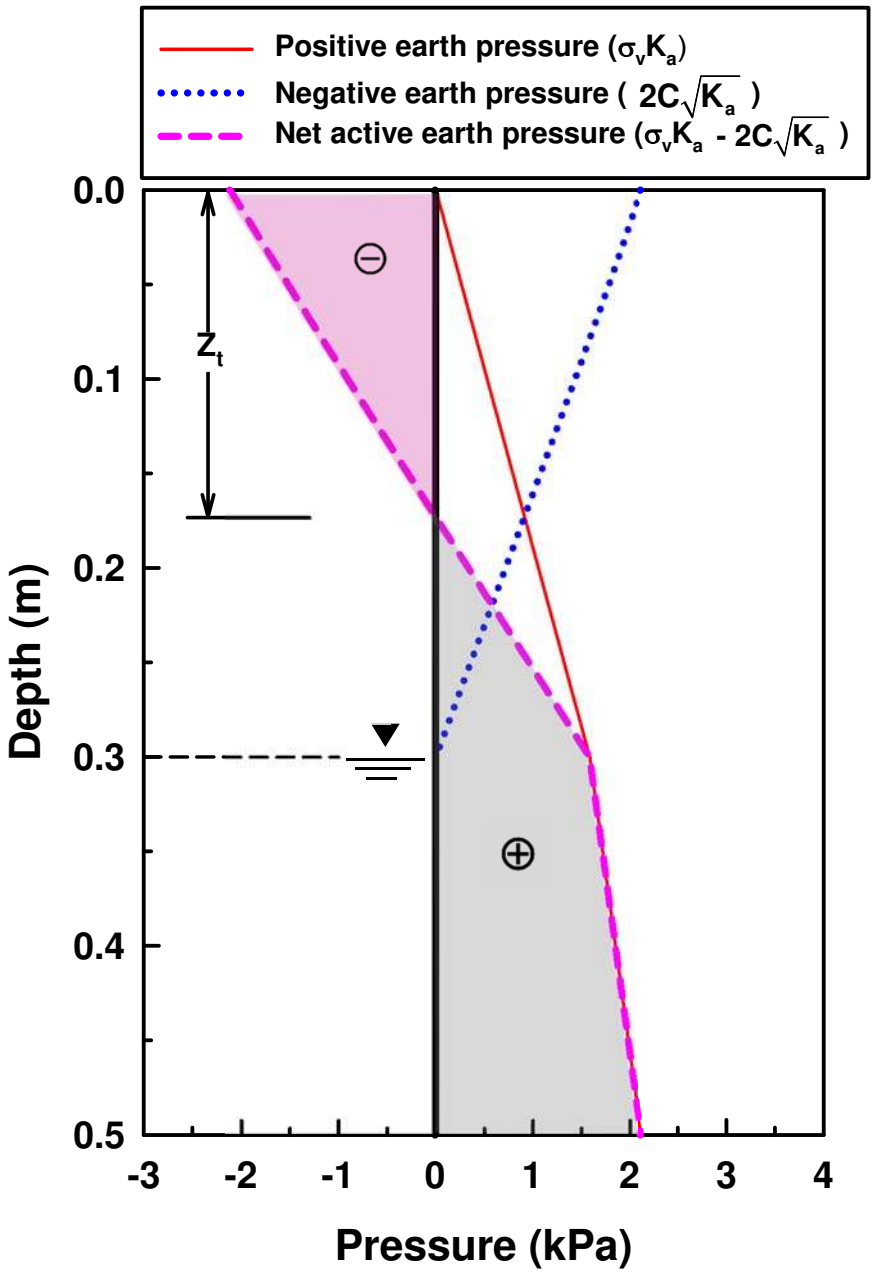

Figure 4.6. Positive, negative, and net AEP distribution (D = 0.3-m)

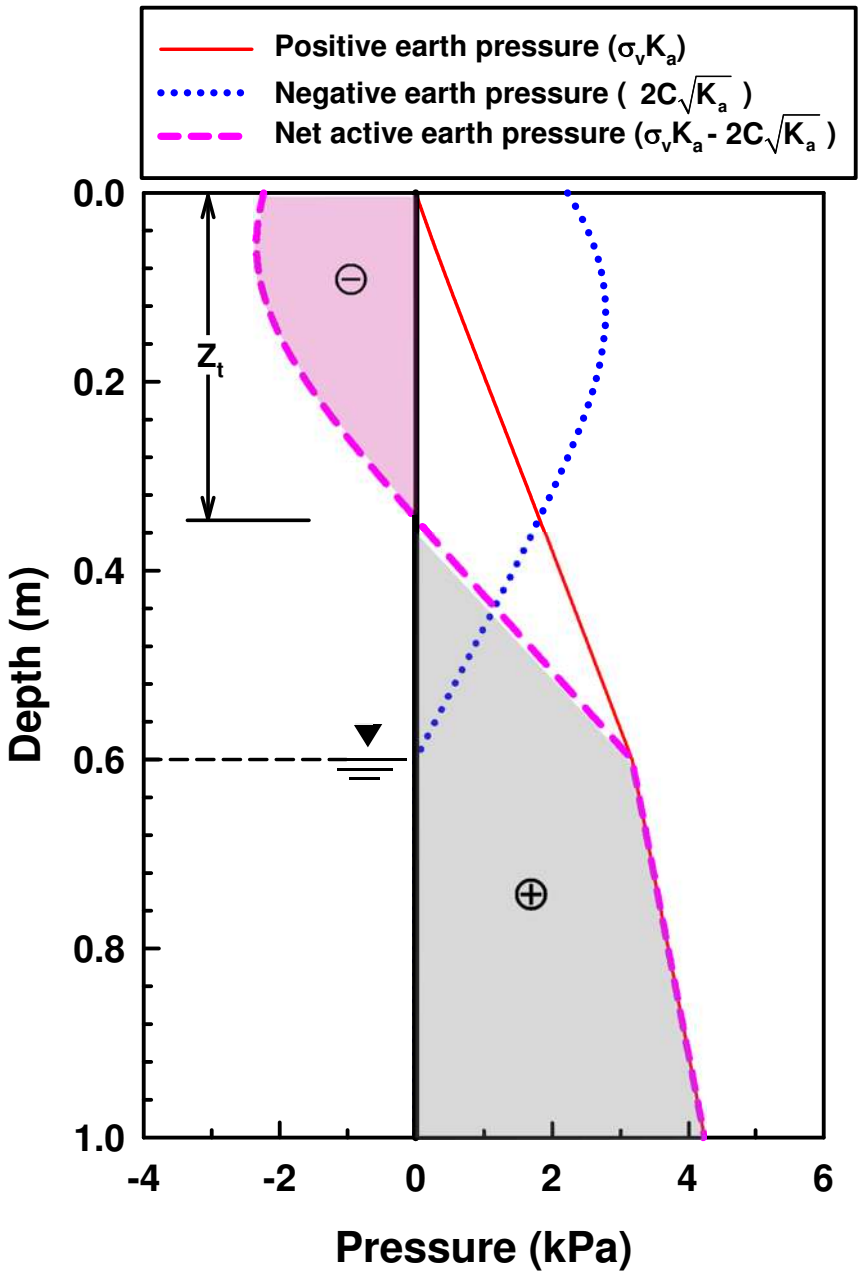

Figure 4.7. Positive, negative, and net AEP distribution (D = 0.6-m)

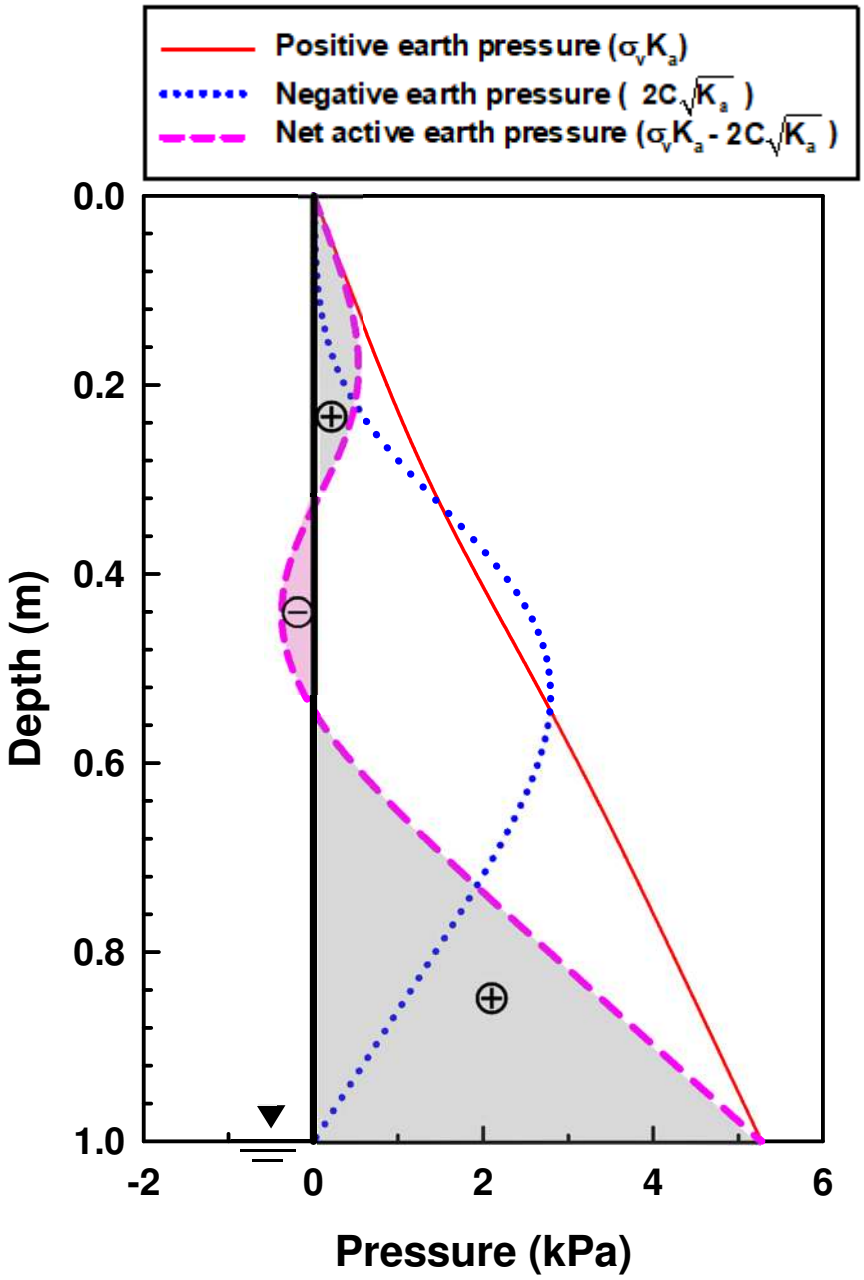

Figure 4.8. Positive, negative, and net AEP distribution (D = 1.0-m)

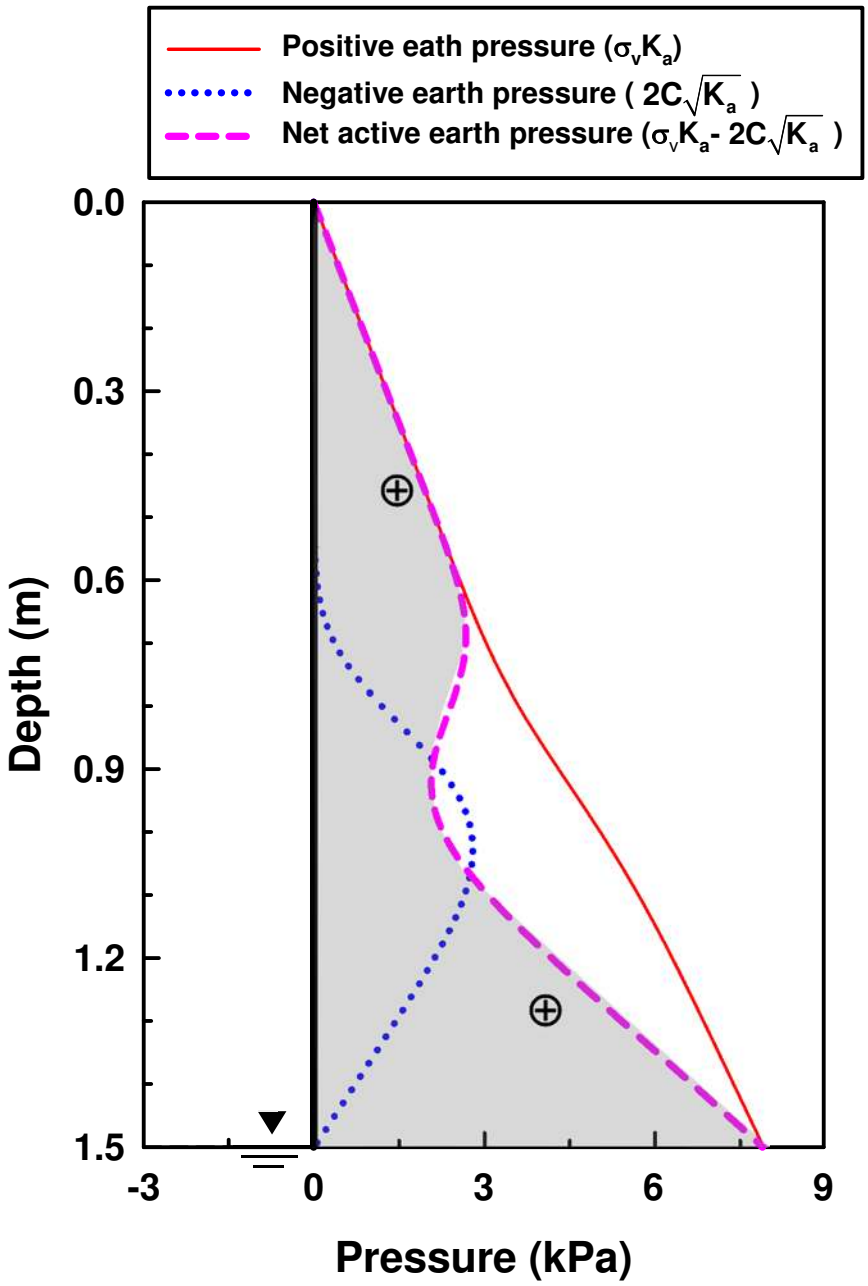

Figure 4.9. Positive, negative, and net AEP distribution (D = 1.5-m)

4.3 Estimating the Critical Height with BSM

In this section, the critical height of an unsupported vertical trench in sand was estimated using Bishop's simplified method with geotechnical modelling software, SLOPE/W. Bishop (1955) assumed that the tangential interslice forces are equal and opposite (i.e. X_1 = X_2 in Figure 4.10) but horizontal forces are not. The FOS is calculated using Eq. (4.3).

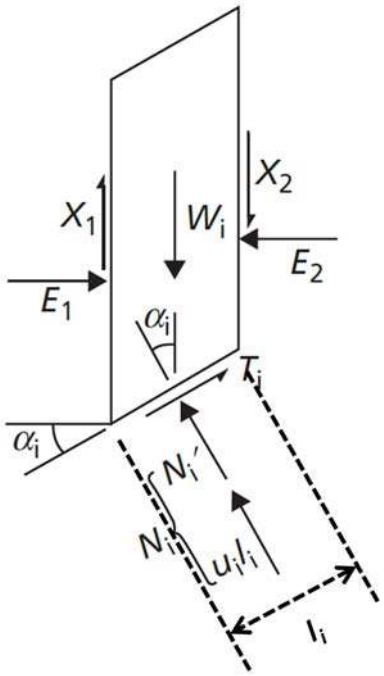

Figure 4.10. Forces acting on the i^{th} slice in Bishop's simplified method of slices (Craig 2004)

$$FOS = \frac{1}{\sum_i W_i \sin\alpha_i} \sum_i \left\{ \left[c'_i \beta_i + \left(W_i - u_i \beta_i \right) \tan\phi'_i \right] \frac{\sec\alpha_i}{\left[1 + \frac{\tan\phi'_i \tan\alpha_i}{FOS} \right]} \right\} \qquad (4.3)$$

where FOS = factor of safety, W_i = weight of i^{th} slice, α_i = inclination of i^{th} slice base, and β = width of i^{th} slice

This method only satisfies moment equilibrium because interslice shear forces are ignored, which implies rotational failure is assumed to happen about a circular slip surface (i.e. negligible internal shearing occurs). This sort of mechanism was deemed plausible for a vertical trench being excavated into sand with apparent cohesion. An iterative procedure is required to solve for equilibrium. The initial guess for the FOS in SLOPE/W is one, in which case the shear strength, and a new FOS are computed. The program continues iterating until convergence occurs at a specified tolerance (i.e. 0.001 between values for the FOS). The critical height was taken as the depth immediately preceding the depth that showed FOS < 1 in the stability analysis.

In-situ analyses in SIGMA/W (Figure 4.11) are used for setting the initial PWP profile and the ground stresses. In-situ analyses require Fixed-X displacement boundaries (i.e. hollow red triangles) on the lateral extents, and Fixed-XY boundaries along the base of the domain. The stresses calculated in SIGMA/W are not used in calculating the FOS for a Bishop analysis in SLOPE/W; therefore, meshing and the material model are not important for this application. However, an in-situ analysis was used as the parent to each SLOPE/W analysis (Figure 4.12) to establish the PWP profile. This was done for convenience, such that the GWT only needed to be changed in one analysis file rather than in each individual excavation stage within SLOPE/W.

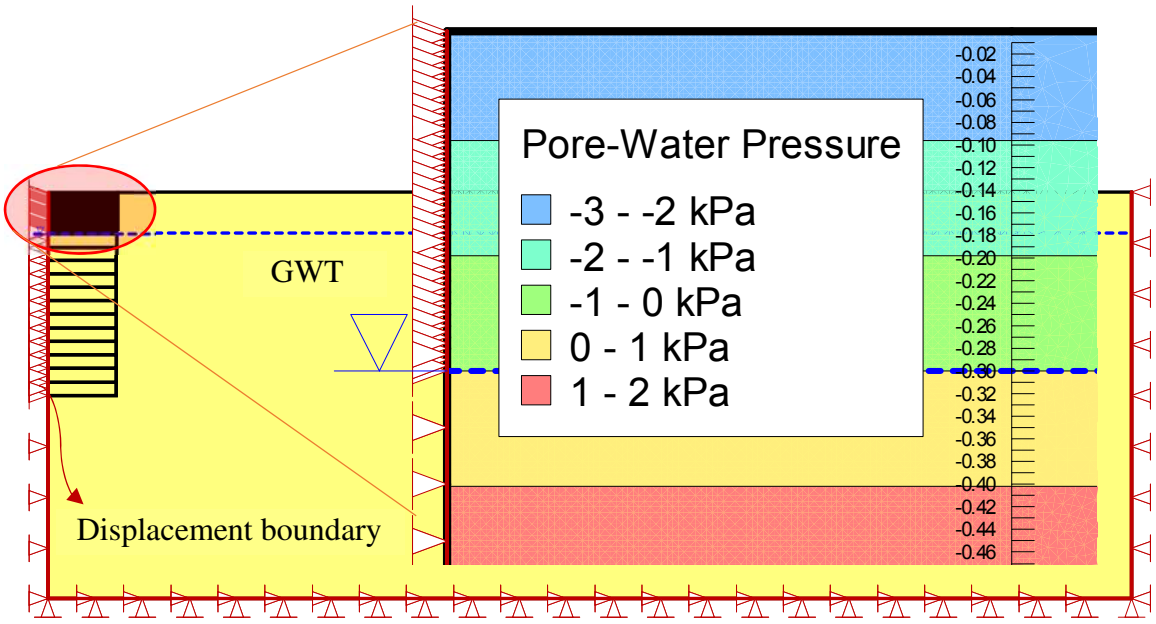

Figure 4.11. Establishing PWP profile with In-situ analysis in SIGMA/W

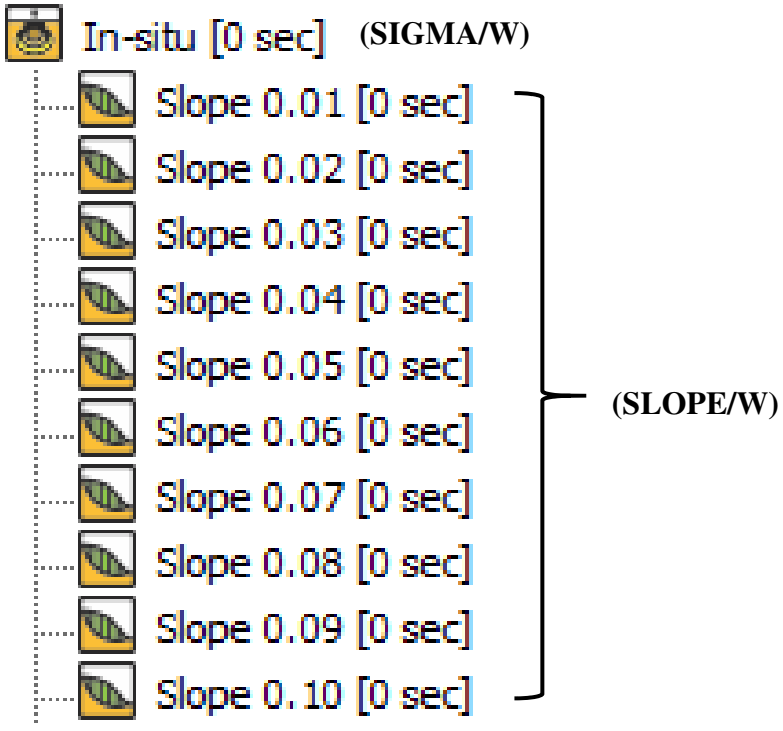

Figure 4.12. Analysis tree for Bishop's simplified method with In-situ as the parent analysis

In SIGMA/W, the initial PWP profile can be simulated by defining a GWT and a maximum negative pressure head based on the assumption that PWP varies hydrostatically with distance above and below the GWT (Figure 4.13). For instance, if the maximum negative pressure head is lower than the height of the unsaturated soil layer (i.e. $H_{max} < H_{unsat}$), the negative PWP is constant up to ground surface beyond the maximum negative pressure head. Conversely, if the maximum negative pressure head is greater than the height of the unsaturated soil layer (i.e. $H_{max} > H_{unsat}$) the negative PWP increases linearly up to ground surface. Alternatively, a spatial function can be used to specify the pressure head at discrete points. The pressure head is determined at intermediate points using linear interpolation. In this study, an initial GWT was assigned to the problem domain to simulate hydrostatic PWP distributions above and below the GWT. The maximum negative pressure head was left as the default setting, 5-m.

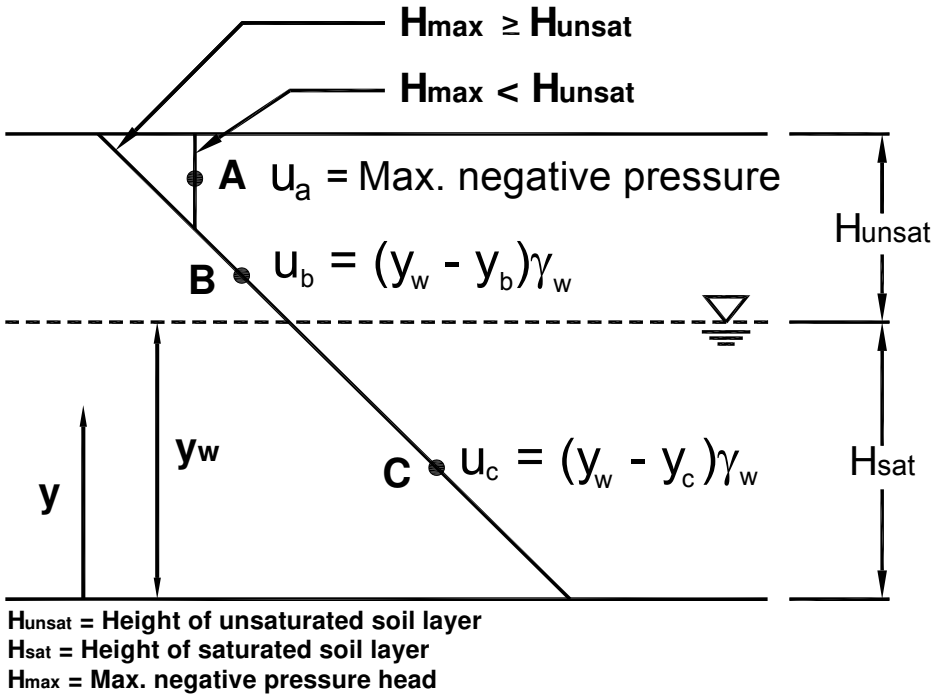

Figure 4.13. Calculation of PWP based on the location of GWT in SIGMA/W

For soil with negative PWP (i.e. matric suction), total cohesion is computed with Eq. (4.4) using effective cohesion and the SWCC. The residual volumetric water content was taken as 5% of the volumetric water content at saturation for calculating total cohesion in SLOPE/W. The Mohr-Coulomb failure criterion was used as the material model.

$$C = c' + \left(u_a - u_w\right)\left(\frac{\theta - \theta_r}{\theta_s - \theta_r}\right)\tan\phi' \tag{4.4}$$

In SLOPE/W, the shape and positions of trial slip surfaces can be defined by four options: i) Entry and Exit, ii) Grid and Radius, iii) Block Specified, and iv) Fully Specified. Each method processes every defined slip surface to find the minimum FOS. The 'Entry and Exit' method was chosen to specify the trial slip surfaces in this chapter (Figure 4.14). The entry was defined as a range as wide as the excavation depth with an entry point every 10-mm, and the exit was specified as a point at the toe of the slope. Figure 4.15 to Figure 4.18 show the results for the stability analyses with D = 0.3, 0.6, 1.0, and 1.5-m, respectively. The contours indicate PWP.

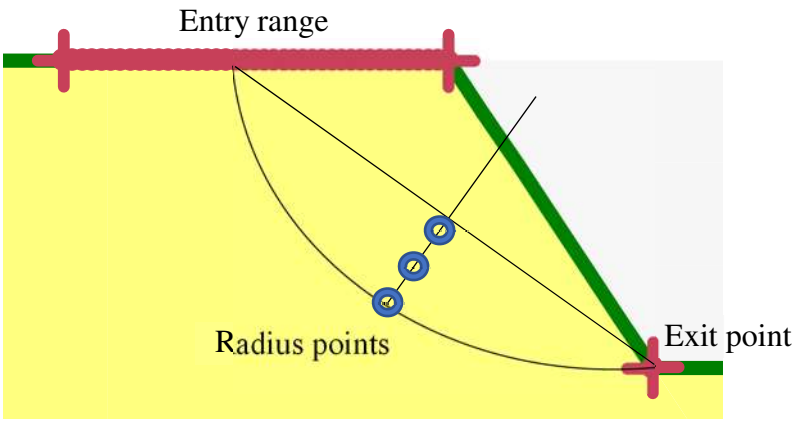

Figure 4.14. Schematic of the 'Entry and Exit' slip surface method in SLOPE/W

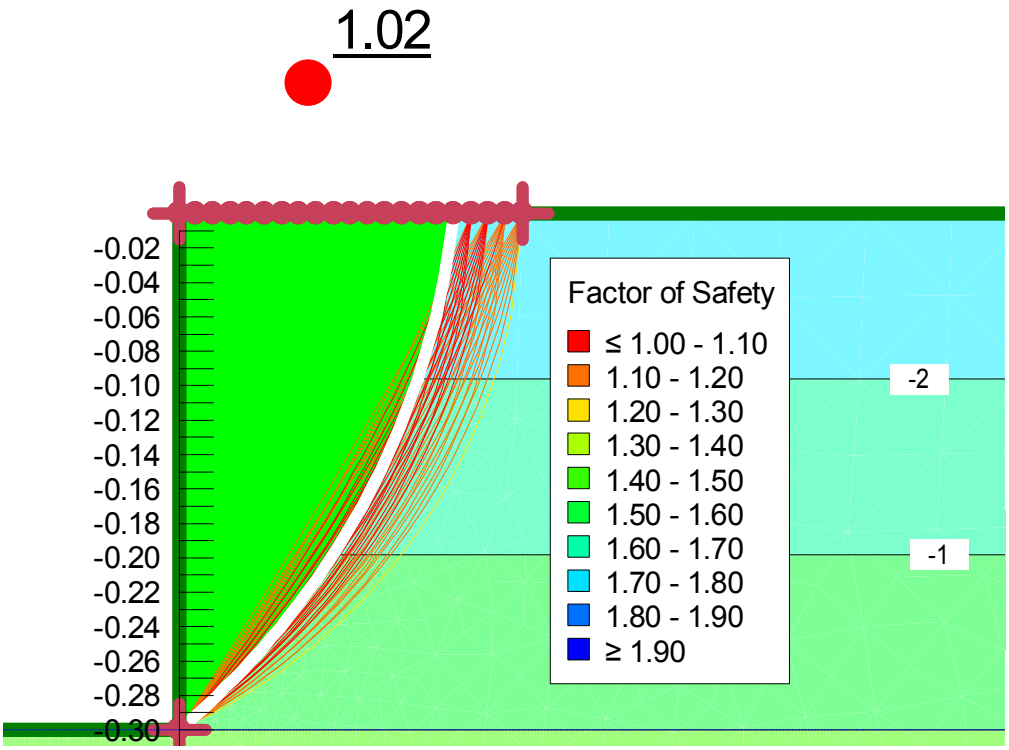

Figure 4.15. Slope stability analysis in SLOPE/W using Bishop's simplified method (D = 0.3-m)

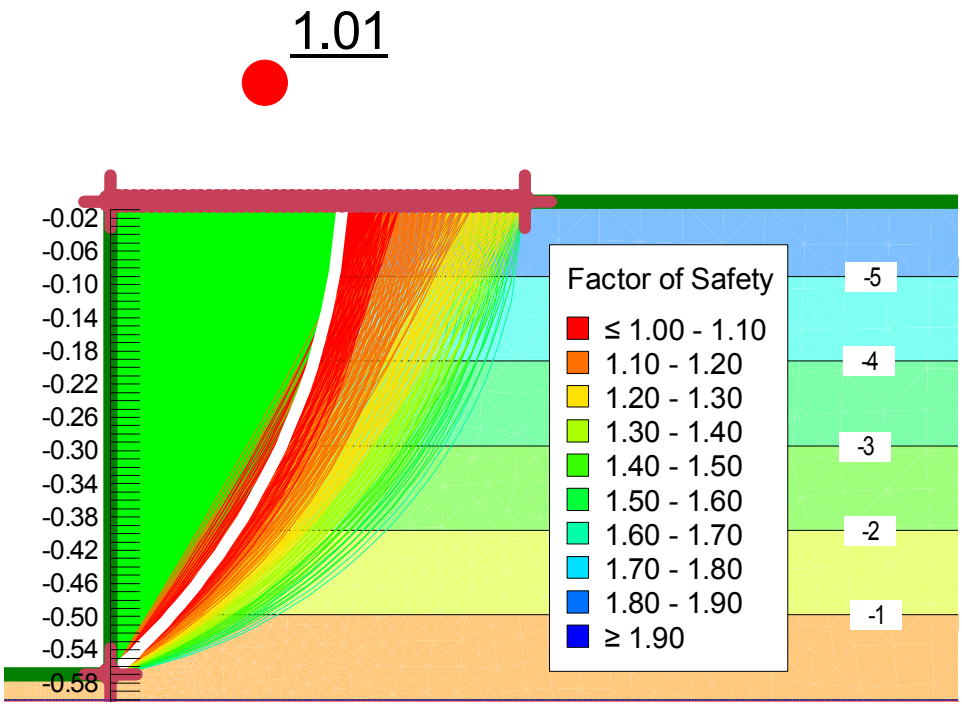

Figure 4.16. Slope stability analysis in SLOPE/W using Bishop's simplified method (D = 0.6-m)

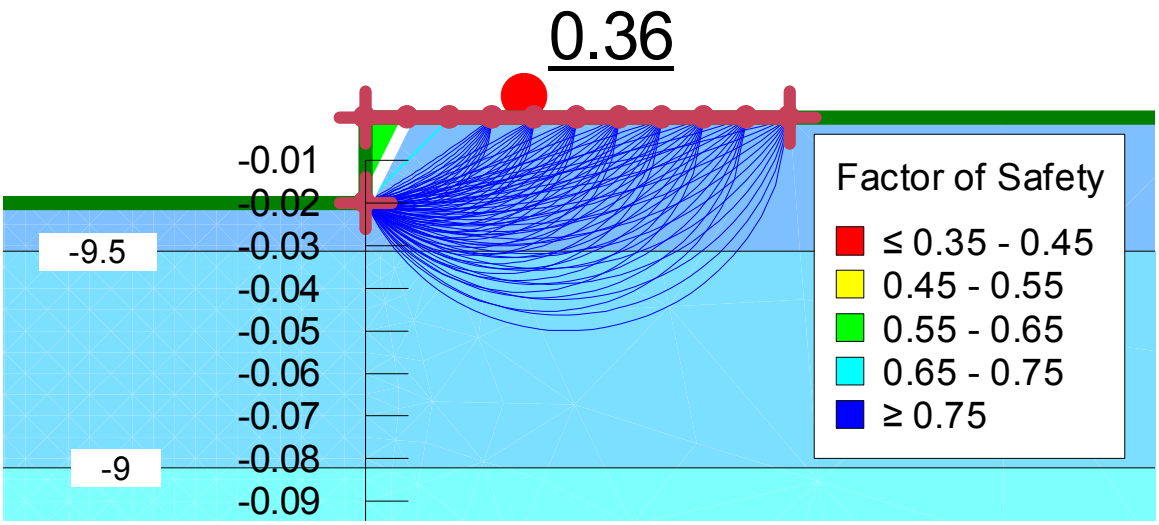

Figure 4.17. Slope stability analysis in SLOPE/W using Bishop's simplified method (D = 1.0-m)

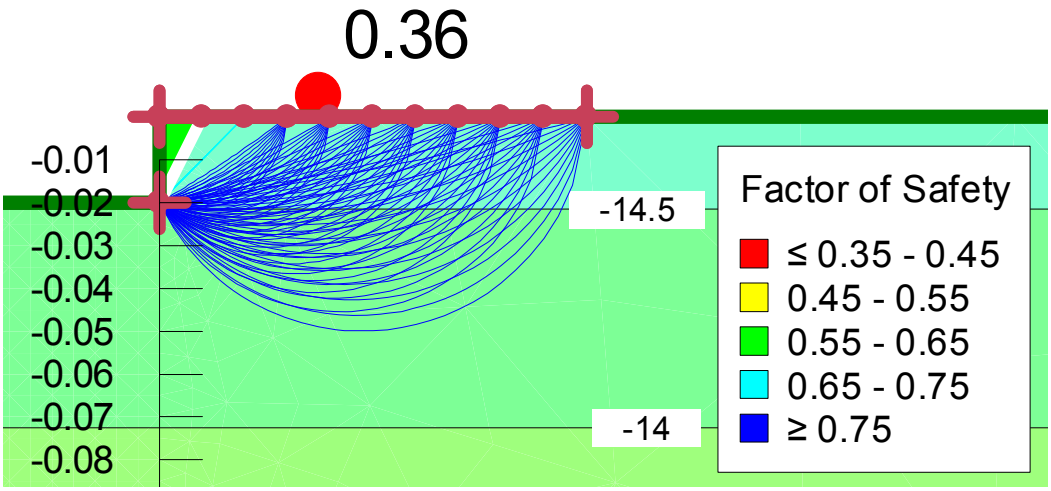

Figure 4.18. Slope stability analysis in SLOPE/W using Bishop's simplified method (D = 1.5-m)

4.4 Comparison of Critical Heights from EREPT and BSM

Multiple analyses were conducted with the GWT at various elevations to establish a relationship between the depth of the GWT and the critical height. Table 4.3 summarizes the critical heights estimated using extended Rankine earth pressure theory and Bishop's simplified method. Based on the results in Table 4.3, the variation of the critical height with respect to the depth of the GWT in Unimin 7030 sand is plotted in Figure 4.19.

Table 4.3. Variation of the critical height in Unimin 7030 sand

GWT (m)	Critical Height (m)	
	Extended Rankine Earth Pressure Theory	**Bishop's Simplified Method**
0	0.00	0.00
0.1	0.11	0.12
0.2	0.20	0.23
0.3	0.30	0.35
0.4	0.39	0.46
0.5	0.48	0.57
0.6	0.57	0.65
0.7	0.64	0.70
0.8	0.68	0.71
0.9	0.00	0.04
1	0.00	0.00
1.1	0.00	0.00
1.2	0.00	0.00
1.3	0.00	0.00
1.4	0.00	0.00
1.5	0.00	0.00

The results from both methods show good agreement. The error ranged from 4% (0.03/0.68-m) with D = 0.8-m, to 19% (0.09/0.48-m) with D = 0.5-m. Both methodologies show that the critical height increases gradually as the depth of the GWT increases up to 0.8-m, and then drops to zero as the depth of the GWT is further increased. The minimum slip surface depth was set at 0.01-m in SLOPE/W, therefore the FOS could not be generated for the 0.01-m excavation stage. In which case, the critical height was taken as 0-m when the 0.02-m excavation stage showed FOS < 1 (e.g. Figure 4.17 and Figure 4.18). This behaviour can be explained by the variation of total cohesion in the sand with respect to matric suction. The contribution of matric suction towards total cohesion increases with increasing matric suction, and then starts decreasing as residual suction is approached (7.8-kPa for Unimin 7030 sand; Vanapalli et al. 1996). In other words, total cohesion becomes zero in the sand near the top of the trench when the depth of the GWT is relatively deep (> 0.8-m), and shear strength becomes fully dependant on frictional resistance. This indicates that trench failure occurs at a shallow depth when the GWT is deep enough to create a residual zone near the ground surface.

For depths of the GWT up to 0.7-m, the critical heights estimated using extended Rankine earth pressure theory are slightly greater than the depths of the GWT. This may not be realistic since the sand used in the present study does not have effective cohesion and an excavation below the GWT can initiate a localized failure near the toe of the slope (i.e. slough-in/cave-in, Figure 2.5(c)), which leads to a general failure. In other words, these methods do not account for localized failures that may trigger general failures.

It is interesting to note that the results show close agreement even though the respective methods are inherently different. Bishop's simplified method only satisfies moment

equilibrium and assumes a circular slip surface, and the shear strength is computed at the base of each slice along the slip surface. Extended Rankine earth pressure theory is purely based on force equilibrium. The lateral pressure along the excavation face is computed and the sum of the forces in the horizontal direction is set to zero to solve for the critical height. The results are likely close because failure naturally occurs at a relatively shallow depth and the soil mass is approximately the same regardless of the assumed failure surface.

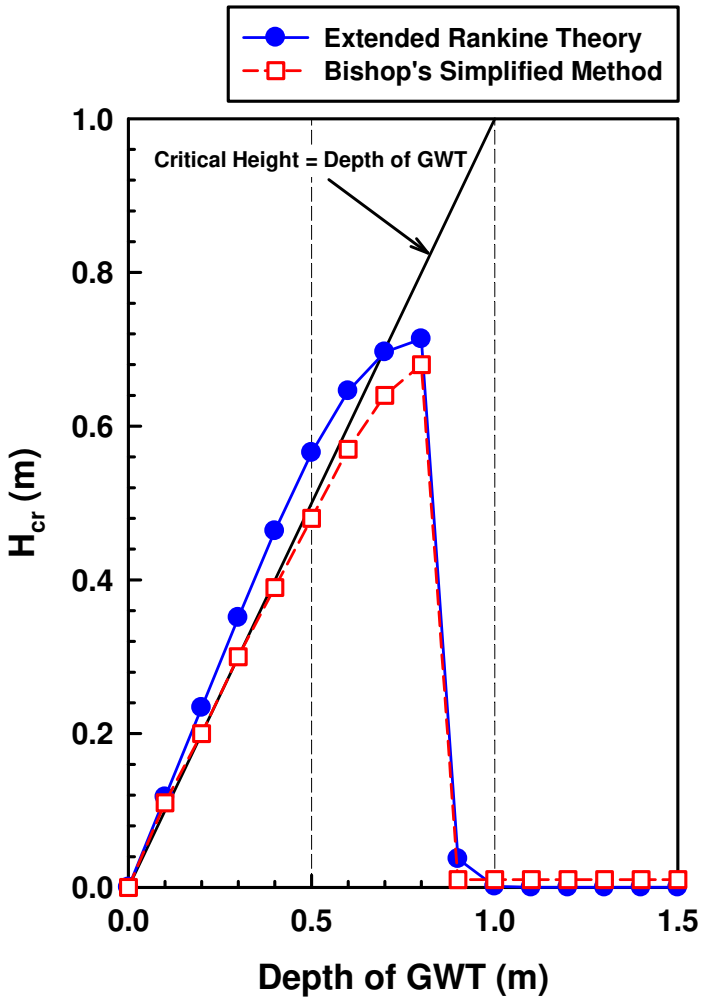

Figure 4.19. Variation of the critical height with respect to the depth of the GWT using extended Rankine earth pressure theory and Bishop's simplified method (Unimin 7030 sand)

4.5 Summary and Conclusions

In this chapter, an attempt is made to estimate the critical height of an unsupported vertical trench in an unsaturated sand using two methodologies; extended Rankine earth pressure theory, and Bishop's simplified method. The results showed that the critical height increases with increasing depth of the GWT up to a point (0.8-m), and then decreases significantly as the depth of the GWT is further increased. This is attributed to the fact that total cohesion of an unsaturated sand becomes close to zero as matric suction exceeds the residual suction value. The agreement between the results suggests that the critical height of an unsupported vertical trench in unsaturated sand is strongly influenced by the variation of shear strength with respect to matric suction.

CHAPTER 5

ESTIMATING THE CRITICAL HEIGHT OF UNSUPPORTED TRENCHES WITH DIFFERENT WALL SLOPES IN SAND

In Chapter 4, trench stability was estimated without considering the change in PWP due to excavating. In practice, excavating a trench relieves stress in the soil within the proximity of the excavation, which results in elastic rebound. This phenomenon leads to an increase in void ratio and a temporary decrease in PWP. The shear strength of an unsaturated soil can either increase or decrease depending on the initial matric suction distribution before excavating. For example, if a trench is excavated into a soil where matric suction is close to or within the residual zone, a further increase in matric suction can lead to a decrease in shear strength and therefore the critical height. Conversely, if most soil above the GWT is within the boundary effect or transition zone, a temporary decrease in PWP may temporarily increase the shear strength of the soil. However, the probability of the trench failing increases with time as negative PWP (i.e. matric suction) dissipates.

Coupled stress-PWP analyses (hereafter referred to as coupled analyses) are conducted in this chapter to investigate the critical height of trenches considering the influence of PWP redistribution caused by excavating. Four different wall slopes (1.5V:1H, 2V:1H, 3V:1H, and 90°) and a vertical trench with the top 0.3-m sloped 1:1 (denoted as 90***, Figure 5.1) were considered with multiple depths of the GWT (0, 0.3, 0.5, 0.7, 0.8, 0.9, 1.0, 1.2, 1.5, and 2.0-m) in Unimin 7030 sand (Table 4.1). For comparison, the critical heights were also estimated using the LEM (Morgenstern-Price method) for the same excavation scenarios used in the coupled analyses.

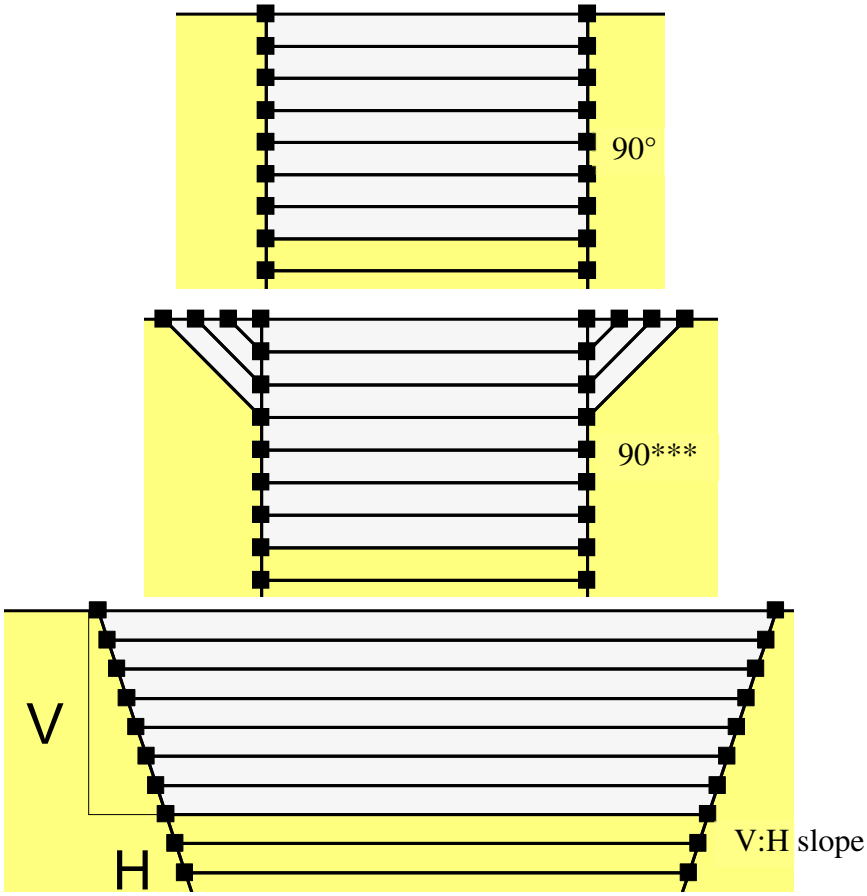

Figure 5.1. Different types of trenches considered in this chapter

5.1 Estimating the Critical Height with the Finite Element Approach

5.1.1 Hydraulic Conductivity Function

The hydraulic conductivity of a soil is maximized when the soil is saturated. As a soil desaturates, air gradually replaces the voids initially occupied by water and the tortuosity of the flow path increases. This phenomenon increases the resistance to flow through the voids. In other words, the hydraulic conductivity of a soil is a function of the degree of saturation (or matric suction) and decreases with increasing matric suction. However, measuring the hydraulic conductivity for various matric suction values is time-consuming

and requires elaborate testing equipment. For this reason, the hydraulic conductivity function proposed by Fredlund et al. (1994), Eq. (5.1), was used in this chapter to estimate the variation of hydraulic conductivity with respect to soil suction. Figure 5.2 shows the hydraulic conductivity function of Unimin 7030 sand.

$$k_{unsat} = k_{sat} \frac{\sum_{i=j}^{N} \frac{\theta\left(e^{y}\right) - \theta\left(\psi\right)}{e^{y_i}} \theta'\left(e^{y_i}\right)}{\sum_{i=1}^{N} \frac{\theta\left(e^{y}\right) - \theta_s}{e^{y_i}} \theta'\left(e^{y_i}\right)} \tag{5.1}$$

where

k_{unsat} = the calculated conductivity for a specified water content or matric suction,

k_{sat} = the measured conductivity for saturated condition,

y = a variable of integration representing the logarithm of negative PWP,

i = the interval between the range of j to N,

j = the least negative PWP to be described by the final function,

N = the maximum negative PWP to be described by the final function,

ψ = the suction corresponding to the j^{th} interval,

θ' = the first derivative of Eq. (4.1)

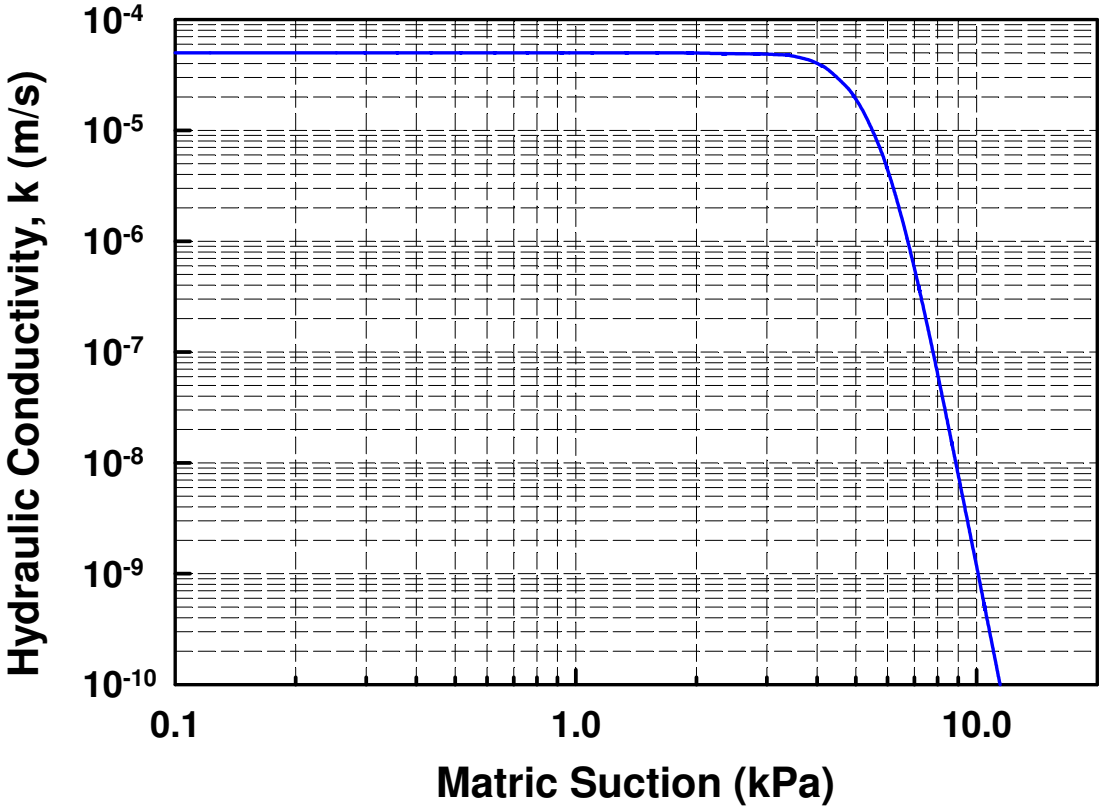

Figure 5.2. Hydraulic conductivity function of Unimin 7030 sand

5.1.2 Analysis in SIGMA/W

The PWP distribution and the initial stresses (i.e. gravity body loads) first must be established with an In-situ analysis prior to excavating (Figure 4.11). A hydrostatic PWP distribution was created by setting a static GWT. The excavations were staged using a coupled analysis. Deformations and stress distributions resulting from each excavation stage were calculated using effective stress parameters and the elastic-plastic constitutive model.

Figure 5.3 shows the boundary conditions required to perform a coupled analysis in SIGMA/W. The left and right ends are restrained in the X-direction (i.e. hollow red

triangles), and the base of the domain is restrained in both the X and Y directions. Total head boundaries equal to the initial water table elevation were placed along the lateral extents of the soil region (i.e. solid blue dots). This allows the GWT to fluctuate in response to excavating while maintaining constant hydraulic head along the extents of the domain.

The mesh is created of 0.1 × 0.25-m elements in the immediate surroundings of the excavation, and transitions to 1 × 1-m elements along the extents of the domain. A finite element mesh pattern of 'quads & triangles' was used to provide a smooth transition between areas of interest. The main reason for using different element sizes was to save on computation time. Mesh sizes were determined based on a mesh-convergence study conducted with different element lengths (1-m, 0.25-m, 0.1-m, and 0.05-m) and a 0.1-m thickness along the excavated surface. The results showed that the critical height is not affected by the mesh size when finer than 0.25-m. 4-point integration was used for the quadrilateral elements, and 3-point integration was used for the triangular elements. A linear interpolation model was used for calculating stresses and deformations at the nodes. The use of secondary nodes was not necessary for this application.

The previous stage in the excavation was used as the parent analysis to the following, such that the stress changes and deformations caused by the previous excavations were compounded as the stages progressed. Excavations were simulated by deactivating regions in 0.1-m increments. Analyses for each slope and GWT were conducted with 10-s and 1,000-s time steps between excavation stages to investigate the variation of PWP caused by different excavation rates. Soil parameters used in the analyses are listed in Table 4.1.

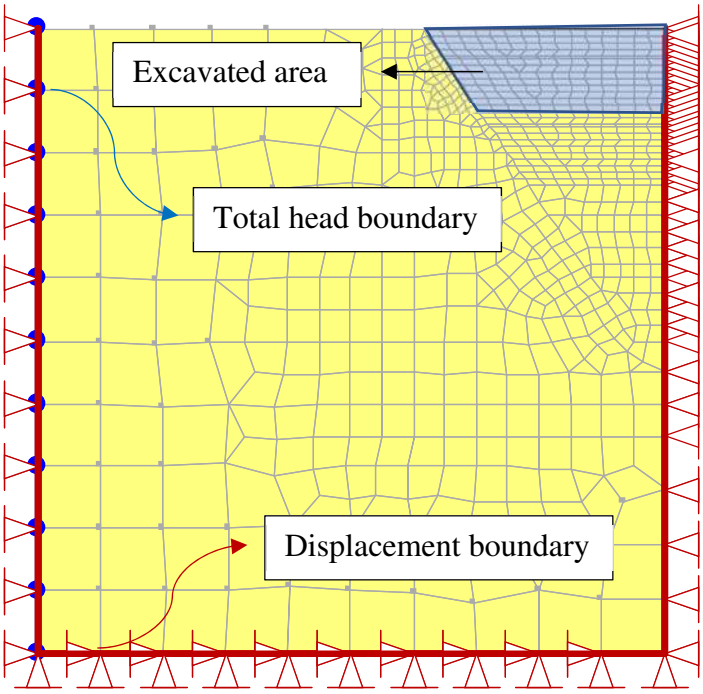

Figure 5.3. Boundary conditions required for coupled analyses in SIGMA/W

5.1.3 Analysis in SLOPE/W

The FOS was calculated at targeted time steps based on the stress-deformation results from SIGMA/W (i.e. SIGMA-Stress type analyses were conducted in SLOPE/W). An example of the analysis tree for 10-s time steps is shown in Figure 5.4. Shear strength is computed with either Eq. (3.4) or Eq. (3.14) depending on the location of the potential slip surface and GWT. The mobilized and resisting shear forces are computed for each slice in finite element analyses, therefore the FOS is computed for each slice. The global FOS is found by summing all forces along the slip surface (Eq. (5.2)).

$$FOS = \frac{\sum S_r}{\sum S_m} \tag{5.2}$$

where S_r = total available shear resistance, and S_m = total mobilized shear force along the base of the slice

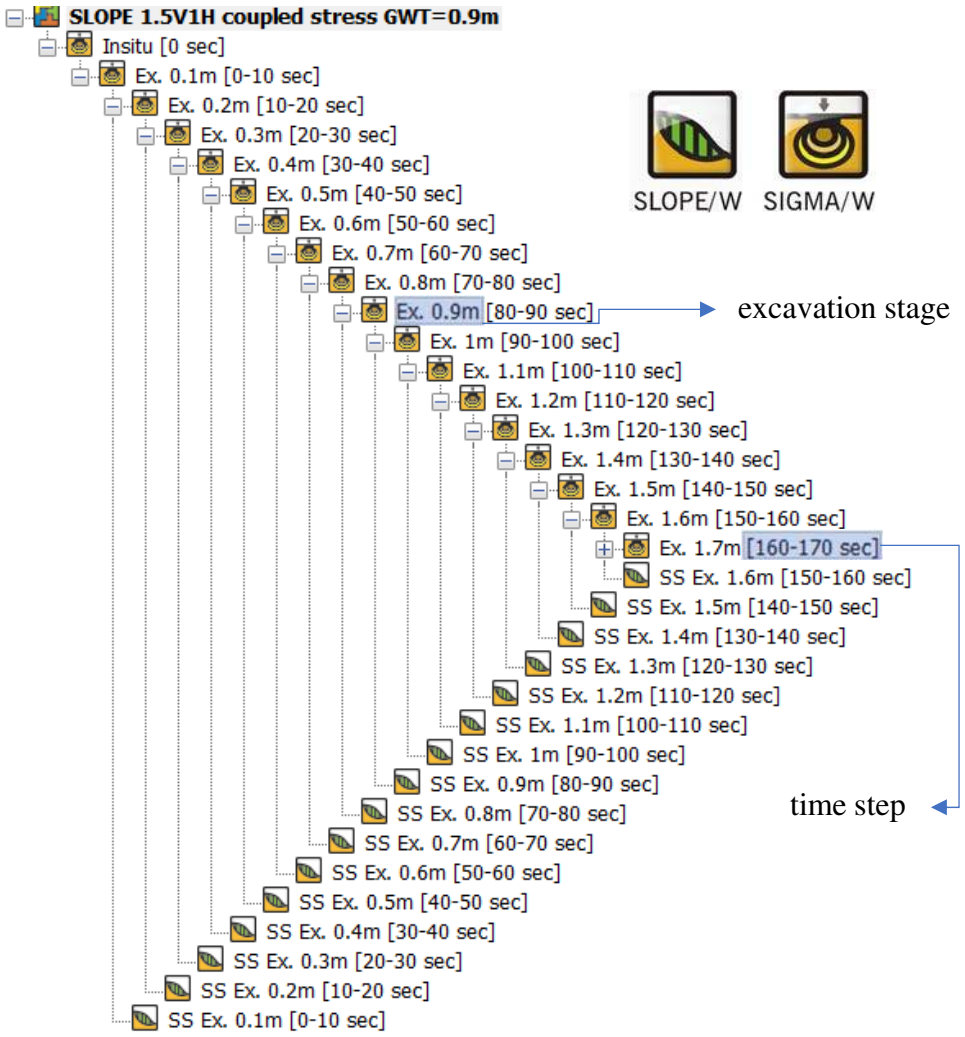

Figure 5.4. Example of slope stability analysis tree used in the coupled analyses (10-s time steps between excavations)

The ‘Entry and Exit’ slip surface method was used for generating potential slip surfaces. The exit was specified as a point at the toe of the excavation, and the entry was defined as a range as wide as the excavation depth with a possible entry point every 10-mm along the ground surface (Figure 4.14). The critical height was defined as the excavation depth that showed FOS = 1.0 (e.g. Figure 5.5), or the depth prior to the excavation stage that showed FOS < 1.0 in the stability analysis. Contours in Figure 5.5 indicates PWP with depth.

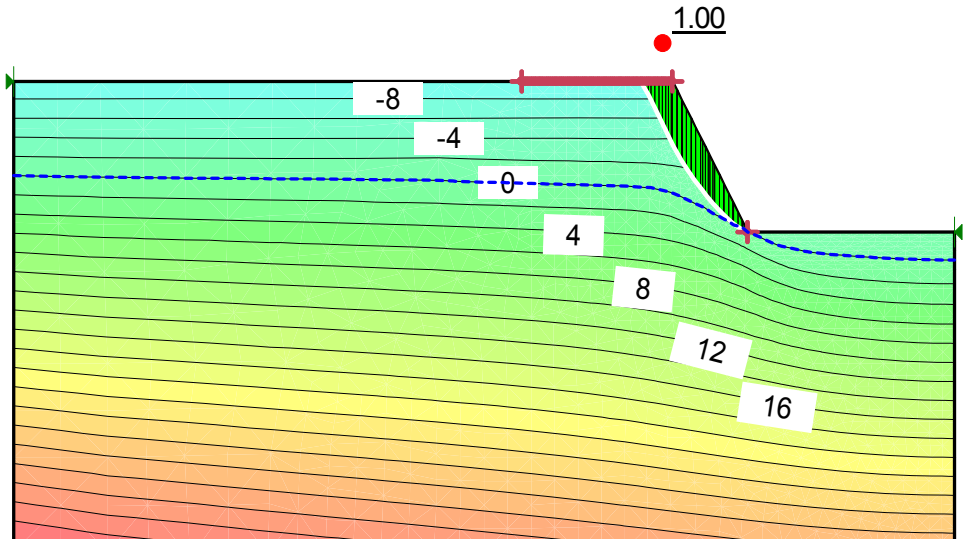

Figure 5.5. Example of slope stability analysis using SIGMA-Stress method in SLOPE/W (1.5V:1H)

5.2 Estimating the Critical Height with the Limit Equilibrium Method

Stability analyses were also conducted with the LEM for the same scenarios used in the coupled analyses to investigate the differences. Among various solutions to the LEM, the method proposed by Morgenstern & Price (1965; hereafter referred to as M-P method) was used in this chapter. Setting up the analysis domain in SLOPE/W for the M-P method is the same as a Bishop analysis as described in Chapter 4 (Figure 4.11, Figure 4.12, and Figure 4.14). The interslice forces are statically indeterminate with the LEM, therefore various solutions exist based on the assumptions made to solve for equilibrium. In Bishop's simplified method, the interslice shear forces are assumed to be equal and opposite to solve for equilibrium. However, the M-P method accounts for both interslice normal and shear forces, assuming that the interslice shear force is a function of a scaling factor, an interslice force function, and the interslice normal force, as shown in Eq. (5.3).

$$X = \lambda f(x) E \tag{5.3}$$

where X = interslice shear force per unit length, E = interslice normal force per unit length, λ = scaling factor, and $f(x)$ = specified interslice force function

The interslice force function describes how the magnitude of X/E varies across the failure surface. The assumption regarding the interslice force function may lead to convergence issues depending on the stress distribution and slope geometry (Ching & Fredlund 1983). The half-sine interslice force function was used in this chapter, because it was chosen as the default setting in SLOPE/W due to user experience and intuition (GEO-SLOPE 2015). The half-sine function causes the slices on the ends of the slip surface to have the lowest

shear-to-normal stress ratio, and the slices in the middle have the highest (Figure 5.6). Once $f(x)$ is specified, λ is varied systematically to determine the value at which moment and force equilibrium have the same FOS. The corresponding λ value is multiplied by the specified $f(x)$ to get the applied $f(x)$, which provides the assumed shear-to-normal stress ratio for each slice (Figure 5.6).

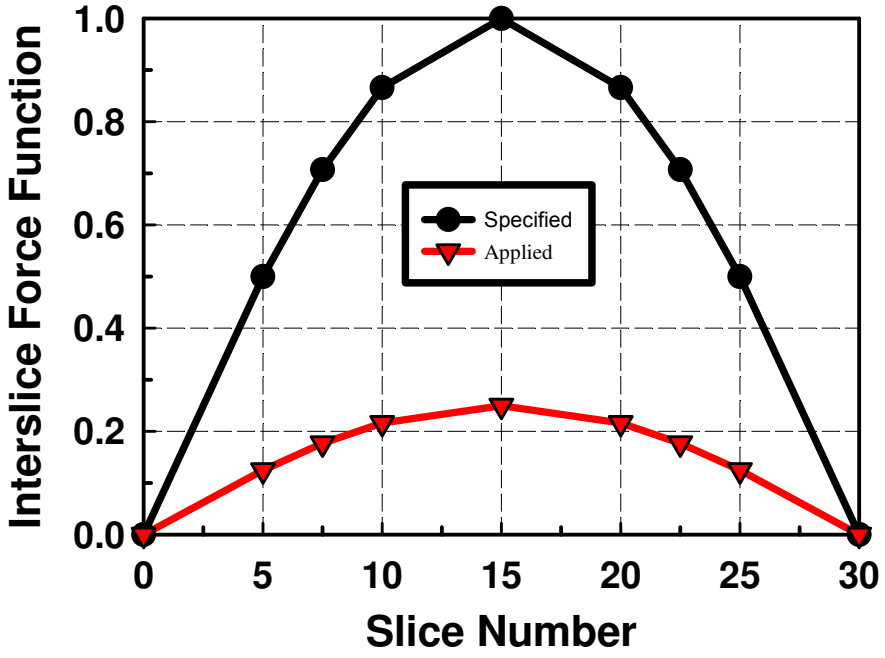

Figure 5.6. Example of half-sine function used in M-P analyses ($\lambda = 0.25$)

If λ equals zero, the M-P method becomes the same as Bishop's simplified method (i.e. internal shear forces are equal and opposite). Bishop's simplified method is appropriate when rotational failure is likely because no slippage between slices is required for a soil mass to rotate along a circular slip surface. However, significant slippage and internal shearing must occur for a soil mass to translate along a circular slip surface. Translational failure becomes more likely in a cohesionless soil as the slope angle approaches the internal friction angle. Therefore, the FOS can be unrealistic using Bishop's simplified method for

sloped excavations in sand. This indicates that the M-P method is more appropriate to analyze trench stability for the cases examined in this chapter. However, it should be noted that the interslice and slip surface forces assumed in the LEM may not represent in-situ stress conditions. Nevertheless, the global FOS from the M-P method is normally acceptable and adequately addresses general failure (Krahn 2003).

Figure 5.7 shows the forces acting on a slice within an arbitrary slip surface and defines all geometric parameters. Lateral pressure due to water in tension cracks (A_R), external point load (D), and seismic loads (kW), were not considered in the analyses and are therefore omitted from the equations for calculating the FOS. In saturated soil, the FOS with respect to moment and force equilibrium is calculated using Eq. (5.4) and Eq. (5.5), respectively. The normal force is computed using Eq. (5.6).

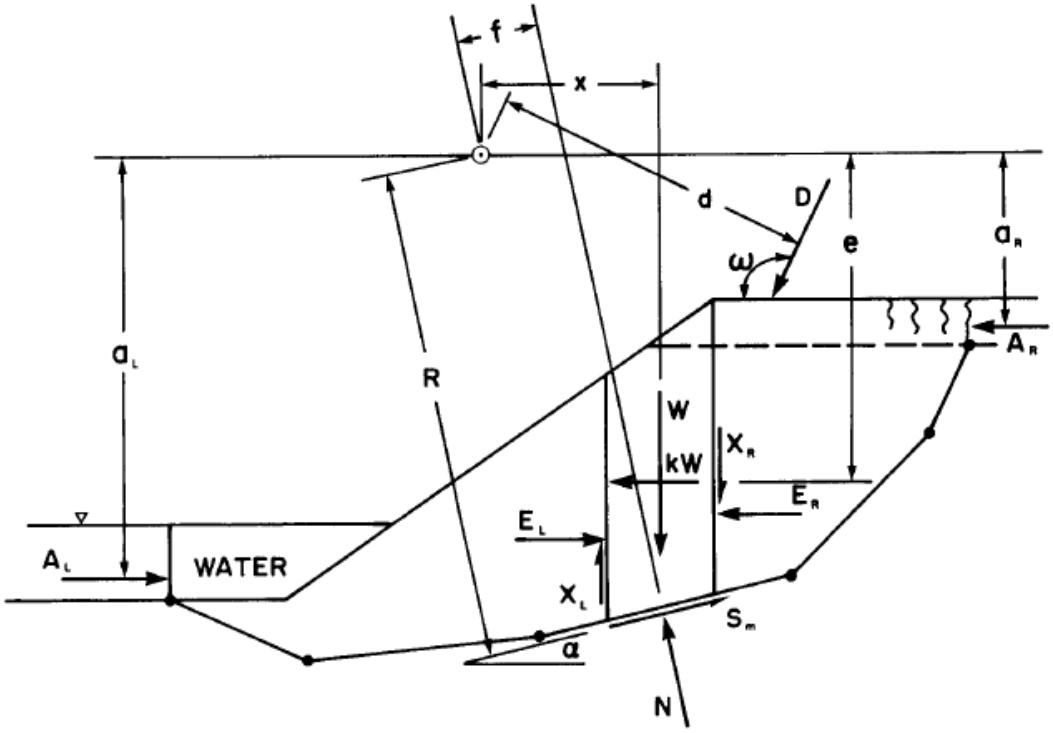

Figure 5.7. Forces acting on a slice within an arbitrary slip surface (GEO-SLOPE 2015)

$$FOS_m = \frac{\sum (c'\beta R + (N - u\beta) R \tan \phi')}{\sum Wx - \sum Nf} \tag{5.4}$$

$$FOS_f = \frac{\sum (c'\beta \cos\alpha + (N - u\beta) \tan \phi' \cos\alpha)}{\sum N \sin\alpha} \tag{5.5}$$

$$N = \frac{W + (X_R - X_L) - \dfrac{c'\beta \sin\alpha + u\beta \sin\alpha \tan\phi'}{FOS}}{\cos\alpha + \dfrac{\sin\alpha \tan\phi'}{FOS}} \tag{5.6}$$

Where FOS_m = factor of safety for moment equilibrium, FOS_f = factor of safety for force equilibrium, N = slice base normal force per unit length ($FOS = FOS_m$ or FOS_f)

Extending Eq. (5.4) and (5.5), SLOPE/W computes the FOS in unsaturated soil for moment and force equilibrium as shown in Eq. (5.7) and (5.8), respectively (Fredlund & Krahn 1977, Fredlund et al. 1981). The normal force, N, is computed as shown in Eq. (5.9).

$$FOS_m = \frac{\sum \left(c'\beta R + \left[N - u_w \beta \dfrac{\tan\phi^b}{\tan\phi'} - u_a \beta \left(1 - \dfrac{\tan\phi^b}{\tan\phi'} \right) \right] R \tan\phi' \right)}{\sum Wx - \sum Nf} \tag{5.7}$$

$$FOS_f = \frac{\sum \left(c'\beta \cos\alpha + \left[N - u_w \beta \dfrac{\tan\phi^b}{\tan\phi'} - u_a \beta \left(1 - \dfrac{\tan\phi^b}{\tan\phi'} \right) \right] \tan\phi' \cos\alpha \right)}{\sum N \sin\alpha} \tag{5.8}$$

$$N = \frac{W + (X_R - X_L) - \dfrac{\left[c'\beta \sin\alpha + u_a \beta \sin\alpha (\tan\phi' - \tan\phi^b) + u_w \beta \sin\alpha \tan\phi^b \right]}{FOS}}{\cos\alpha + \dfrac{\sin\alpha \tan\phi'}{FOS}} \tag{5.9}$$

5.3 Comparison of Limit Equilibrium and Finite Element Approaches

The FOS of a trench may be relatively high immediately after excavating but may decrease over time as the GWT and PWP return to equilibrium. This sort of scenario may occur in practice if an excavation is made rapidly to a desired depth and left open for some period. Figure 5.8 shows the variation of deformation, PWP, and FOS with time for the case of a 1.5V:1H sloped excavation staged in 0.1-m increments up to 1.3-m at 10-s time steps, with the GWT initially set at 0.7-m. The time step for the 1.3-m stage was increased to 1,000-s (Figure 5.4) to allow the GWT to rebound. The black arrows represent hydraulic velocity vectors, and the magnitude decreases with time as PWP approaches equilibrium. The sequence in Figure 5.8 shows how an excavation may appear stable but fail shortly thereafter (i.e. 750-s in this example). As discussed previously, removing soil from the ground relieves confining pressures which results in expansion of the soil adjacent to the excavated surface. Figure 5.8 clearly shows that the deformations along the excavation face gradually increase over time. This phenomenon contributes to the decrease in FOS with time as shown in Figure 5.9.

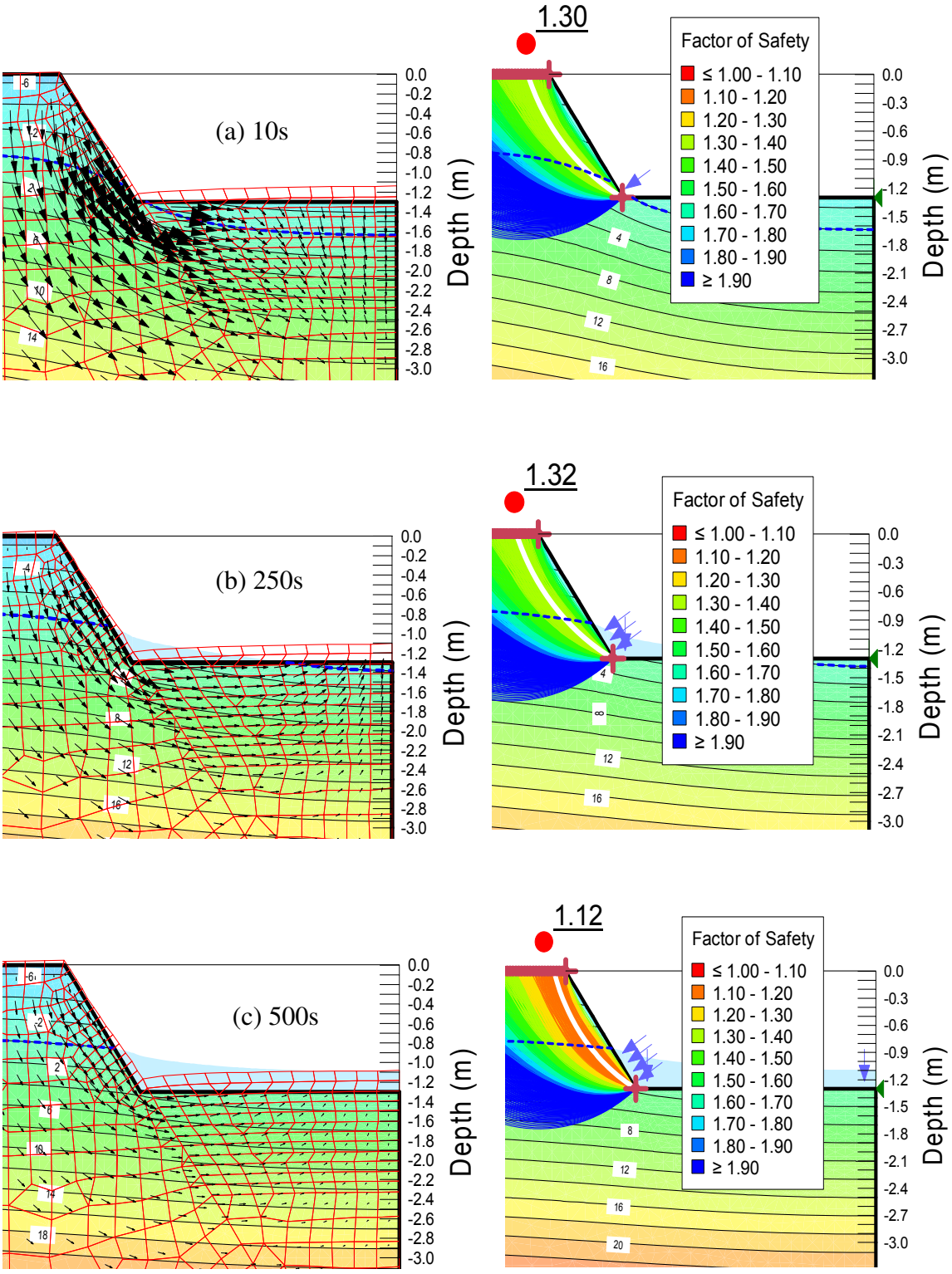
(a) 10s
1.30
Factor of Safety
≤ 1.00 - 1.10
1.10 - 1.20
1.20 - 1.30
1.30 - 1.40
1.40 - 1.50
1.50 - 1.60
1.60 - 1.70
1.70 - 1.80
1.80 - 1.90
≥ 1.90
Depth (m)
(b) 250s
1.32
Factor of Safety
Depth (m)
(c) 500s
1.12
Factor of Safety
Depth (m)

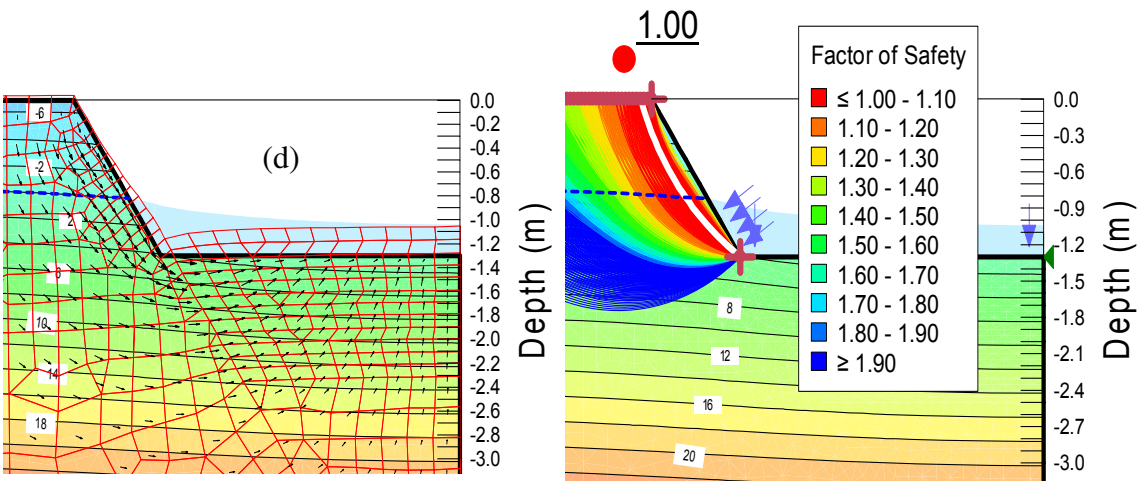

Figure 5.8. Variation of deformation, PWP, and FOS with time for (a) 10-s, (b) 250-s, (c) 500-s, and (d) 750-s after 1.3-m excavation stage with initial D = 0.7-m

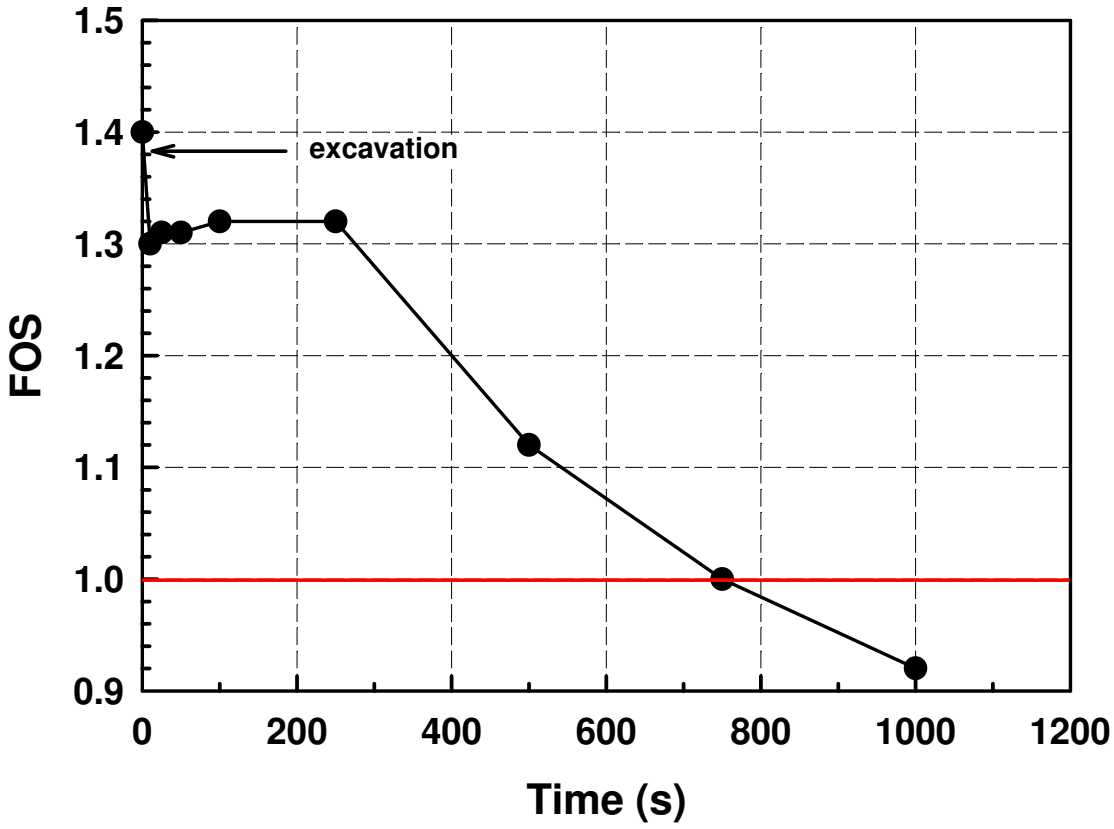

Figure 5.9. FOS vs. Time for 1.3-m excavation stage (1.5V:1H) with initial D = 0.7-m

Negligible changes in matric suction are observed near the ground surface throughout the time steps used in the analysis. This implies that the slope failure is governed by the change in matric suction distribution between the initial GWT and the toe of the slope. The FOS remains relatively constant during the first 250-s because the length of slip surface below the GWT is relatively unchanged, even though the GWT increases with time. However, the FOS drops rapidly with time once the length of slip surface below the GWT exceeds what can be considered the critical length of the slip surface under saturated condition.

In geotechnical engineering practice, trenches may be excavated at a relatively fast rate between stages without allowing the GWT to rebound to its original level. However, once a trench is excavated up to the targeted depth, PWP will gradually approach equilibrium. This may occur while field workers are completing their jobs in the trench. As shown in Figure 5.9, a trench may appear stable initially but can fail over time as the GWT rebounds. It is interesting to note that failure can occur even before PWP reaches equilibrium. Figure 5.8(d) shows FOS = 1 after 750-s without equilibrium being reached, as evidenced by the hydraulic velocity vectors.

To further investigate how the redistribution of PWP caused by excavating affects the critical height of unsupported trenches, slope stability analyses were carried out for two different time steps; namely, 10-s and 1000-s. These time steps were chosen to simulate fast and slow excavation rates, respectively. Figure 5.10 and Figure 5.11 show the variation of the critical height with respect to the depth of the GWT for five different excavation scenarios with 10-s and 1,000-s time steps, respectively. Figure 5.12 shows the variation of the critical heights estimated using the M-P method for the same scenarios used in the coupled analyses. The critical height increases as trench slope is reduced regardless of the

level of the GWT. This indicates that sloping trenches is an effective way to increase the critical height. For 10-s time steps, the critical height of the 1.5V:1H slope was estimated to be 2.6 times higher compared to the vertical trench for some cases. The critical height of the vertical trench increases as the depth of the GWT increases and then declines sharply once the GWT is deeper than 1-m.

The critical heights estimated from the three methods are plotted for the 90°, 3V:1H, 2V:1H, and 1.5V:1H excavation scenarios in Figure 5.13 to Figure 5.16, respectively (90*** is explained later).

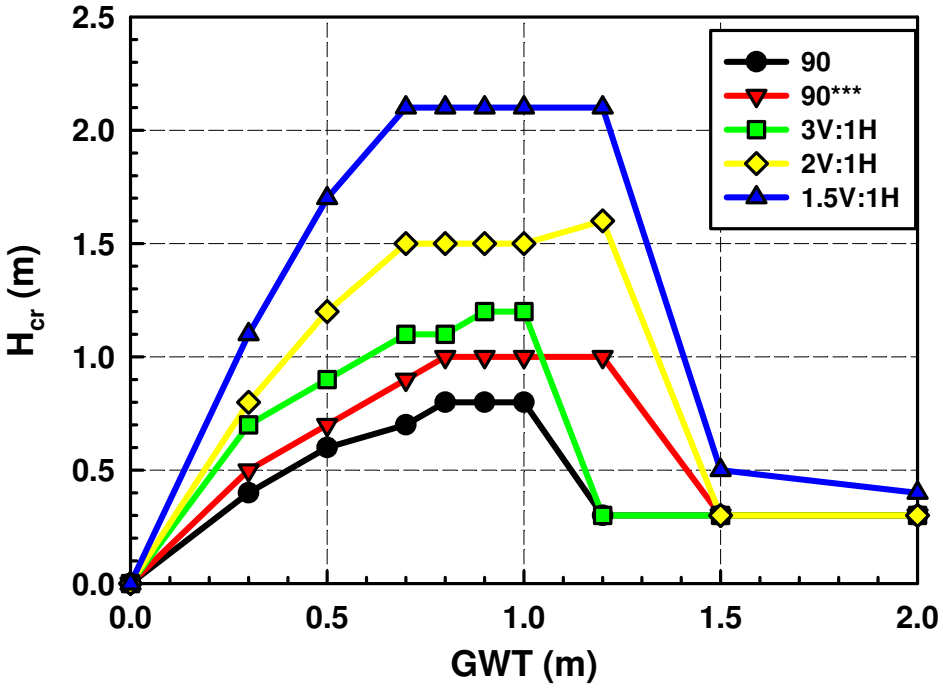

Figure 5.10. Variation of the critical height for different sloping angles in Unimin 7030 sand (10-s time steps, coupled analysis)

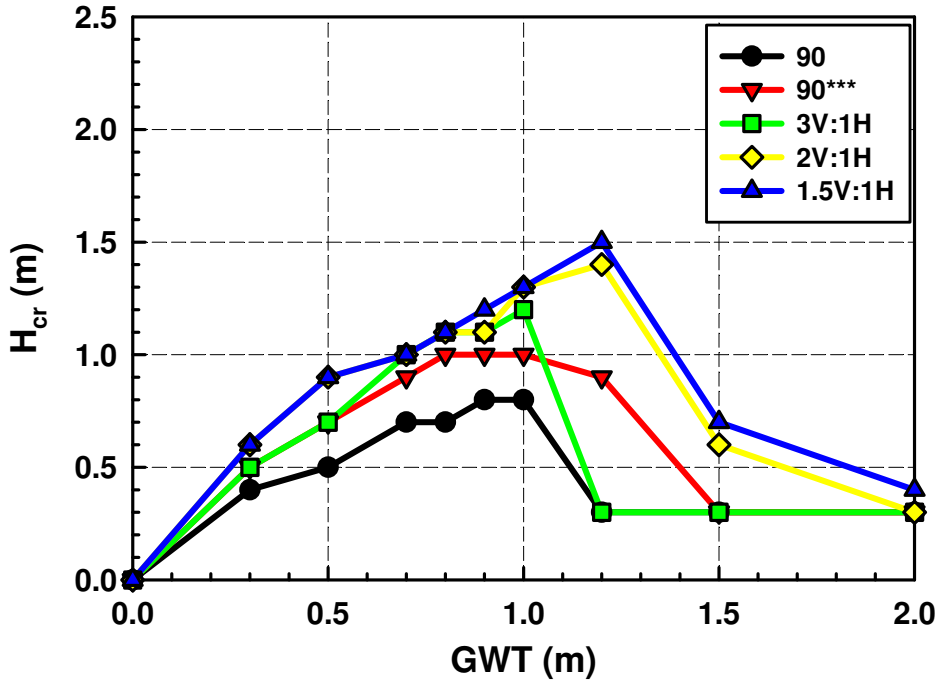

Figure 5.11. Variation of the critical height for different sloping angles in Unimin 7030 sand (1,000-s time steps, coupled analysis)

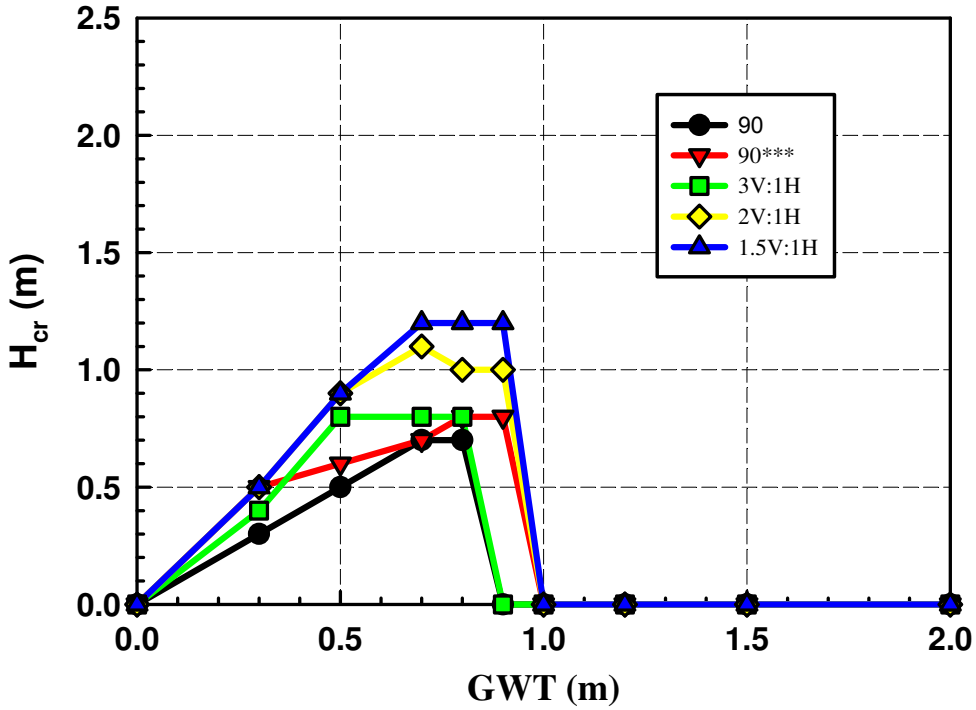

Figure 5.12. Variation of the critical height for different sloping angles in Unimin 7030 sand (M-P method)

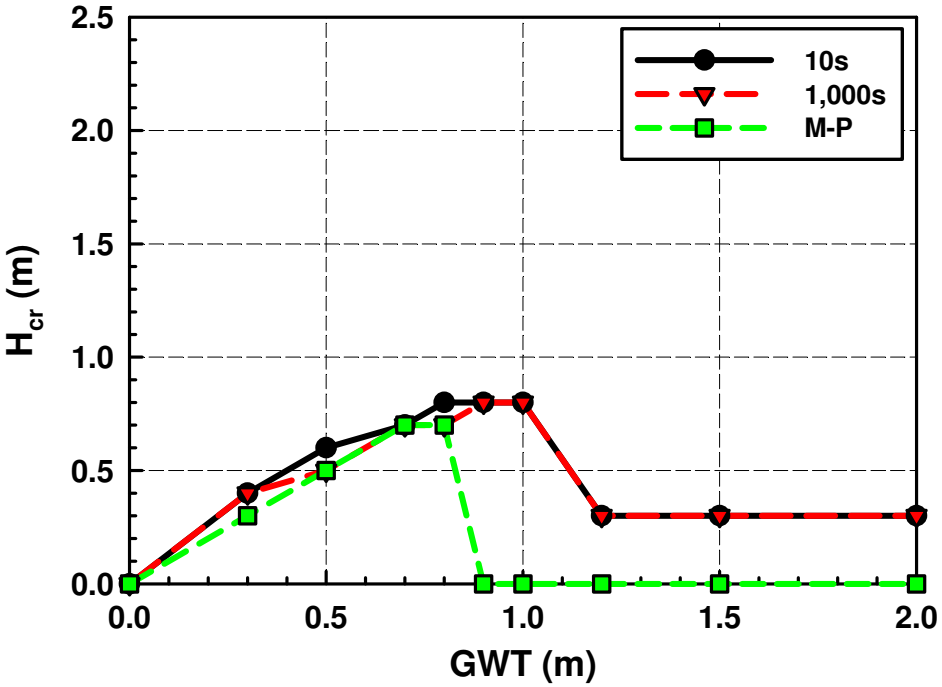

Figure 5.13. Variation of the critical height for 90° slope in Unimin 7030 sand

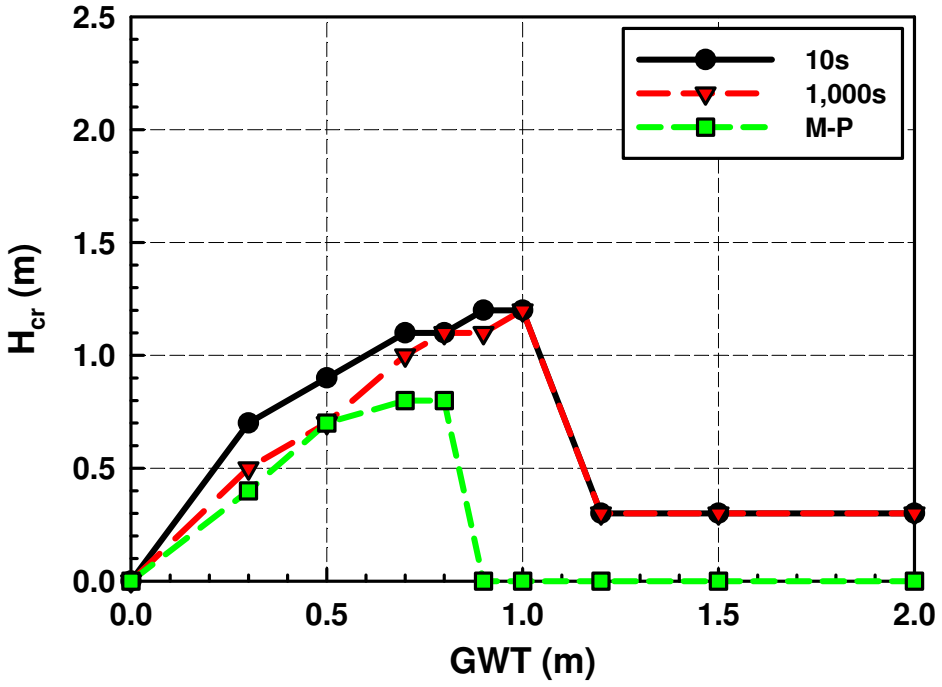

Figure 5.14. Variation of the critical height for 3V:1H slope in Unimin 7030 sand

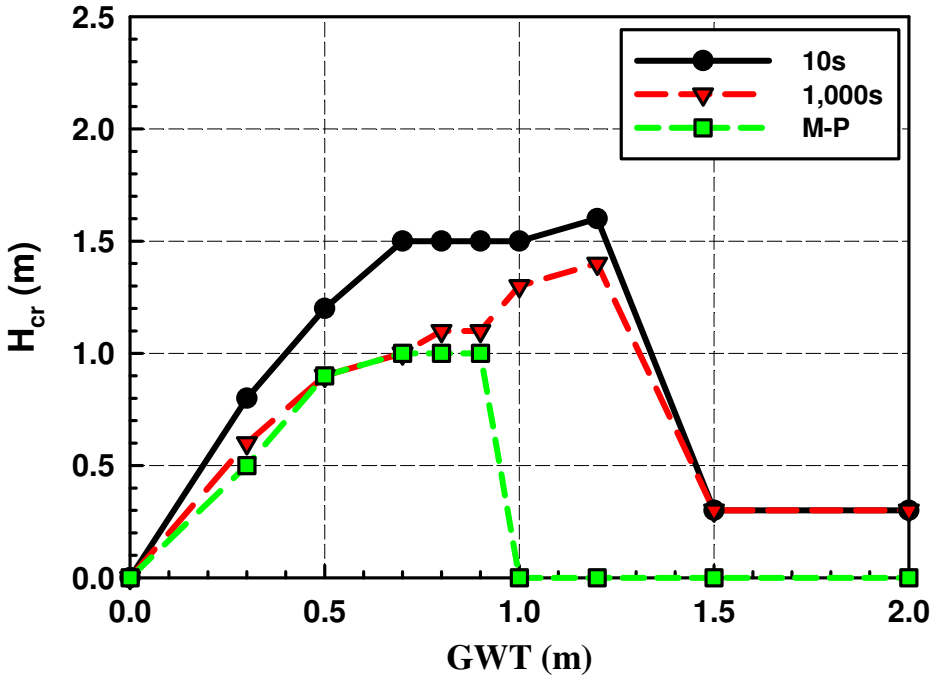

Figure 5.15. Variation of the critical height for 2V:1H slope in Unimin 7030 sand

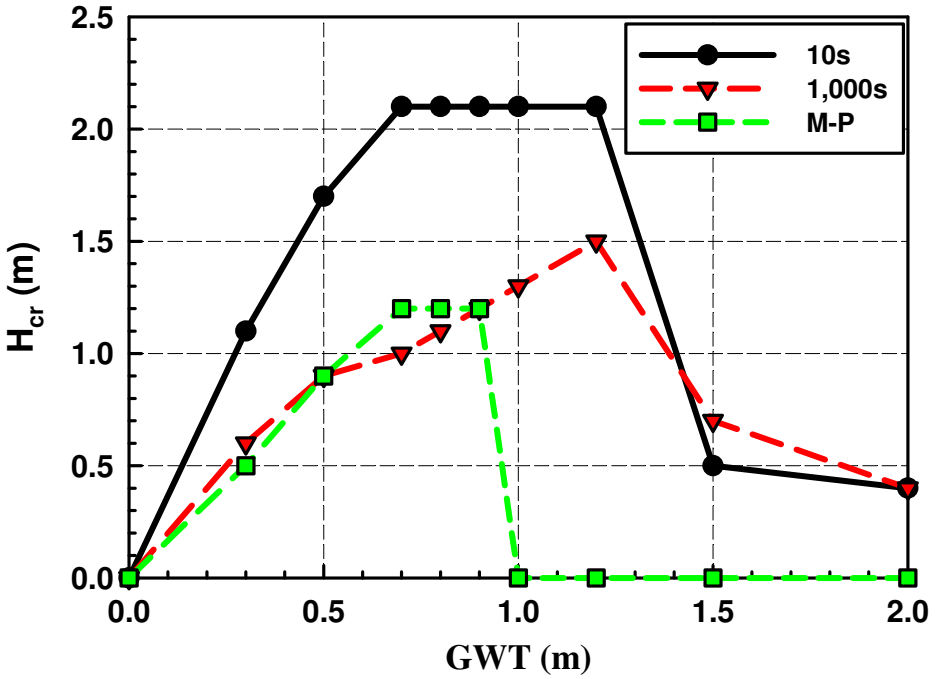

Figure 5.16. Variation of the critical height for 1.5V:1H slope in Unimin 7030 sand

As expected, the critical heights estimated using the M-P method showed the lowest values. The critical height decreases as the period between excavation stages increases (i.e. 10-s to 1,000-s time steps). This is because 10-s time step excavations force the GWT to continue dropping without giving enough time to rebound a significant amount.

When a soil mass is removed from the ground, the soil within the proximity of the excavation experiences stress relief ranging from $K_0\sigma_z$ to σ_z in the horizontal and vertical directions, respectively (where σ_z is the vertical stress at a depth z, and K_0 is the coefficient of earth pressure at-rest). This indicates that the stress relief in the soil near the ground surface is minimal (or close to zero), and PWP changes are negligible. Therefore, as the slope of a trench decreases, more stress relief occurs along the face of the slopes and the change in PWP increases accordingly. For this reason, the largest difference in the critical heights between the coupled analysis (10-s) and the M-P method is observed for the 1.5V:1H slope. For coupled analyses with 1,000-s time steps, most negative excess PWP dissipates and the critical heights show small discrepancies with the M-P method when the GWT is less than 1-m. When the GWT is deeper than 1-m, the critical heights estimated with the M-P method are zero, but the coupled analyses show minimum values of 0.3-m.

Stability analyses based on limit equilibrium conditions are normally more conservative compared with that of finite element stress-based analyses. However, there are advantages to using finite element stress-based stability analyses such as i) displacement compatibility is satisfied and ii) the ground stresses are much closer to reality (Krahn 2003). The main reason for this difference is related to the concentration of normal and shear stress in the toe area of a slope as shown in Figure 5.17 and Figure 5.18, respectively. This phenomenon

may increase frictional resistance and in turn increase the local FOS in the slices near the toe of the slope. For this reason, a sloped trench can be can be excavated past the residual zone near the ground surface even when the GWT is relatively deep (i.e. deeper than 1-m).

The critical height increases for the vertical excavation as the depth of the GWT increases up to 0.8-m, and then declines sharply thereafter. As explained previously, a deep GWT creates a residual suction zone near the ground surface which results in a complete loss of total cohesion (Figure 5.19). To further investigate this behavior, additional analyses were conducted for a vertical trench with the first 0.3-m of excavation sloped 1:1 (denoted as 90***) as shown in Figure 5.20. The results from the three methods for the 90*** case are plotted in Figure 5.21. For the M-P method, the maximum attainable critical height in a vertical trench was increased by 0.1-m and was sustained for an additional 0.1-m increase in the depth of the GWT by sloping the soil in the residual zone. For the coupled analyses, the 90*** case provides higher critical heights with the GWT between 0.5 and 1.5-m. This indicates that benching or sloping the soil in the residual zone can effectively increase the critical height. Furthermore, sloping the residual zone may be more effective in some cases than sloping the entire trench wall (Figure 5.10, Figure 5.11, and Figure 5.12).

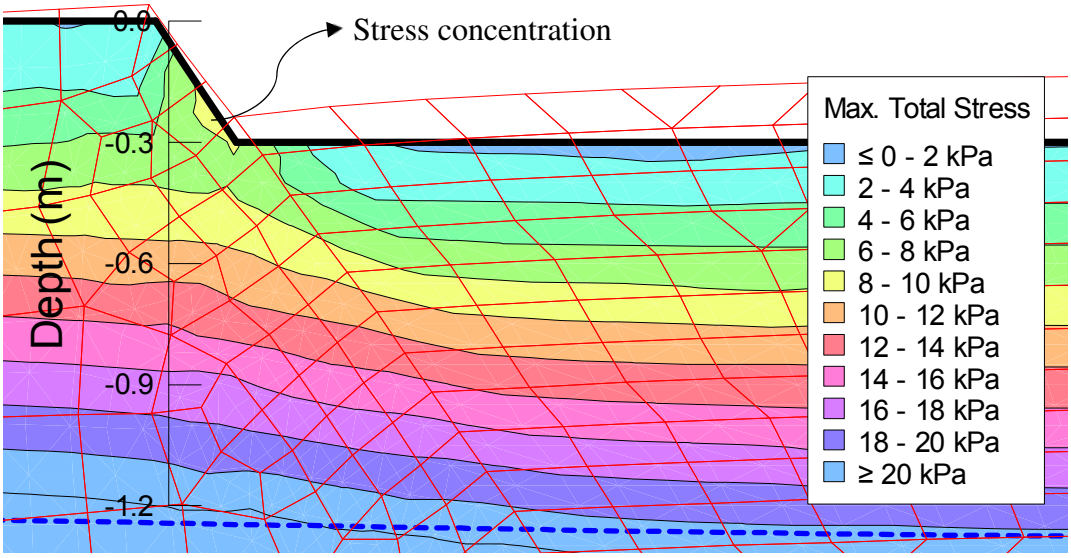

Figure 5.17. Distribution of total normal stress during 0.3-m excavation stage for 1.5V:1H slope with initial D = 1.2-m (10-s time steps)

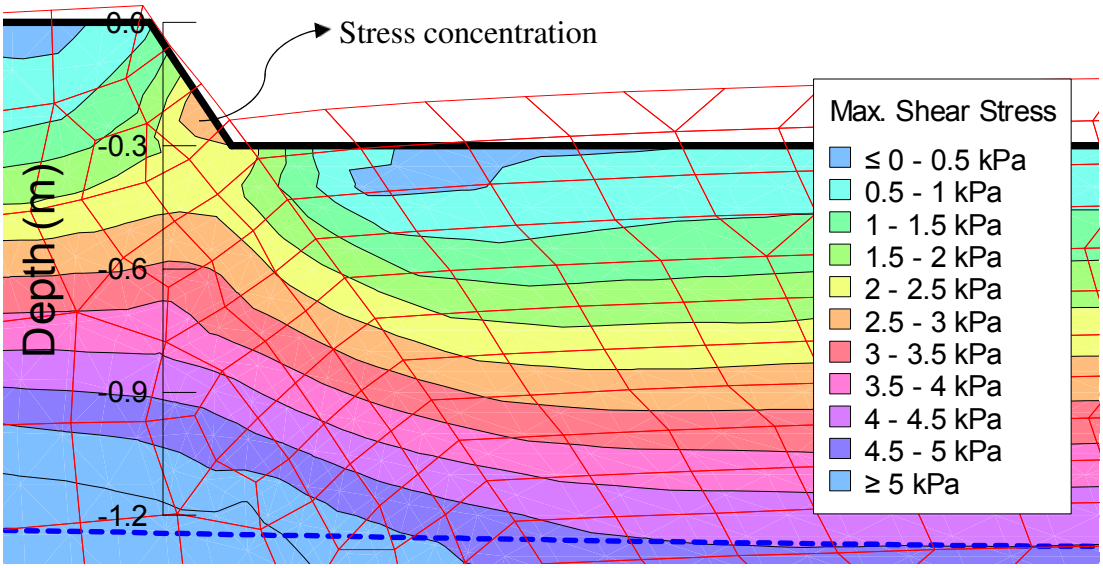

Figure 5.18. Distribution of shear stress during 0.3-m excavation stage for 1.5V:1H slope with initial D = 1.2-m (10-s time steps)

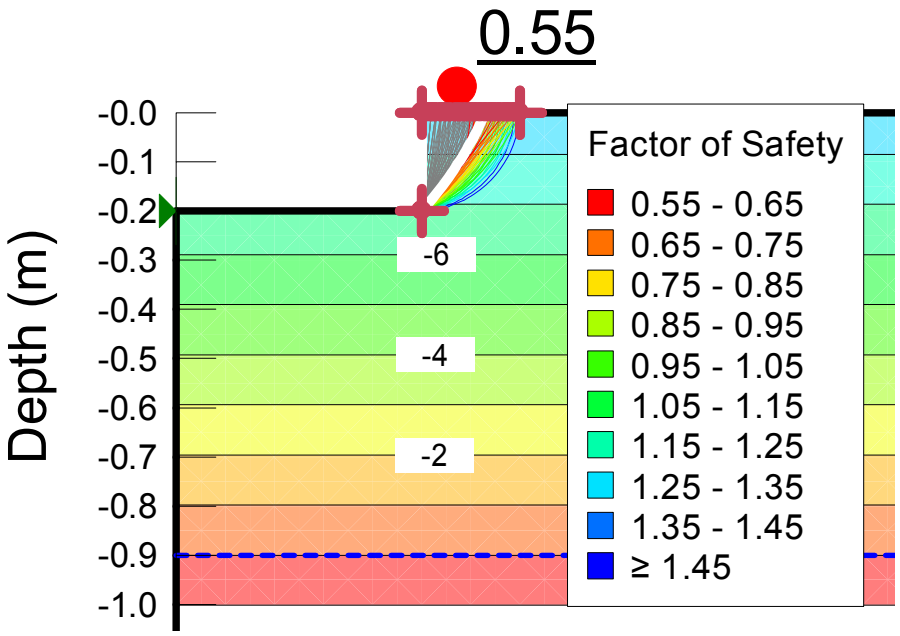

Figure 5.19. Vertical trench with D = 0.9-m (M-P method)

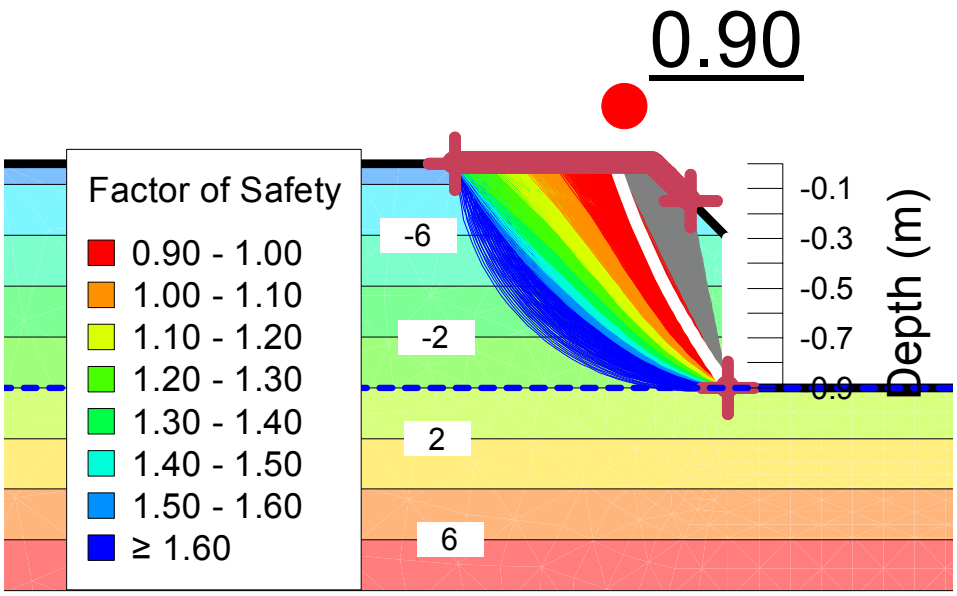

Figure 5.20. Partially sloped (1:1) vertical trench with D = 0.9-m (M-P method)

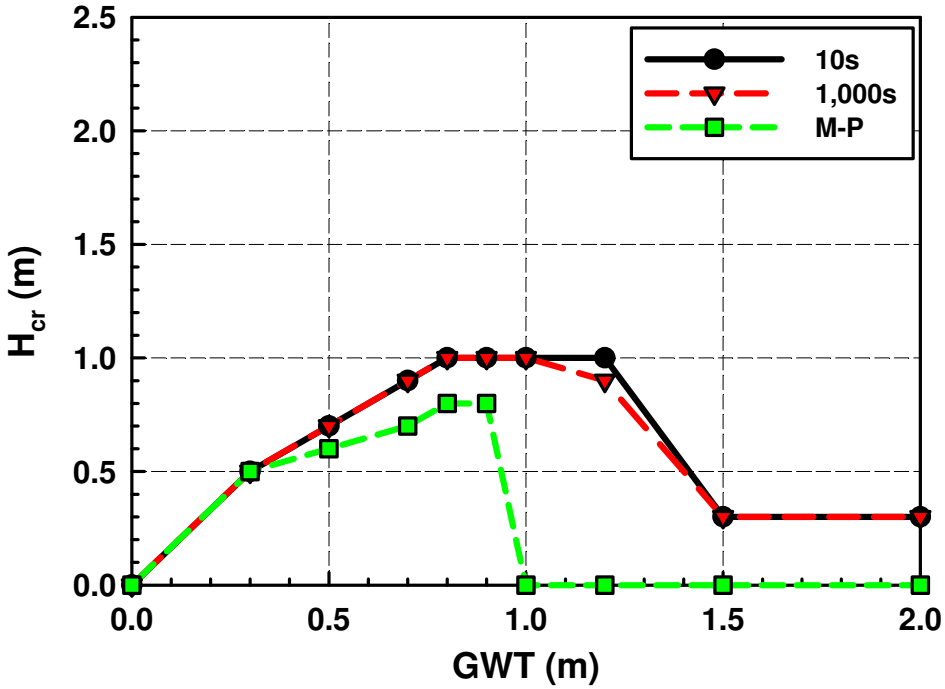

Figure 5.21. Variation of the critical height for 90*** slope in Unimin 7030 sand

5.4 Summary and Conclusions

M-P and coupled analysis methods were used to investigate the influence of various slopes and matric suction distributions on the critical height of unsupported trenches in an unsaturated sand. The coupled analyses show that a trench may appear stable initially and result in failure as PWP returns to equilibrium conditions. Thus, it is more conservative to assume a hydrostatic PWP distribution when estimating the critical height. Overall, sloping the trench greatly increases the critical height. This lends credibility to Canadian provincial standards (Ontario 2017), as they state a 1:1 slope is sufficient for most excavations where a vertical trench cannot be excavated to a significant depth. The results also show that the critical height can be almost doubled by flattening the slopes compared to a vertical excavation. The main advantage of flattening the slope is that a greater critical height can

be achieved even when residual suction is reached near the ground surface. The critical height was increased as the slope angle was reduced; however, it may not always be possible to provide a gentle slope to the excavation in geotechnical engineering practice due to limited space. In this case, a combination of sloping and benching can be used effectively to achieve targeted critical heights, especially when the soil surface is within the range of residual suction.

CHAPTER 6

ESTIMATING THE CRITICAL HEIGHT OF UNSUPPORTED VERTICAL TRENCHES SUBJECTED TO SURCHARGE PRESSURE

In this chapter, the critical height of unsupported vertical trenches in an unsaturated fine-grained soil is investigated considering practical scenarios. The trenches were assumed to be excavated into Indian Head till (hereafter referred to as IHT).

In well-developed cities, there are circumstances where trenches must be excavated adjacent to an existing superstructure to install or remediate municipal infrastructure such as storm drains or utility lines. In these cases, the critical height of unsupported vertical trenches is affected by the stress beneath an existing shallow foundation (hereafter referred to as foundation stress). Hence, analyses were conducted for multiple foundation stresses (10, 20, 30, and 50-kPa) located at various distances from the edge of an excavation (1, 2, 3, and 5-m) to simulate this practical scenario. Each scenario was modelled with the GWT at a depth of 0, 1, 2, 3, and 5-m below the shallow foundation (referred to as depth, D).

6.1 Soil Properties

Basic soil properties of IHT are shown in Table 6.1. The grain size distribution curve and the SWCC of IHT are shown in Figure 6.1 and Figure 6.2, respectively. The SWCC was best-fitted using Eq. (4.1) and the parameters, *a, m*, *n* are shown in the figure. The shear strength parameters, *c'* and ϕ' determined by Vanapalli et al. (1997) and Oh &Vanapalli (2010) were used in the analyses.

Table 6.1. Basic soil properties of IHT (Vanapalli et al. 1997, Oh & Vanapalli 2010)

Properties	Value
Plasticity Index, I_p (%)	15.5
Saturated unit weight, γ_{sat} (kN/m^3)	20.7
Void ratio, e	0.55
Specific gravity, G_s	2.72
Effective cohesion, c' (kPa)	5
Effective internal friction angle, ϕ' (˚)	23.1

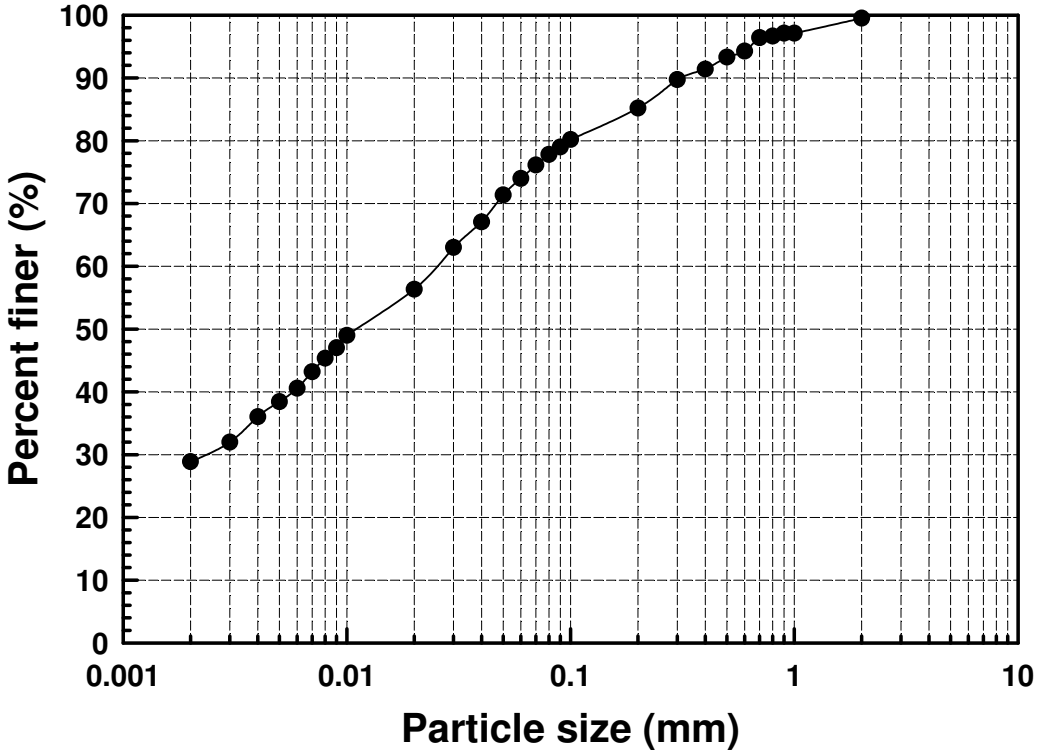

Figure 6.1. Grain size distribution curve of IHT (Oh &Vanapalli 2010)

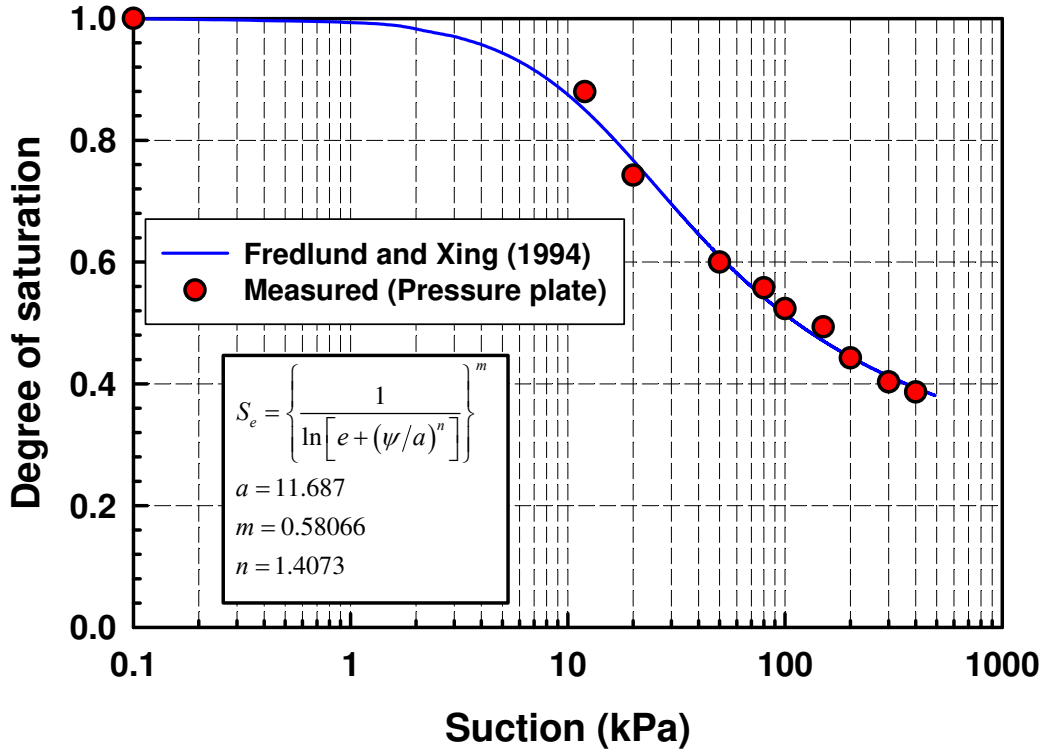

Figure 6.2. SWCC of IHT (Oh & Vanapalli 2018)

6.2 Estimating the Critical Height without Foundation Stress

In this section, critical heights are estimated using extended Rankine earth pressure theory and Bishop's simplified method (see sections 4.2 and **Error! Reference source not found.** for more details) without considering foundation stress. This scenario represents the case where an arbitrary foundation stress is sufficiently far away from the trench such that the critical height of an unsupported vertical trench is not affected by the foundation.

6.2.1 Estimating the Critical Height with EREPT

The positive, negative, and net AEP distributions for cases with D = 0, 1, 3, and 5-m are shown in Figure 6.3 to Figure 6.6, respectively.

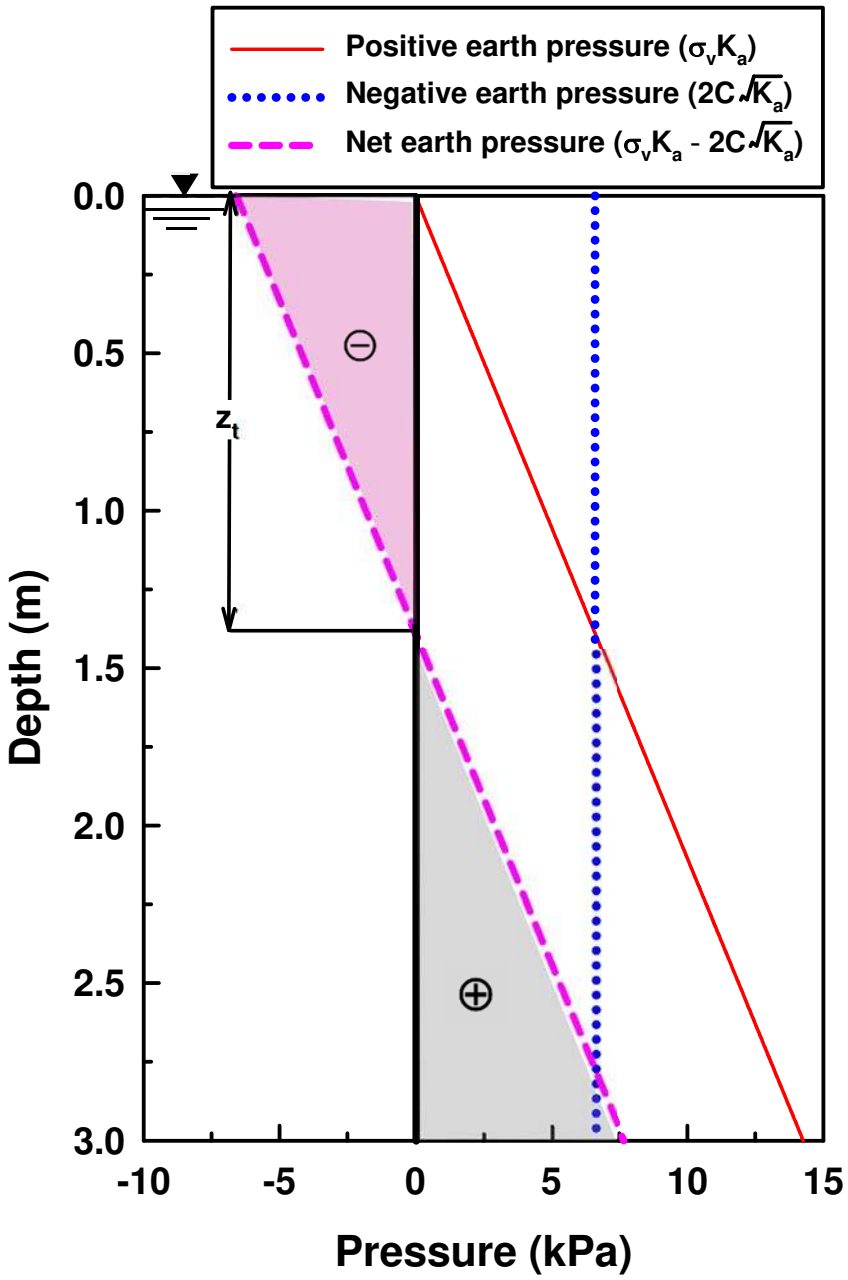

Figure 6.3. Positive, negative, and net AEP distribution (D = 0-m)

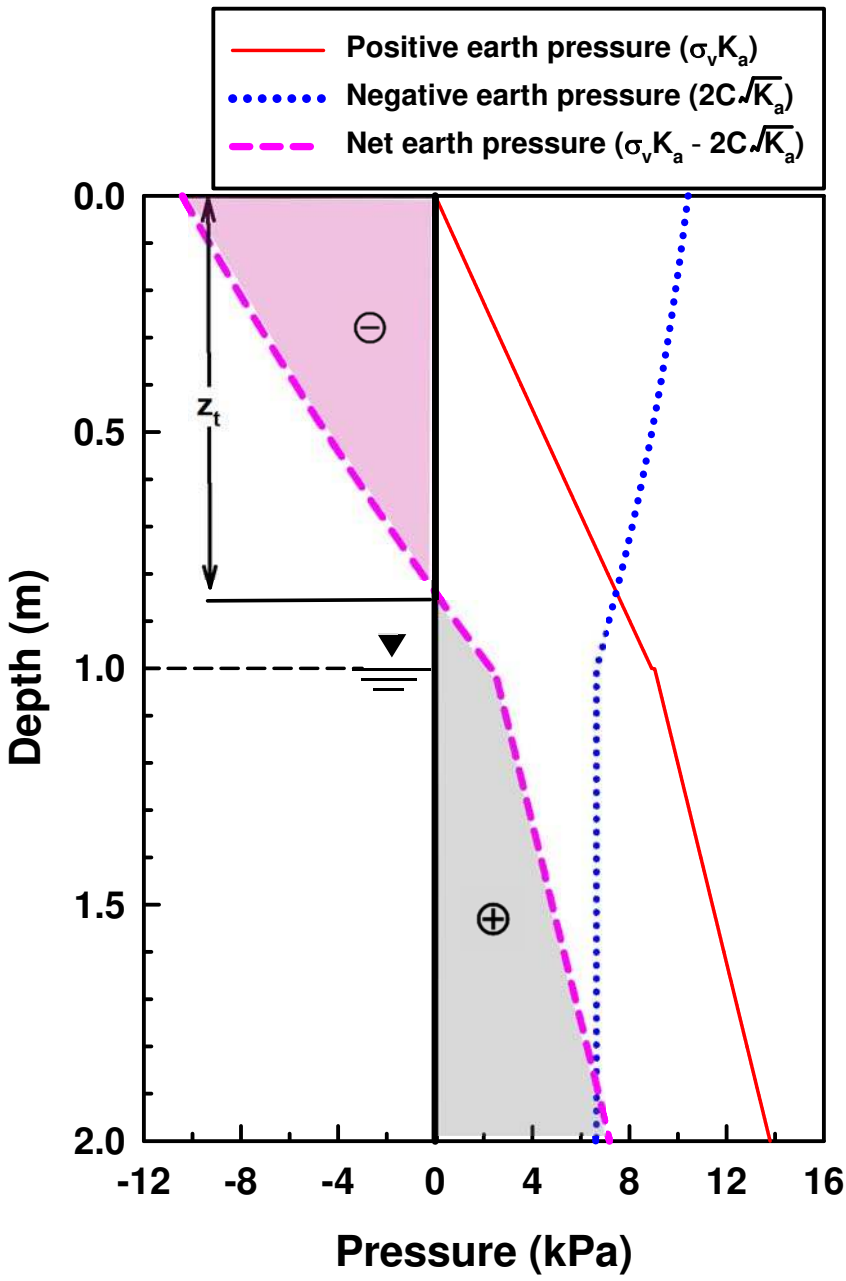

Figure 6.4. Positive, negative, and net AEP distribution (D = 1-m)

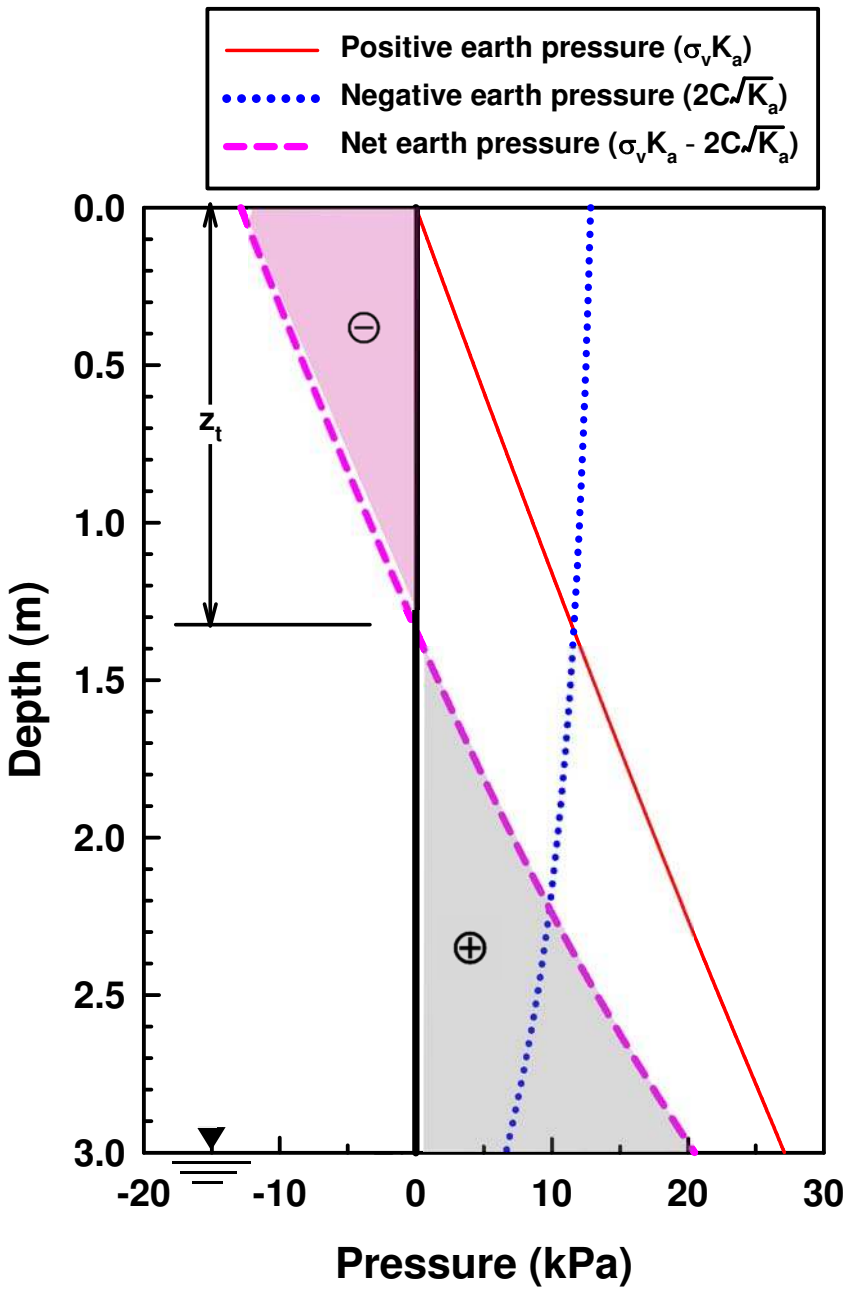

Figure 6.5. Positive, negative, and net AEP distribution (D = 3-m)

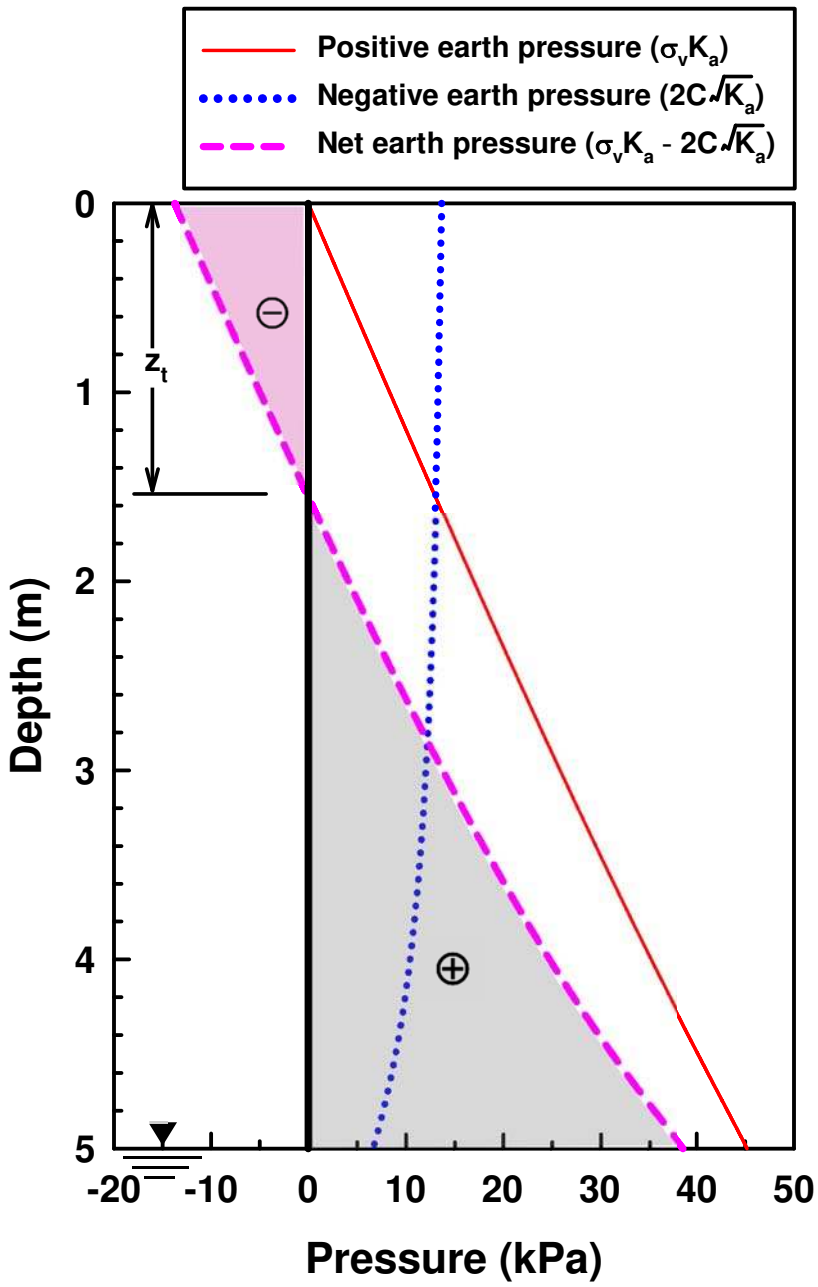

Figure 6.6. Positive, negative, and net AEP distribution (D = 5-m)

6.2.2 Estimating the Critical Height with BSM

Figure 6.7 to Figure 6.10 show the slope stability analyses using Bishop's simplified method with D = 0, 1, 3, and 5-m, respectively.

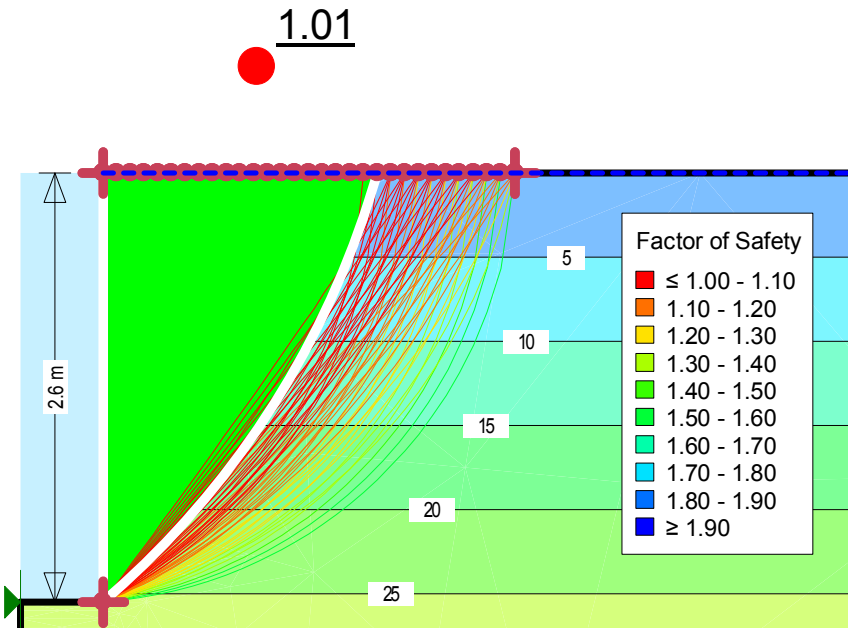

Figure 6.7. Slope stability analysis in SLOPE/W using Bishop's simplified method (D = 0-m)

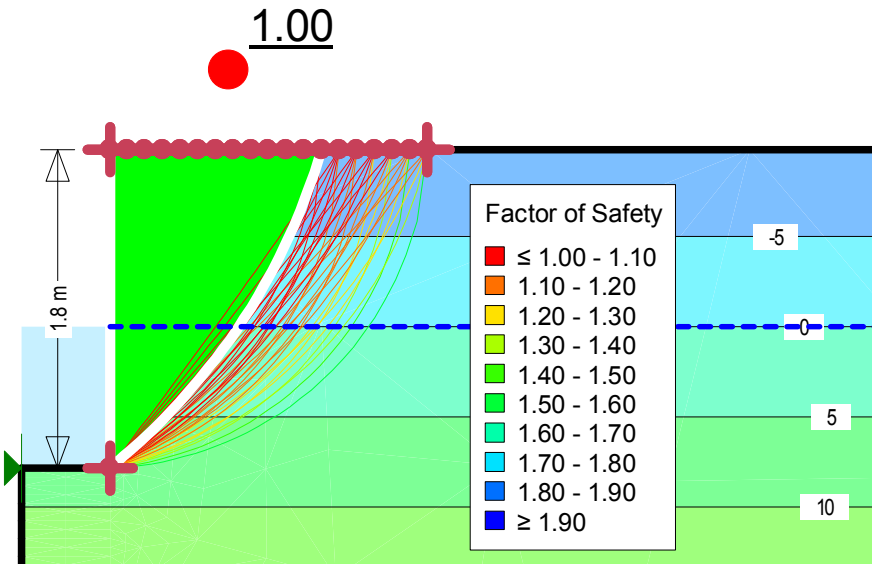

Figure 6.8. Slope stability analysis in SLOPE/W using Bishop's simplified method (D = 1-m)

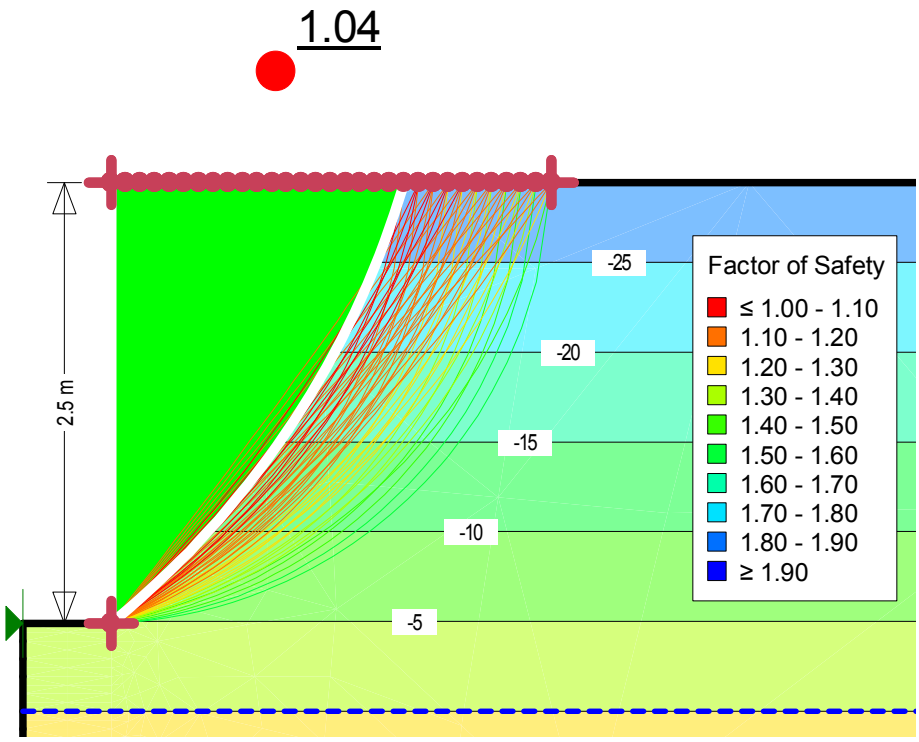

Figure 6.9. Slope stability analysis in SLOPE/W using Bishop's simplified method (D = 3-m)

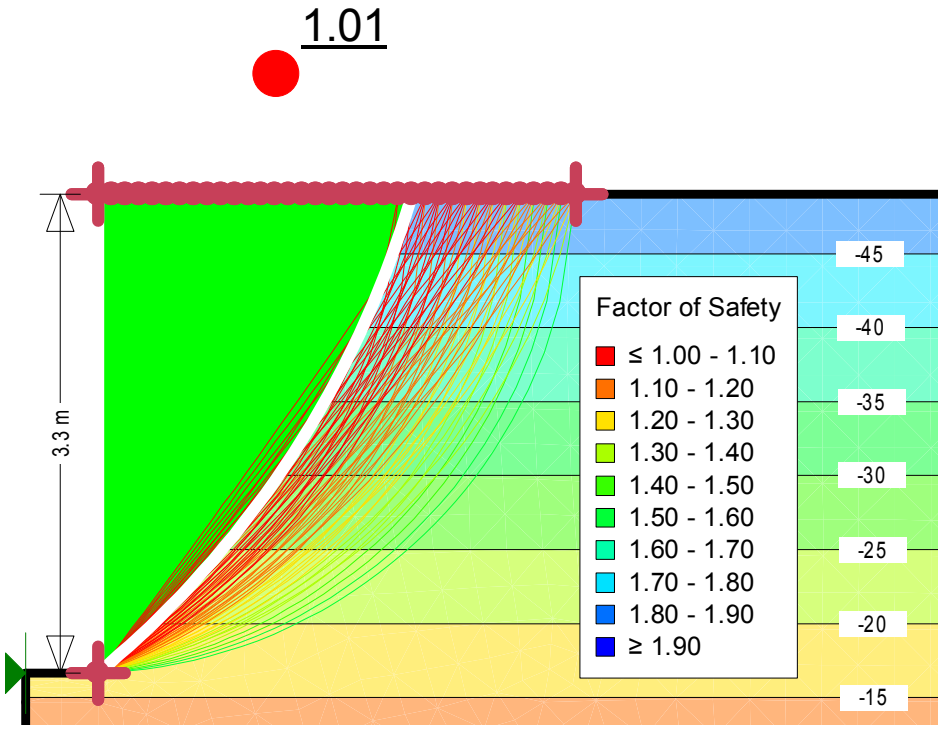

Figure 6.10. Slope stability analysis in SLOPE/W using Bishop's simplified method (D = 5-m)

6.2.3 Comparison of Critical Heights from EREPT and BSM

The critical heights obtained from extended Rankine earth pressure theory and Bishop's simplified method are summarized in Table 6.2 for various levels of the GWT. The results are plotted in Figure 6.11 for better comparison.

Table 6.2. Variation of the critical height in IHT

Depth of GWT (m)	Critical Height (m)	
	Extended Rankine Earth Pressure Theory	**Bishop's Simplified Method**
0	2.6	2.8
0.3	2.2	2.3
0.5	2.0	2.1
0.7	1.9	2.0
1	1.8	1.9
1.2	1.8	2.0
1.5	1.9	2.0
2	2.0	2.2
2.5	2.3	2.4
3	2.5	2.6
4	3.0	2.9
5	3.3	3.1

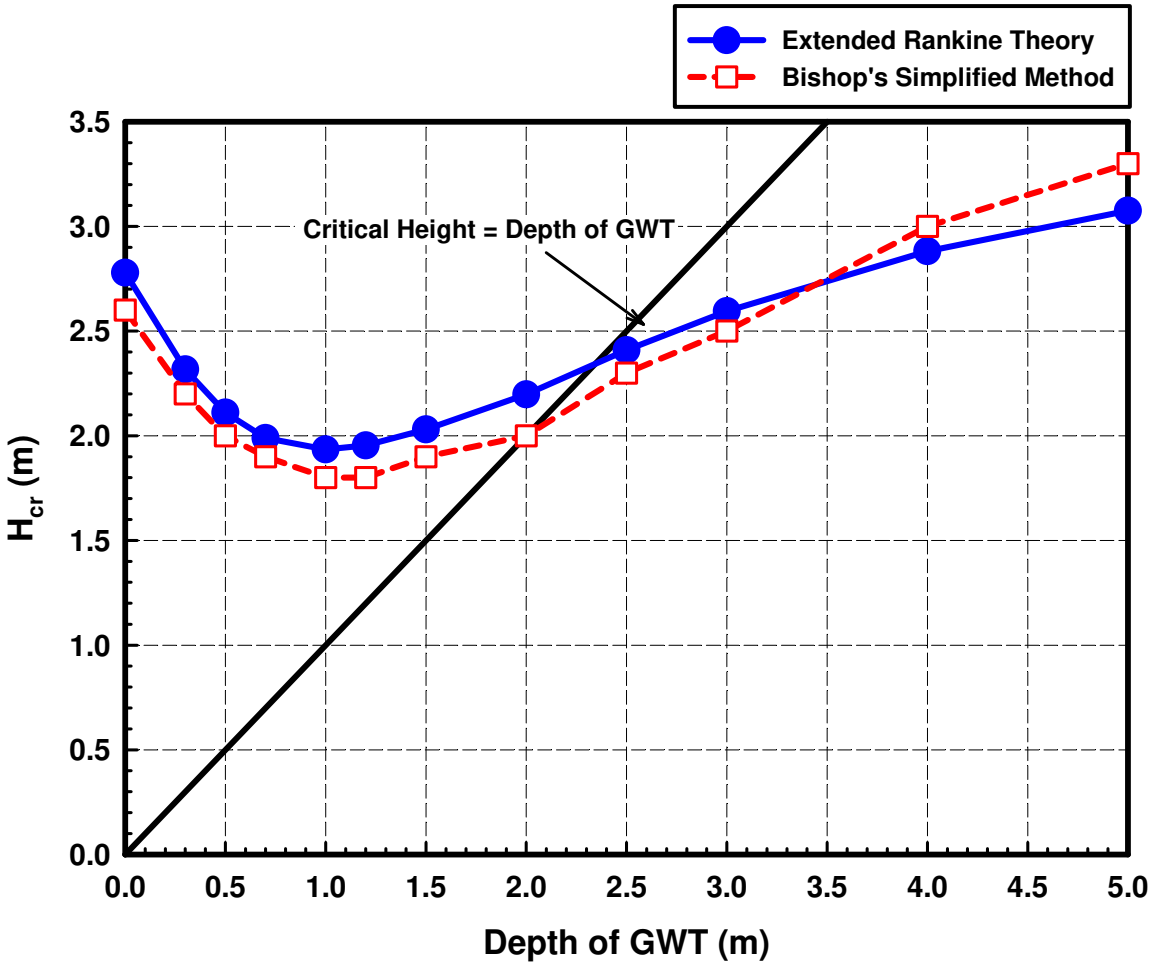

Figure 6.11. Variation of the critical height with respect to the depth of the GWT using extended Rankine earth pressure theory and Bishop's simplified method (IHT)

The results show that there is good agreement between the critical heights obtained from extended Rankine earth pressure theory and Bishop's simplified method. This suggests that extended Rankine earth pressure theory is a simple and efficient way to estimate the critical height of unsupported vertical trenches in both coarse and fine-grained unsaturated soils. It is interesting to note that the critical height does not continuously increase with increasing depth of the GWT, but instead decreases gradually to a minimum value when D = 1-m, and then starts increasing.

In a cohesive soil, net AEP is the sum of positive and negative earth pressure that are caused by effective weight and total cohesion of the soil, respectively. The SWCC of a cohesive soil is distributed over a large range of suction and the rate of change in the total cohesion to that of soil suction is less compared to sandy soils. Hence, when the GWT is at a shallow depth (i.e. less than 1-m), the contribution of total cohesion towards negative earth pressure is less than that of effective weight of soil towards positive earth pressure. This becomes opposite as the GWT is further decreased, which leads to an increase in the critical height. In the case where the GWT is at the surface, total cohesion is minimized (= effective cohesion); however, the unit weight of soil is minimized at the same time (i.e. effective unit weight). For this reason, the critical height with D = 0-m is greater than that with the GWT at a depth less than 3.5-m in this soil.

6.3 Estimating the Critical Height with Foundation Stress

The variation of the critical height of an unsupported vertical trench subjected to foundation stress was estimated with the M-P method (details in section 5.2) to simulate excavations nearby existing foundations. It was assumed that all soil was removed up to the wall of the structure before proceeding to excavate below the foundation depth regardless of the foundation stress. The scenario was modelled as shown in Figure 6.12.

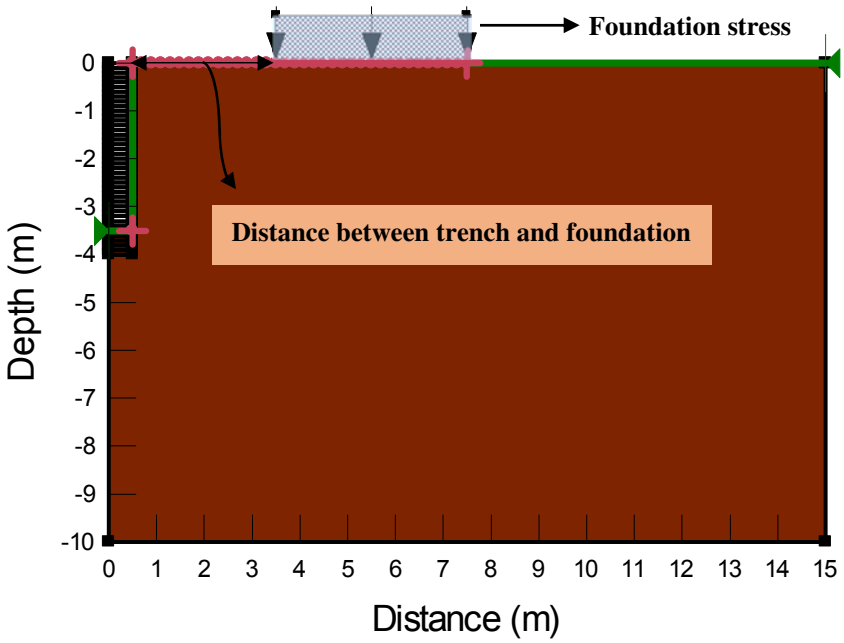

Figure 6.12. SLOPE/W model used to consider foundation stress

The critical heights were estimated considering three variables; i) level of the GWT (0, 1, 2, 3 and 5-m), ii) foundation stress (10, 20, 30 and 50 kPa), and iii) distance between the excavation and the foundation stress (0, 1, 2, and 3-m). The entry range of potential slip surfaces was defined as double the depth of excavation, spanning from the edge of excavation towards the foundation with an entry point every 10-cm. The exit was specified as a point at the toe of the slope. An example of a stability analysis is shown in Figure 6.13. Figure 6.14 to Figure 6.18 show the variation of the critical height with respect to the distance from the edge of excavation to the foundation for different GWTs.

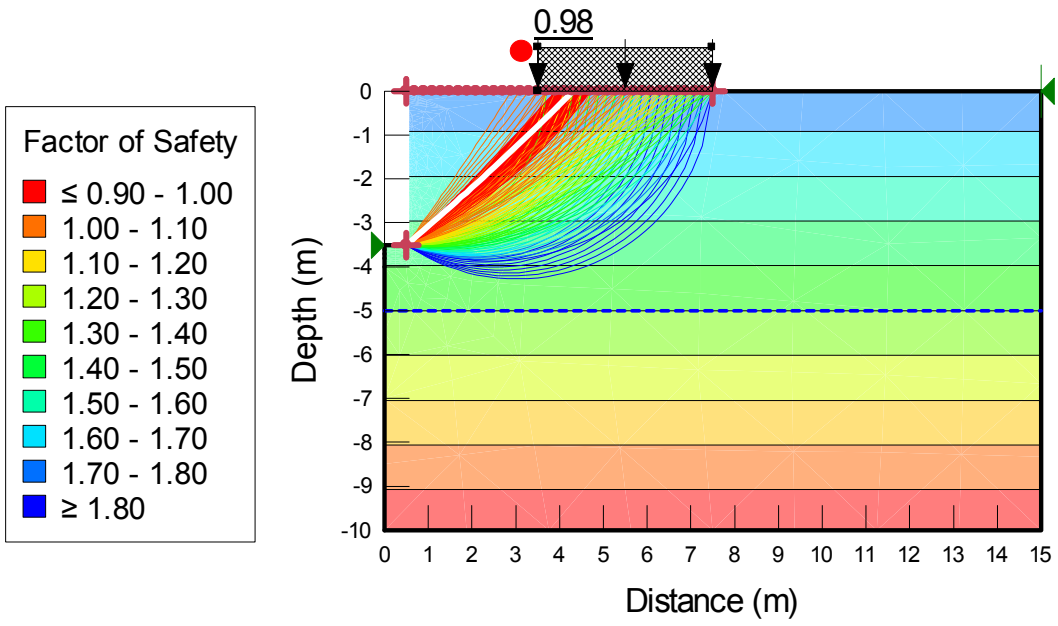

Figure 6.13. Stability analysis considering 50-kPa surcharge at a distance of 3-m (D = 5-m)

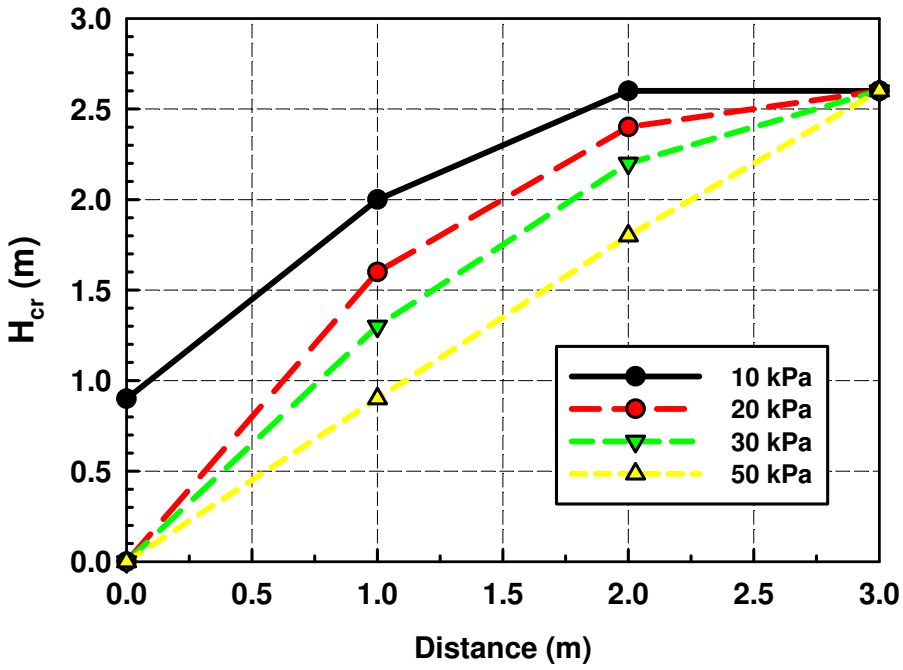

Figure 6.14. Critical height vs. distance of foundation stress from excavation (D = 0-m)

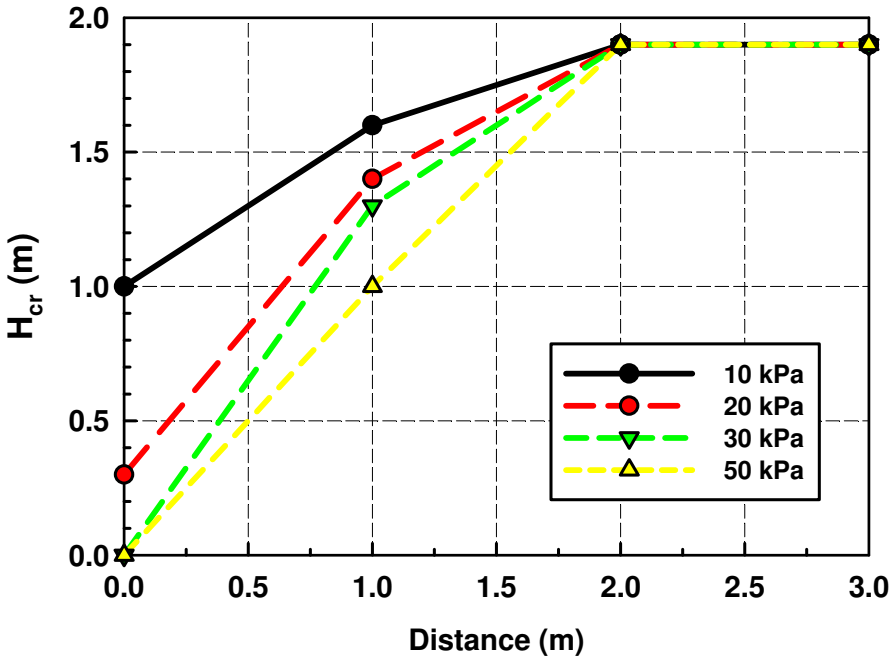

Figure 6.15. Critical height vs. distance of foundation stress from excavation (D = 1-m)

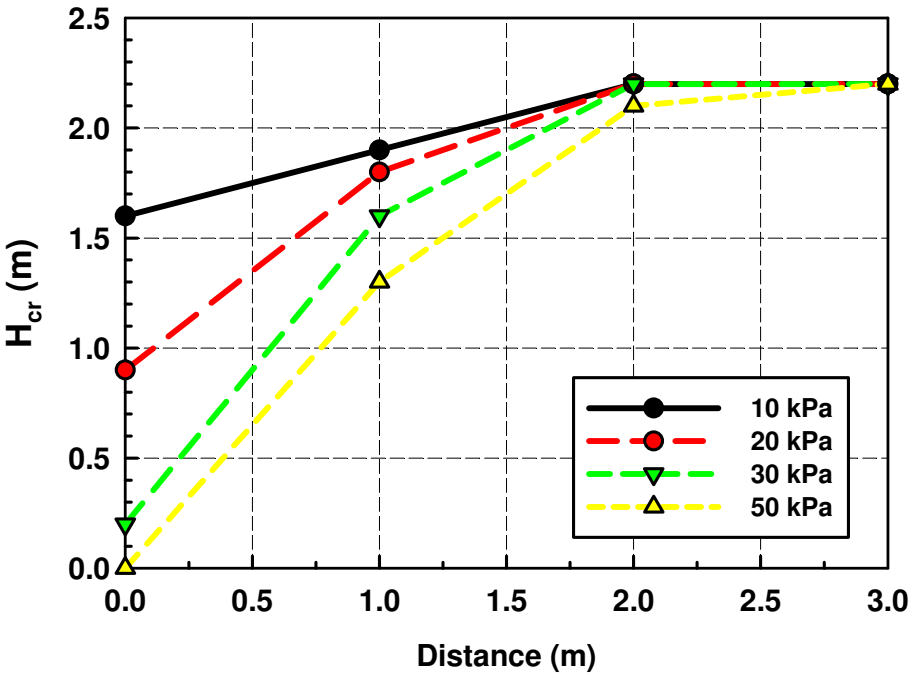

Figure 6.16. Critical height vs. distance of foundation stress from excavation (D = 2-m)

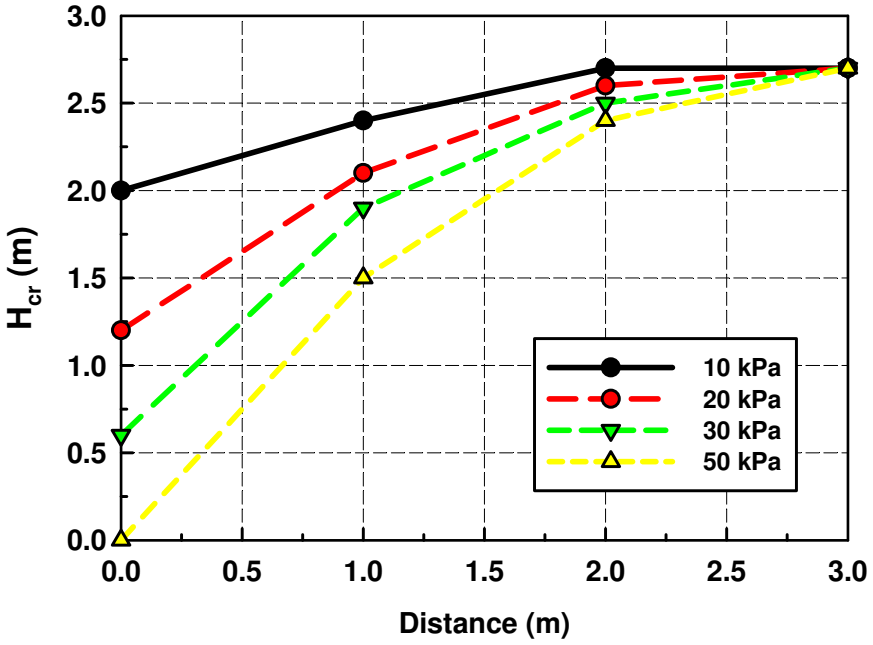

Figure 6.17. Critical height vs. distance of foundation stress from excavation (D = 3-m)

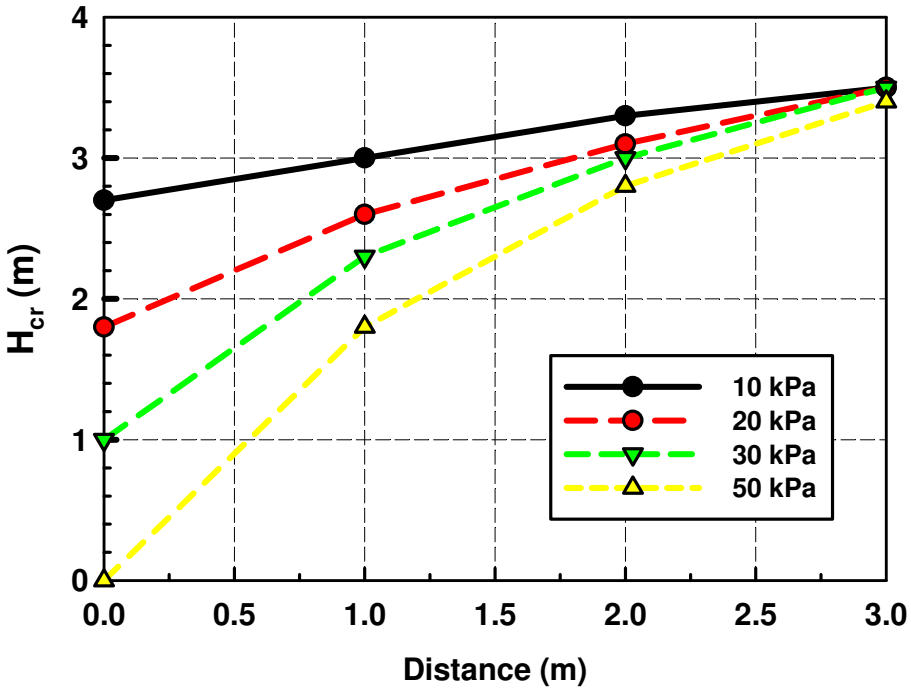

Figure 6.18. Critical height vs. distance of foundation stress from excavation (D = 5-m)

The estimated critical heights decrease with increasing foundation stress. The distance at which the curves converge in Figure 6.14 to Figure 6.18 shall be referred to as the 'significant distance'. This is the distance at which the critical height is not affected by the foundation stress. In other words, failure occurs due to the self-weight of the soil overcoming the resistance from total cohesion, rather than being influenced by the foundation stress when the significant distance is reached. For this reason, the critical heights obtained at the significant distance show good agreement (maximum 8% discrepancy) compared to those found without any applied foundation stress (Figure 6.11). This discrepancy exists because different LEMs were used to estimate the critical heights in section 6.2 and 6.3 (i.e. Bishop's simplified method and M-P method). The significant distance is approximately 3-m, 2-m, and 3-m, when D = 0-m, 1-m, and 5-m, respectively. The shallowest critical height occurs when D = 1-m without any applied foundation stress, therefore the significant distance is also lowest when D = 1-m. This is because the significant distance is a function of the desired excavation depth in addition to applied surcharge pressure (i.e. foundation stress).

The critical height vs. depth of the GWT is plotted in Figure 6.19 to Figure 6.22 for different foundation stresses that are 0, 1, 2, and 3-m away from the excavation, respectively. Except for when the distance is 0-m, the critical height is at a minimum for D = 1-m, which is consistent with the case of no foundation stress. Figure 6.22 clearly shows that the significant distance is no greater than 3-m in IHT for the foundation stresses and levels of the GWT used in this chapter, as indicated by the overlapping surcharge curves.

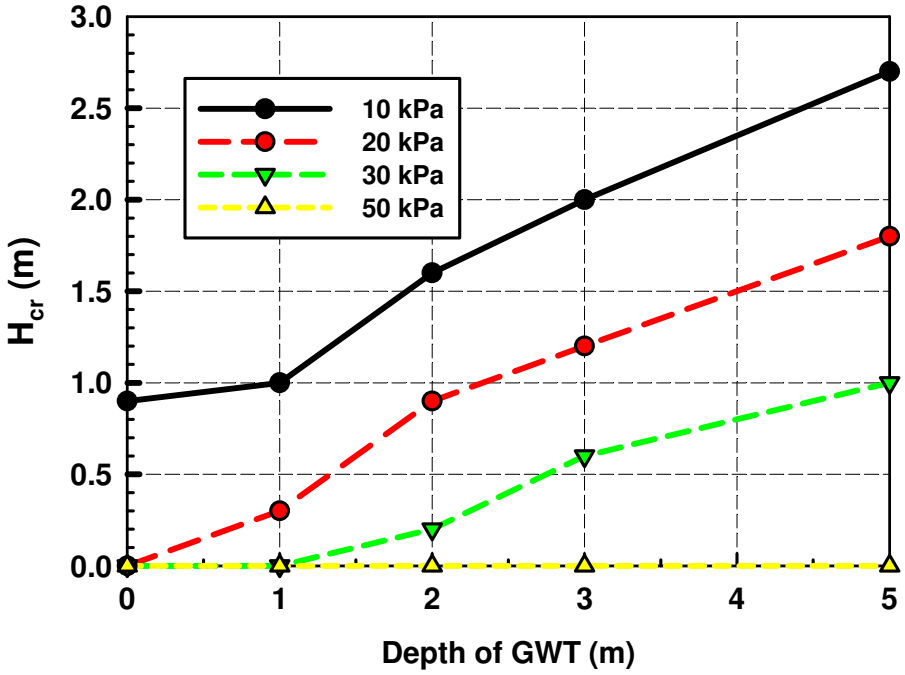

Figure 6.19. Critical height vs. depth of the GWT with distance of foundation stress from excavation = 0-m

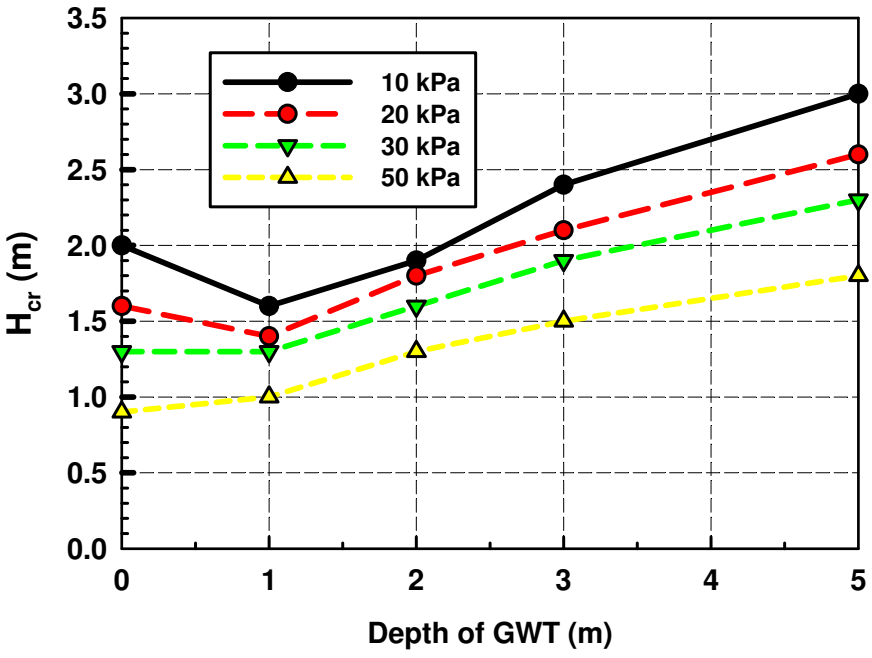

Figure 6.20. Critical height vs. depth of the GWT with distance of foundation stress from excavation = 1-m

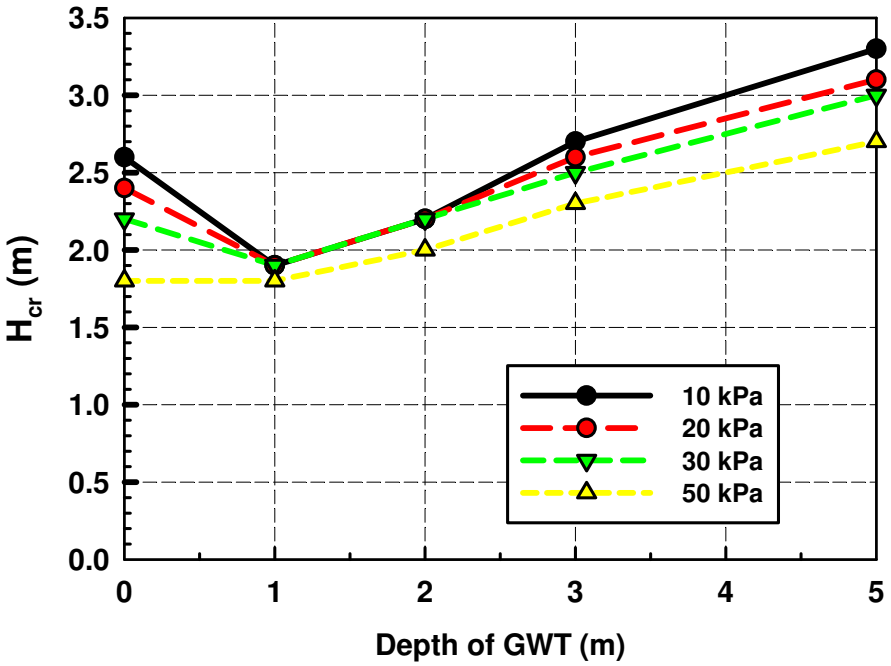

Figure 6.21. Critical height vs. depth of the GWT with distance of foundation stress from excavation = 2-m

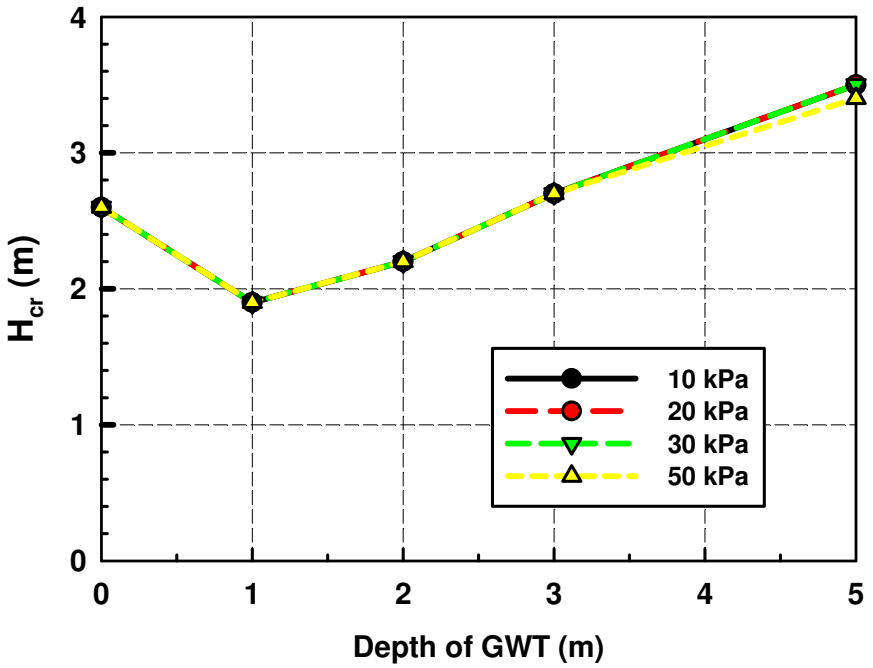

Figure 6.22. Critical height vs. depth of the GWT with distance of foundation stress from excavation = 3-m

6.4 Summary and Conclusions

The variation of the critical height of an unsupported vertical trench was investigated with respect to the proximity and magnitude of adjacent foundation stresses. The critical height is less dependant on the magnitude of the foundation stress as the distance from the edge of the excavation to the foundation stress is increased. The significant distance was estimated to be approximately 3-m regardless of the level of the GWT used in this chapter. The results show that in cases where a trench is excavated near existing superstructures, a combination of the foundation stress, distance from the excavation to the foundation, and level of the GWT (i.e. matric suction distribution) should be considered to reliably estimate the critical height.

CHAPTER 7

GENERAL CONCLUSIONS

Being able to assess the critical height helps facilitate more efficient production in trench-related work. Canadian provinces enforce strict regulations for excavations that workers are required to enter (e.g. Regulation 181(1) of the Occupational Health & Safety Act (1991)). In the case where workers are not required to enter the excavation, the regulations state that contractors can use shoring at their own discretion. For example, machinery alone may be capable of performing the task in the trench and no workers are subjected to a collapse; however, a collapse can still damage the equipment and/or disrupt the work. Thus, knowing the critical height for a jobsite allows the contractor to make informed decisions with respect to supporting the excavation walls. Although this study provides framework for estimating the critical height of unsupported trenches, it is recommended to use shoring if soil deformations in the proximity of a trench (which can damage existing foundations or utilities) is a concern.

An attempt was made to investigate the influence of the matric suction distribution on the critical height of unsupported trenches in unsaturated soil. Extended Rankine earth pressure theory and Bishop's simplified method were used to independently estimate the variation of the critical height of an unsupported vertical trench with respect to the depth of the GWT in Unimin 7030 sand (Chapter 4), and Indian Head till (Chapter 6). The soils have inherently different shear strength properties (cohesionless and cohesive soils), yet the critical heights estimated using both methods showed good agreement for both soils. This

suggests that extended Rankine earth pressure theory and Bishop's simplified method are reliable methods for estimating the critical height of unsupported vertical trenches in unsaturated soils where it is necessary to extend the effective stress approach.

Coupled stress analyses that account for changes in PWP over time were used to investigate the critical height of unsupported excavations with various wall slopes and matric suction distributions in Unimin 7030 sand. The results showed that the FOS is relatively high immediately after the excavation, and then decreases over time as the PWP approaches equilibrium conditions. The critical height increases with increasing depth of the GWT up to a point and then decreases rapidly as the depth of the GWT is further increased, regardless of the wall slope. This is due to the decrease in the contribution of matric suction towards shear strength as matric suction of a soil near the ground surface reaches the residual condition. The critical height was increased as the slope angle was reduced; however, it may not be always possible to provide a gentle slope to the excavation in geotechnical engineering practice due to limited work space in the field. In this case, a combination of sloping and benching can be used effectively to achieve targeted critical heights, especially when matric suction nearby the soil surface is in the range of residual suction.

The Morgenstern-Price method was used in SLOPE/W to examine the influence of foundation stress, the level of the GWT, and the distance between a trench and a foundation. All soil should be removed up to the wall of the structure before proceeding with an excavation below the foundation depth. The significant distance (i.e. the distance that the critical height is not affected by the foundation stress) was estimated to be approximately

3-m for the foundation stresses and levels of the GWT used in this study. The significant distance is a function of excavation depth and the applied surcharge pressure.

Most Canadian provinces impose a maximum allowable depth of 1.2-m for unsupported vertical trenches, regardless of soil type and field conditions. The results from this study suggest that imposing a universal safe height is flawed, and the safe height should be estimated considering soil type, field conditions, and practical scenarios. In Unimin 7030 sand, only a 0.9-m critical height is the best-case scenario for an unsupported vertical trench, which is less than the safe height recommended by any Canadian province. Conversely, the worst-case scenario for the critical height in Indian Head till (i.e. 1.8-m) is greater than the recommended safe height in all Canadian provinces.

In the case where the critical height is much less than what Canadian provinces suggest, the critical height can be further increased by benching or sloping the trench walls, especially in the residual zone. Ontario standards (2017) suggest that sloping the walls 1:1 from the base of excavation where it is not possible to excavate vertically to any significant depth, and the findings from the current study reinforce this suggestion.

In the long-term, the effective cohesion of soil can be lost due to excessive strain, and apparent cohesion may be lost due to excessive rainfall or evaporation. However, it is unrealistic to omit these components of strength in the short-term design of unsupported trenches.

7.1 Recommendations for Future Research

The long-term objective of this study is to provide field engineers and contractors with guidelines for estimating the critical height of unsupported trenches with given field conditions (i.e. soil type, matric suction distributions) and circumstances (e.g. surcharge pressure). This research may facilitate more efficient trench related work by assisting contractors in determining the depth at which shoring or a trench box is required to perform any necessary tasks.

The findings from this study are based on analytical and numerical analyses, hence it is necessary to conduct a series of laboratory and/or field tests to validate the findings. There are also various practical scenarios that should be considered before estimating the critical height of unsupported trenches for a jobsite by extending the findings from this study. For example, if a trench must extend deeper than the GWT, de-watering the trench by pumping induces seepage through the sidewalls of the trench. Seepage forces can decrease the effective stress at the toe of the slope, and in turn lower shear strength. Another common scenario that needs to be considered is heavy equipment operating near the top of a slope. This induces vibration and affects the PWP and matric suction distribution within the soil. Thus, the influence of seepage forces and dynamic loading should be studied to improve the reliability of the methodologies for estimating the critical height of an unsupported vertical trench.

REFERENCES

Alberta - Occupational Health & Safety Division. 2009. Occupational Health & Safety Code - Explanation Guide.

Bishop, A.W. 1955. The Use of the Slip Circle in the Stability Analysis of Slopes. Geotechnique, **5**(1): 7–17.

Bishop, A.W. 1959. The Principle of Effective Stress. Teknisk ukeblad, **106**(39): 859–863.

Bishop, A.W., and Blight, G.E. 1963. Some Aspects of Effective Stress in Saturated and Partly Saturated Soils. Géotechnique, **13**(3): 177–197.

Bowles, J.E. 2001. Foundation Analysis and Design. *In* 5th edition. McGraw-Hill.

Ching, R.K.H., and Fredlund, D.G. 1983. Some difficulties associated with the limit equilibrium method of slices. Canadian Geotechnical Journal, **20**(4): 661–672.

Craig, R.F. 2004. Craig's Soil Mechanics. *In* 7th edition. Spon Press, New York.

Dai, B.B., Yang, J., and Zhou, C.Y. 2016. Observed Effects of Interparticle Friction and Particle Size on Shear Behavior of Granular Materials. International Journal of Geomechanics, **16**(1): 1–11.

De Vita, P., Angrisani, A.C., and Di Clemente, E. 2008. Engineering geological properties of the Phlegraean pozzolan soil (Campania region, Italy) and effect of the suction on the stability of cut slopes. Italian Journal of Engineering Geology and Environment, **2**: 5–22.

Donald, I.B. 1957. Effective stresses in unsaturated non-cohesive soils with controlled negative pore pressure. University of Melbourne, Melbourne, Australia.

Eivemark, M., and Hall, B. 2000. Geotechnical Considerations in Trench Design for Lifelines. Jacques Whitford & Associates Ltd.

Escario, V., and Saez, J. 1987. Shear strength of partly saturated soils versus suction. *In* International Conference on Expansive Soils. pp. 141–143.

Fredlund, D.G., and Krahn, J. 1977. Comparison of slope stability methods of analysis. Canadian Geotechnical Journal, **14**(3): 429–439.

Fredlund, D.G., Krahn, J., and Pufahl, D. 1981. The relationship between limit equilibrium slope stability methods. *In* Tenth International Conference on Soil Mechanics and Foundation Engineering. Stockholm. pp. 409–416.

Fredlund, D.G., and Morgenstern, N.R. 1977. Stress State Variables for Unsaturated Soils. Journal of the Geotechnical Engineering Division, **103**(5): 447–466.

Fredlund, D.G., Morgenstern, N.R., and Widger, R.A. 1978. The shear strength of unsaturated soils. Canadian Geotechnical Journal, **15**(3): 313–321.

Fredlund, D.G., and Rahardjo, H. 1993a. An overview of unsaturated soil behavior. Geotechnical special publication, **1**(1).

Fredlund, D.G., and Rahardjo, H. 1993b. Soil Mechanics for Unsaturated Soils. John Wiley & Sons.

Fredlund, D.G., Rahardjo, H., and Fredlund, M.D. 2012. Unsaturated Soil Mechanics in Engineering Practice. John Wiley & Sons, Inc.

Fredlund, D.G., and Xing, A. 1994. Equations for the soil-water characteristic curve. Canadian Geotechnical Journal, **31**(4): 521–532.

Fredlund, D.G., Xing, A., and Huang, S. 1994. Predicting the permeability function for unsaturated soils using the soil-water characteristic curve. Canadian Geotechnical Journal, **31**(4): 533–546.

Gan, J.K.M., Fredlund, D.G., and Rahardjo, H. 1988. Determination of the shear strength parameters of an unsaturated soil using the direct shear test. Canadian Geotechnical Journal, **25**(3): 500–510.

Garven, E.A., and Vanapalli, S.K. 2006. Evaluation of Empirical Procedures for Predicting the Shear Strength of Unsaturated Soils. *In* Unsaturated Soils 2006. American Society of Civil Engineers. pp. 2570–2592.

GEO-SLOPE International Ltd. 2015. Stability Modeling with SLOPE/W - An Engineering Methodology. Calgary, Alberta.

Goh, S.G., Rahardjo, H., and Leong, E.C. 2014. Shear Strength of Unsaturated Soils under Multiple Drying-Wetting Cycles. Journal of Geotechnical and Geoenvironmental Engineering, **140**(2).

Hilf, J. 1956. An Investigation of Pore-water Pressure in Compacted Cohesive Soils. PhD Dissertation, Technical Memorandum No. 654, U.S. Bureau of Reclamation, Denver, Co.

Hinze, J. 2005. Use of Trench Boxes for Worker Protection. Journal of Construction Engineering and Management, **131**(4): 494–500.

Jennings, J.E.B., and Burland, J.B. 1962. Limitations to the Use of Effective Stresses in Partly Saturated Soils. Geotechnique, **12**(2): 125–144.

Khalili, N., and Khabbaz, M.H. 1998. A unique relationship of chi for the determination of the shear strength of unsaturated soils. Geotechnique, **48**(5).

Krahn, J. 2003. The 2001 R.M. Hardy Lecture: The limits of limit equilibrium analyses. Canadian Geotechnical Journal, **40**: 643–660.

Krahn, J., and Fredlund, D.G. 1983. Variability of the engineering properties of natural soil deposits. *In* Fourth International Conference on Applications of Statistics and Probability in Soil and Structural Engineering. Florence, Italy. pp. 1017–1029.

Manitoba - Workplace Safety & Health Division. 2011. Guide for Excavation Work.

Ministry of Labour Alberta. (2009). Occupational Health and Safety Code.

Mohamed, F., and Vanapalli, S.K. 2006. A semi-empirical approach for the interpretation of the bearing capacity of unsaturated soils. University of Ottawa.

Morgenstern, N.R., and Price, V.E. 1965. The Analysis of the Stability of General Slip Surfaces. Geotechnique, **15**(1): 79–93.

National Institute of Occupational Safety & Health. 2013. Trenching and Excavation - Workplace Safety and Health Topic. US Department of Health and Human Services.

New Brunswick. 1991. Occupational Health and Safety Act.

Nishimura, T., Toyota, H., Vanapalli, S.K., and Oh, W.T. 2008. The shear strength behavior of a silty soil in the residual zone of unsaturation. *In* 12th International Conference of International Association for Computer Methods and Advances in Geomechanics. Goa, India. pp. 2213–2221.

Oh, W.T., and Vanapalli, S.K. 2010. Influence of Rain Infiltration on the Stability of Compacted Soil Slopes. Computers and Geotechnics, **37**: 649–657.

Oh, W.T., and Vanapalli, S.K. 2018. Modeling the stress versus settlement behavior of shallow foundations in unsaturated cohesive soils extending the modified total stress approach. Soils and Foundations, **58**(2): 382–397.

Ontario - Infrastructure Health & Safety Association. 2017. Trenching Safety.

Pufahl, D.E., Fredlund, D.G., and Rahardjo, H. 1983. Lateral earth pressures in expansive clay soils. Canadian Geotechnical Journal, **20**(2): 228–241.

Rahardjo, H., Heng, O.B., and Choon, L.E. 2004. Shear strength of a compacted residual soil from consolidated drained and constant water content triaxial tests. Canadian Geotechnical Journal, **41**(3): 421–436.

Rankine, W.J.M. 1857. On the Stability of Loose Earth. Philosophical Transactions of the Royal Society of London, **147**: 9–27.

Richard, A., Oh, W.T., and Brennan, G. 2017. Critical height of an unsupported vertical trench in an unsaturated sand. *In* 70th Canadian Geotechnical Conference. Ottawa, Canada.

Slipp, B., and Gulf Operators. 2018. Construction costs associated with trenching.

Suruda, A., Smith, G., and Baker, S. 1988. Deaths from Trench Cave-in in the Construction Industry. Journal of Occupational and Environmental Medicine, **30**(7): 552–555.

Symons, I.F., Chard, B., and Carder, D.R. 1982. Ground movements caused by deep trench construction. *In* Restoration of Sewerage Systems. Thomas Telford Ltd., London.

Terzaghi, K. 1936. The shearing resistance of saturated soils and the angle between the planes of shear. First international conference on soil Mechanics, 1936, **1**: 54–59.

Thompson, L.J., and Tanenbaum, R.J. 1977. Survey of Construction Related Trench Cave-Ins. Journal of the Construction Division, **103**(3): 501–512.

Thu, T.M., Rahardjo, H., and Leong, E.-C. 2006. Shear Strength and Pore-Water Pressure Characteristics during Constant Water Content Triaxial Tests. Journal of Geotechnical and Geoenvironmental Engineering, **132**(3): 411–419.

Trench Shoring Company. 2016. Trench & Manhole Boxes.

Vanapalli, S.K. 2009. Shear strength of unsaturated soils and its applications in geotechnical engineering practice. *In* 4th Asia Pacific Conference on Unsaturated Soils. Newcastle, Australia. pp. 579–598.

Vanapalli, S.K., and Fredlund, D.G. 2000. Comparison of Different Procedures to Predict Unsaturated Soil Shear Strength. *In* Advances in Unsaturated Geotechnics. American Society of Civil Engineers. pp. 195–209.

Vanapalli, S.K., Fredlund, D.G., and Pufahl, D.E. 1997. Saturated-unsaturated shear strength and hydraulic conductivity behavior of a compacted glacial till. *In* 50th Canadian Geotechnical Conference. Ottawa, Canada. pp. 625–632.

Vanapalli, S.K., Fredlund, D.G., and Pufahl, D.E. 1999. The influence of soil structure and stress history on the soil-water characteristics of a compacted till. **49**(2): 143–159.

Vanapalli, S.K., Fredlund, D.G., Pufahl, D.E., and Clifton, A.W. 1996. Model for the prediction of shear strength with respect to soil suction. Canadian Geotechnical Journal, **33**(3): 379–392.

Vanapalli, S.K., and Oh, W.T. 2012. Stability Analysis of Unsupported Vertical Trenches in Unsaturated Soils. *In* GeoCongress 2012. American Society of Civil Engineers. pp. 2502–2511.

Whenham, V., Vos, M.D., Legrand, C., Charlier, R., Maertens, J., and Verbrugge, J.-C. 2007. Influence of Soil Suction on Trench Stability. *In* Experimental Unsaturated Soil Mechanics. Springer Berlin Heidelberg. pp. 495–501.

White, F. 2008. National Institute for Occupational Safety and Health (NIOSH) Prevention through Design (PtD) Workshop Closing Remarks. Journal of Safety Research, **39**(2): 203–204.

WorkSafeNB. 2017. Number of trench-related fatalities in New Brunswick.

Yang, H., Rahardjo, H., Leong, E.-C., and Fredlund, D.G. 2004. Factors affecting drying and wetting soil-water characteristic curves of sandy soils. Canadian Geotechnical Journal, **41**(5): 908–920.

CURRICULUM VITAE

Candidate's full name:	Adin Alexander Richard
Universities attended:	B.Sc.E. (Civil), University of New Brunswick, 2016
Journal publications:	N/A
Conference presentations:	"Critical height of an unsupported vertical trench in an unsaturated sand". *In Proceedings of the 70th Canadian Geotechnical Conference*. Ottawa, Canada. (2017).